# Advanced thermal management system driven by phase change materials for power lithium-ion batteries: A review

Jiangyun Zhang[a,*], Dan Shao[d], Liqin Jiang[c], Guoqing Zhang[a], Hongwei Wu[b], Rodney Day[b], Wenzhao Jiang[a]

[a] *School of Materials and Energy, Guangdong University of Technology, Guangzhou, Guangdong 510006, China*

[b] *School of Physics, Engineering and Computer Science, University of Hertfordshire, Hatfield, AL10 9AB, United Kingdom*

[c] *Guangdong Zhuhai Supervision Testing Institute of Quality And Metrology, Zhuhai, 519000, China*

[d] *Guangdong Key Laboratory of Battery Safety, Guangzhou Institute of Energy testing, Guangzhou, Guangdong 511447, China*

## ABSTRACT

Power lithium-ion batteries are widely utilized in electric vehicles (EVs) and hybrid electric vehicles (HEVs) for their high energy densities and long service-life. However, thermal safety problems mainly resulting from thermal runaway (TR) must be solved. In general, temperature directly influences the performance of lithium-ion batteries. Hence, an efficient thermal management system is very necessary for battery modules/packs. One particular approach, phase change material (PCM)-based cooling, has exhibited promising applicability due to prominent controlling-temperature and stretching-temperature capacities. However, poor thermal conductivity performance, as the main technical bottleneck, is limiting the practical application. Nevertheless, only promoting the thermal conductivity is far from enough considering the practical application in EVs/HEVs. To fix these flaws, firstly, the heat generation/transfer mechanisms of lithium-ion power batteries were macro- and

* Corresponding author.

*E-mail address*: roseyyun@163.com (J. Zhang)

microscopically reviewed. Following that, the thermal conductivity, structural stability, and flame retardancy of PCM are thoroughly discussed, to which solutions to the aforementioned performances are systematically reviewed. In addition, battery thermal management system (BTMS) employing PCM is illustrated and compared. Eventually, the existing challenges and future directions of PCM-based BTMS are discussed. In summary, this review presents effective approaches to upgrade the PCM performances for high-density lithium-ion BTMS. These strategies furtherly accelerate the commercialization process of PCM BTMS.

**Highlights**

(1) The classification and heat production/transfer principles of power lithium-ion batteries are elaborated.

(2) The categories of PCM and the enhanced key performances are summarized.

(3) The application of PCM-based BTMS in the module/pack is particularly described.

(4) The existing challenges and the future directions of PCM-based BTMS are discussed.

***Keywords*:** Lithium-ion power batteries, thermal safety, thermal management, phase change materials, hybrid cooling system, preheating system

**Contents**

**Abbreviations**

| | | | |
|---|---|---|---|
| EVs | Electric vehicles | HEVs | Hybrid electric vehicles |
| TR | Thermal runaway | PCM | Phase change material |
| BTMS | Battery thermal management system | HP | Heat pipe |
| TE | Thermoelectric | CNT | Carbon nanotube |
| PCC | Phase change composite | LFP | $LiFePO_4$ |
| LMO | $LiMn_2O_4$ | LCO | $LiCoO_2$ |
| NCA | $Li(NiCoAl)O_2$ | NCM | $Li(NiCoMn)O_2$ |
| SSPCM | Solid-solid PCM | SLPCM | Solid-liquid PCM |
| SGPCM | Solid-gas PCM | LGPCM | Liquid-gas PCM |
| PA | Paraffin | EG | Expanded graphite |
| EG-MWC | Expanded | EG-CNF | Expanded graphite-carbon |

| | | | |
|---|---|---|---|
| NT | graphite-multi-walled carbon nano-tube | | nano-fiber |
| HDPE | High density polyethylene | Microencapsulated phase change materials | MicroPCM |
| LDPE | Low density polyethylene | SEBS | Styrene-b-(ethylene-co-butylene)-b-styrene |
| SSPoPCM | Solid-solid polymer PCM | FS | Form stabilized |
| DEEP | Diethyl ethylphosphonate | LOI | Limiting oxygen index |
| HRR | Heat release rate | PHRR | Peak heat release rate |
| TSR | Total smoke rate | THR | Total heat release |
| APP | Ammonium polyphosphate | RP | Red phosphorus |
| IFR | Intumescent flame retardant | PP | Polypropylene |
| SPR | Smoke produce rate | PNDA | Phosphorus–nitrogen containing diamine |
| CFA | Char forming agent | CP | Chlorinated paraffin |
| AT | Antimony trioxide | CF | Copper foam |
| OBC | Olefin block copolymer | SBS | Styrene butadiene styrene |
| B-CPCM | Block-shaped CPCM | S-CPCM | Serpentine CPCM |
| PCS | Personal cooling system | CM | Copper mesh |
| OHP | Oscillating heat pipe | TECs | TE coolers |
| SEI | Solid electrolyte interphase | AC | Alternating current |
| AlN | Aluminium nitride | | |

## 1. Introduction

Significant energy shortage and environmental pollution have increased the need for developing new energy storage technologies. In general, minimizing carbon emissions has always been prioritized in the global scale, particularly with an average emission reduction target of 40% for 2015–2025 [1]. As such, the development of new energy vehicles has become a global trend. Environmentally friendly electric vehicles (EVs) and hybrid electric vehicles (HEVs) have been considered as a possible solution to the aforementioned world-wide issues. Many countries have announced the future plans (Table 1) to target fuel vehicle withdrawal to encourage the development of electric-driven EVs and HEVs. The driving miles, performance, service life, and safety of EVs and HEVs are largely dependent on their power systems. In particular, lithium-ion power batteries are considered a primary option for power battery systems due to their high energy density, high voltage, low self-discharge rate, long cycle-life, and specific energy. However, the pressure [2,3], vibration [4], and operation temperature [5] of lithium-ion batteries require careful consideration for their application in EVs and HEVs. In particular, the charge–discharge electrochemical reactions are significantly dependent on the operating temperature, which in turn directly affect the power battery electrochemical performance and heat generation behavior for reliability and safety considerations. In general, lithium-ion batteries operate within an optimum temperature range of 20ºC–40ºC and at a temperature uniformity of 5ºC [6]. However, lithium-ion power battery heat dissipation is difficult during continuous temperature increase and heat accumulation due to a lack of efficient dissipation approaches, which in turn aggravate the electrochemical reactions. As a result, thermal runaway (TR), especially in abusive conditions (Fig. 1), produces flame, fire, and explosive accidents [7]. Recent TR-induced accidents are described in Table 2. There are higher chances of executing TR scenarios during stressful and abusive battery operations, such as operating at high discharge rates, high ambient temperatures (>40°C), and under thermal, electrical (excessive charging and discharging), and mechanical abuse conditions. Therefore, the development of a high-efficiency, scientific, and appropriate battery thermal management system (BTMS) is crucial to produce the

desired performances. Particularly, the following functions must be met: 1) accurate monitoring and measuring of battery operating temperatures in real time; 2) efficient ventilation and heat dissipation of high-temperature battery packs; 3) rapid heating of low-temperature battery packs; 4) continuous maintenance of specified operation temperature range; and 5) improved the uniform temperature distribution across the battery cells.

**Table 1**

Future plans to ban the sale of traditional fuel vehicles [8-10]

| Countries | Detailed time / year | Specific target |
|---|---|---|
| France | 2040 | A blanket ban on the fuel vehicle sale |
| United Kingdom | 2040 | A complete ban on the sale of traditional diesel-powered cars |
| Germany | After 2030 | Banning the sale of traditional internal combustion engine cars |
| India | 2030 | Banning the sale of conventional fuel cars |
| Holland | 2025 | Banning the sale of conventional fuel cars |
| Norway | 2025 | Banning the sale of conventional fuel cars |
| China | 2040 | Banning the sale of conventional fuel cars |

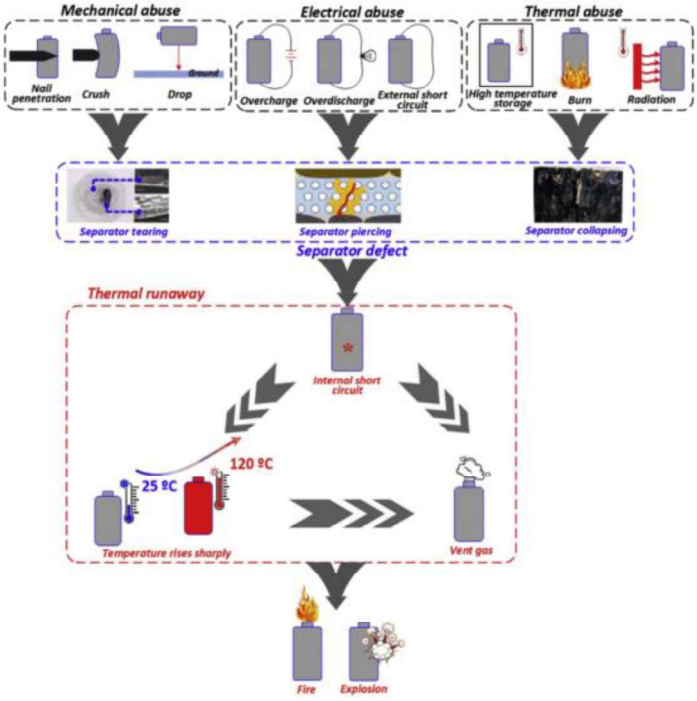


**Fig. 1.** Schematic of lithium-ion battery TR mechanism under different abusive conditions [7].

**Table 2**
Selected lithium-ion battery TR mechanism-induced severe accidents

| Date of accident | Location | Source of accident |
|---|---|---|
| January 6, 2016 | Norway | Tesla Model S suddenly fired when charging in the charge station [11] |
| August 17, 2016 | Biarritz, France | Tesla Model 90D suddenly fired when testing driving [12] |
| September 27, 2017 | Newman Company, Shenzhen City, China | Short circuit-induced spontaneous combustion of stored batteries in a warehouse [13] |
| May 12, 2018 | Florida, USA | Tesla Model S resulted in fire accidents after collisions [14] |
| April 7, 2019 | Hangzhou, China | Battery spontaneously ignited and occurred propagation during the charging process [15] |
| July 18, 2019 | Beijing, China | Batteries suddenly ignited during the rest-time period [16] |
| June 11, 2019 | Daly City, California, USA | Lithium-ion battery-induced fire during charging, which ignited surrounding combustible materials and spread the fire accident [13] |
| May 8, 2020 | Dongguan City, China | Lithium-ion battery-induced |

| | | |
|---|---|---|
| | | spontaneous combustion of car, resulting in a fire [13] |
| August 16, 2020 | Taiyuan City, China | Lithium-ion battery-induced spontaneous combustion of electric car during charging [13] |
| November 6, 2020 | Haikou City, China | EC 30-type electric car suddenly began to smoke and burn [17] |
| November 9, 2020 | Pingxiang City, China | New energy vehicle burst into flames, accompanied by large amount of smoke and explosion [18] |
| November 22, 2020 | Shenzhen City, China | New energy car suddenly sent up smoke, which spread the fire and resulted in an explosion [19] |

At present, the development of an optimal BTMS approach has been based on air-based cooling [20,21], liquid-based cooling [22-24], and phase change material (PCM)-based cooling [25-27]. Cooling methods can also be categorized as active cooling or passive cooling based on their energy consumption [28]. In particular, active cooling, such as air-conditioning refrigeration and refrigerator cooling, defines cooling methods with additional energy consumption costs. In contrast, passive cooling, such as natural convection cooling and PCM-based cooling, define cooling methods that do not consume energy. In general, air cooling BTMSs can be easily installed and exhibit low production and maintenance costs, and are thus the most commonly applied approach in EVs/HEVs [21]. However, with the ascension of the energy density and driving miles, this system cannot fully meet the cooling demand, especially with maintaining temperature homogeneity. Although the liquid cooling strategy possesses higher heat transfer coefficients due to the excellent thermal conductivity of the coolant, the system is very complicated, expensive, difficult to maintain, and has a risk of experiencing short circuits from the leakage of the cooling medium [23]. In contrast, Al-Hallaj and Selman proposed a PCM-based BTMS in 2000 for the heat generation management of eight 100 Ah cells as an alternative heat dissipation technique. The PCM BTMS does not have additional energy requirements, making it appropriate for simple filling systems [29]. In addition, PCM is able to absorb/release abundant latent heat during phase transition stage, thereby producing somewhat constant temperature distributions and controlling the temperature rise (Fig.

2). However, the primary PCM technology bottleneck, specifically its low thermal conductivity, impedes the heat transfer rate and lowers the cooling capacity during storing/releasing heat. Hence, many research efforts contributed to the promotion of the thermal conductive coefficient through diverse optimization and modification of PCM [30,31]. Rehman et al. [32] reported PCM heat transfer changes with porous materials/foams, specifically enhancements in its thermal conductive performance. Malik et al. [33] examined EVs and HEVs and reviewed its use of PCM/carbon nanotube (CNT) materials. Jaguemont and Mierlo [34] reported prospective BTMS through various passive and active cooling strategies, and traditional BTMS development trends. Liu et al. [35] reviewed various systematic techniques to increase virgin PCM thermal conductivity. Chen et al. [36] examined the relationship between various PCM thermal management strategies and power lithium-ion battery cooling performances, particularly with regards to improving its thermal conductivity performance. Previous research has focused on enhanced PCM heat transfer. However, only PCM thermal conductivity enhancement is insufficient considering PCM applied in EVs and HEVs at various operating conditions. PCM mechanical strength, leak-proof, electrical insulation, and flame retardancy significantly affect lithium-ion battery safety, all of which must fulfill high EV and HEV standard demands. To our best knowledge, the aforementioned several properties have been minimally reported. Therefore, this review organized the thermal management of PCM for high energy-density lithium-ion batteries as follows: 1) classification of power lithium-ion batteries and heat production/transfer principles; 2) categories for PCM and increased key performances (thermal conductivity, mechanical strength and flame retardant performance); 3) detailed application of PCM in the BTMS in the modules/packs; and 4) current challenges, prospective PCM-based BTMS development approaches and future directions. This overview aims to cohesively reference all current and future PCM properties for PCM loading application and commercialization in new energy vehicles. In addition, this review aims to provide in-depth, systematic engineering guidance for PCM-based BTMS.

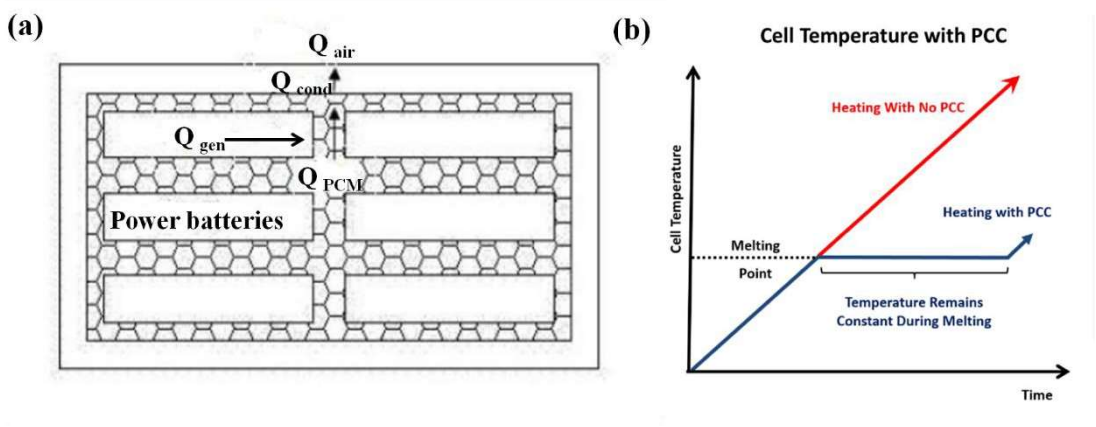


**Fig. 2.** Working principles of BTMS using PCM: (a) heat transfer mechanism of PCM-based cooling technology and (b) temperature-controlling and temperature-balancing theories of the phase change composite (PCC) BTMS [25,27].

## 2. Power lithium-ion batteries

### *2.1. Power lithium-ion batteries categorization*

Electricity-driven vehicles rely very significantly on lithium-ion batteries. Lithium-ion batteries can be distributed across three categories based on their external shape and appearance: (1) cylindrical, (2) prismatic, and (3) pouch (Fig. 3). These batteries have four primary components: (1) a positive electrode (cathode); (2) a negative electrode (anode); (3) an electrolyte; and (4) a separator [37,38]. In general, the anode is composed of carbon such as graphite or silicon-carbon composites, whereas the cathode is composed of a lithium oxide composite. A lithium salt is generally dissolved in organic solvents, such as ethylene carbonate, diethyl carbonate, or dimethyl carbonate, to produce the electrolyte, which stimulates ion transport between the anode and cathode [39,40]. The separator mainly controls electron transport to minimize short circuiting between the positive and negative poles [41]. Cylindrical cells, such as 18650 (diameter=18 mm; length=65 mm), 26650, 32650, and 42110, have electrodes distributed as layers spiraling around a “jelly roll,” which is stuffed into a metal shell (Fig. 3d). At present, standard and typical cylindrical cells are regarded as the most commonly used assembly for battery module/packs because

of their mature technology, excellent consistency, good mechanical stability [42-44]. However, these cells still exhibit thermal safety issues that must be resolved carefully. For example, the power systems of Tesla Roadster, which are composed of 6831 18650-type cells, and Tesla Model S with 7104 cells, are all designed with an efficient BTMS to guarantee a high heat dissipation efficiency. Compared with cylindrical cells, the "jelly roll" assembly can also be applied in rigid prismatic cells but is inserted into a cuboid can (Fig. 3e). However, prismatic cells are able to more easily disperse heat during discharge due to their large heat dissipation area [45,46]. Enough space can be provided when utilizing rectangular cells in EVs/HEVs. In contrast, pouch cells have stacking multiple-layered anode–separator–cathode slice structures that are placed and sealed in electrolyte pouches (Fig. 3f). The none-rigid feature is beneficial for decreasing the weight and increasing the high energy density and packaging efficiency, although this generates additional mechanical destructive properties and swelling [47-49]. Power battery modules/packs constituted by the cylindrical/prismatic cells will be matched with different PCM forms, which will be concretely elaborated in Section 4.

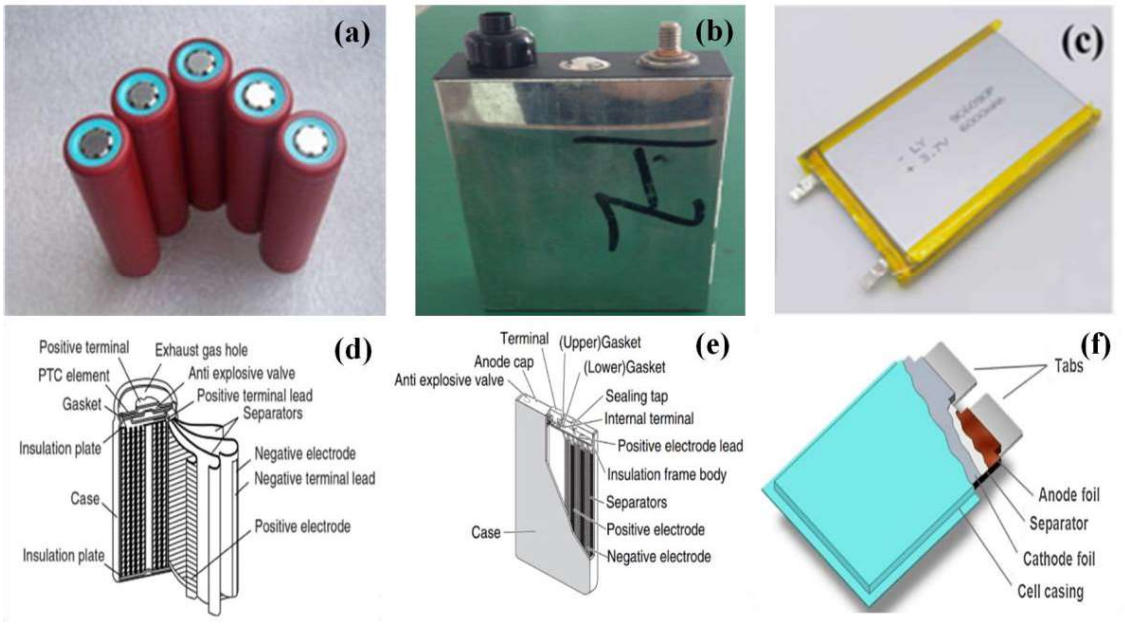


**Fig. 3.** Commonly used power lithium-ion batteries and their internal structure: (a) cylindrical cells, (b) rigid prismatic cells, (c) pouch cells, (d) cylindrical lithium-ion cell structure, (e) prismatic lithium-ion cell structure, and (f) lithium-ion cell pouch structure [37,38].

Lithium-ion power battery electrochemical patterns can be categorized as lithium-iron phosphate ($LiFePO_4$, LFP), lithium manganese oxide ($LiMn_2O_4$, LMO), lithium cobalt oxide ($LiCoO_2$, LCO), lithium nickel cobalt aluminum ($Li(NiCoAl)O_2$, NCA), and lithium nickel cobalt manganese ($Li(Ni_xCo_yMn_{1-x-y})O_2$, NCM) [50]. The overall performance comparison of the aforementioned lithium-ion batteries is listed in Table 3. At present, lithium-ion batteries with LFP and ternary electrochemical patterns have been the primary technological route choices of designing the power system. The ternary power batteries have relatively high energy and power densities, which aggravates the TR given its material crystal structure and chemical reaction during lithium-ion insertion and extraction processes under heat-intensive conditions [51]. Therefore, the development of an appropriate BTMS technique is of the essence to optimize heat output of lithium-ion batteries (Section 2.2) and to enhance their lifespan, safety performance, and driving miles.

**Table 3**

Trade-off analysis of the mainstream lithium-ion power batteries [52,53].

| Cathode chemistry | LCO | LMO | LFP | NCM | NCA |
|---|---|---|---|---|---|
| Voltage (V) | 3.7 | 3.8 | 3.2 | 3.6 | 3.7 |
| Specific energy (mAh/g) | 150 | 120 | 150 | 160 | 170 |
| Energy density (Wh/kg) | 120-150 | 105-120 | 130 | 160-220 | 220-250 |
| Cycles life | 500 | 300 | 2000 | 1000 | 1000 |
| Thermal Safety | Poor | Excellent | Excellent | Preferable | Poor |
| Operating temperature range/$^oC$ | -20–60$^oC$ | -20–60$^oC$ | -20–60$^oC$ | -20–55$^oC$ | -20–60$^oC$ |
| Cost | Expensive | Cheap | Cheap | More expensive | Low |
| Advantages | Stable charge/discharge properties and simple technology | Low cost and admirable safety | High security, environmentally friendly and longer | Good circulation | Eminent low-temperature property and high energy |

| | | | | | |
|---|---|---|---|---|---|
| | | | service life | | density |
| Disadvantages | Expensive Co and reduced cycle life | Low energy density | Poor low-temperature performance and discharge voltage | High cost of Co | Poor high-temperature property and high technical barrier |

*2.2. Lithium-ion battery heat generation/transfer mechanisms*

*2.2.1. Heat production mechanism*

The embedding and disembedding electrochemical reaction processes of $Li^+$ can be interpreted as follows: $Li^+$ is embedded from the positive to negative directions during charging and, in contrast, is embedded from the negative to positive directions during discharging (Fig. 4). This reversible electrochemical process does not damage the original internal lithium battery crystal structure.

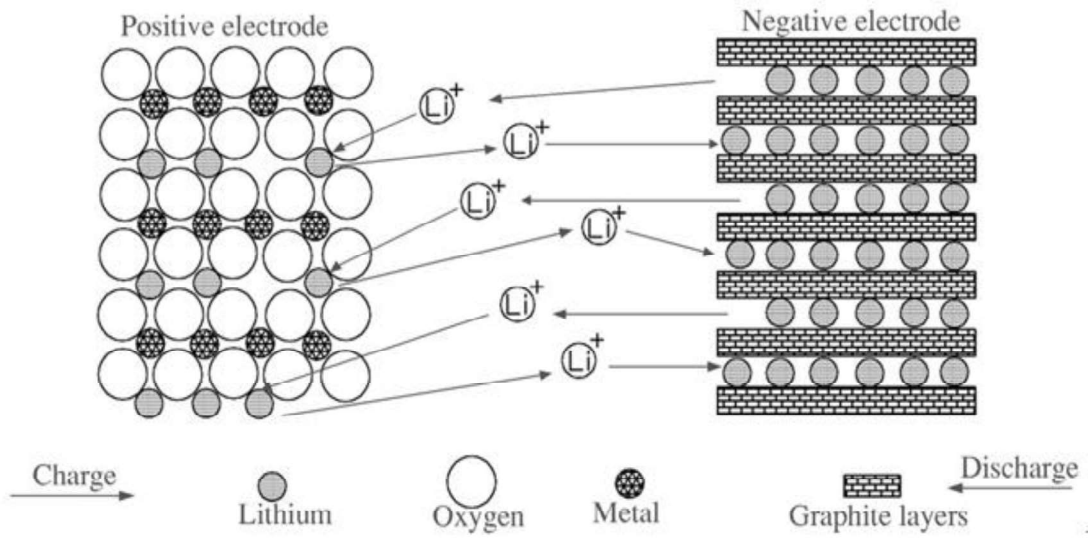


**Fig. 4.** Lithium-ion power battery working principle.

A chain of electrochemical reactions proceeds during charging/discharging to generate heat. As known, lithium-ion battery heat generation is highly dependent on the temperature (Table 4).

**Table 4**

Lithium-ion power battery heat generation under different temperature ranges.

| Temperature range /°C | Chemical reactions | Heat generation/J·g$^{-1}$ | Mechanism analysis |
|---|---|---|---|
| 110–150 | $Li_xC_6$ + | 350 | Rupture of passivation film |
| 130–180 | Melting of PE diaphragm | -190 | Heat absorption |
| 160–190 | Melting of PP diaphragm | -90 | Heat absorption |
| 180–500 | Decomposition of $Li_{0.3}NiO_2$ and electrolyte | 600 | Releasing oxygen temperature 200°C |
| 220–500 | Decomposition of $Li_{0.45}CoO_2$ and electrolyte | 450 | Releasing oxygen temperature 230°C |
| 150–300 | Decomposition of $Li_{0.1}MnO_4$ and electrolyte | 450 | Releasing oxygen temperature 300°C |
| 130–220 | Solvent and $LiPF_6$ | 250 | Lower energy |
| 240–350 | $Li_xC_6$ and PVDF | 1500 | Violent chain growth |
| 660 | Aluminum melting | -395 | Heat absorption |

Lithium-ion battery heat production is primarily divided into three heat components: reversible chemical reaction heat, Joule heat, and polarization heat. In general, cell heat generation is an unsteady, internal process, as described by Eq. (1). According to Eq. (2), the heat generation in the battery is mainly comprised of the total heat generation rate (q), internal reaction heat ($q_{reaction}$), increased heat ($q_{heat\text{-}capacity}$), heat caused by the phase transition process inside the cell ($q_{phase\text{-}change}$), and additional heat rate ($q_{mixing}$) caused by the uneven concentration of cells. Uniform cell concentration under ideal conditions is assumed during normal charging and discharging, such that inner-cell phase transitions can be deemed negligible. Therefore, the Eq. (2) can be simplified as Eq. (3):

$$\rho C\frac{\partial t}{\partial \tau} = \frac{\partial}{\partial x}\left(\lambda\frac{\partial t}{\partial x}\right) + \frac{\partial}{\partial y}\left(\lambda\frac{\partial t}{\partial y}\right) + \frac{\partial}{\partial z}\left(\lambda\frac{\partial t}{\partial z}\right) + q \ , \qquad (1)$$

where

$\rho$ = density of the power lithium-ion cell, kg/m$^3$,

C= specific heat capacity of the lithium-ion cell, J/kg • K,

q= heat production per unit volume of the cell, J/m$^3$,

$$q - IV = q_{reaction} + q_{heat-capacity} + q_{phase-change} + q_{mixing} \ , \qquad (2)$$

$$q - IV = q_{reaction} + q_{heat-capacity} \quad , \quad (3)$$

$$Q = I(U - E) + IT\frac{\partial U}{\partial T} \quad , \quad (4)$$

where

Q=total heat generation of the cell, J,

I = total current of the cell, A,

U = open-circuit voltage, V,

E = electromotive force, V,

T = the average temperature of the cell during the discharge process, $^{o}$C, and

$I(U-E) = I^2R$, including the Joule heat caused by internal resistance of the lithium-ion cell and the polarization heat caused by mass transfer loss, J; and R is the total of the polarization resistance and Joule resistance, Ω.

*2.2.2 Heat transfer approaches*

Lithium-ion power battery electrochemical reactions exhibit three primary heat transfer modes: heat conduction, heat convection, and heat radiation. Practical application generally only follows the first two transfer modes and ignores heat radiation. The detailed calculations are shown as follows:

(1) Heat conduction includes the heat transfer between the materials within the cell, such as the electrodes, the electrolyte, and current collectors. The cell can be regarded as an entirety, and the heat is dissipated from the inside to the surface cell.

$$Q_1 = -\lambda A\frac{dt}{dx} \quad , \quad (5)$$

where

$Q_1$ = heat generation caused by heat conduction, W,

A = heat transfer area, $m^2$,

λ = thermal conductivity coefficient, W/(m • K), and

dt/dx= temperature gradient.

(2) Heat convection refers to the exchanging heat of the cell surface with the surrounding cooling medium, such as water or air.

$$Q_2 = hA\Delta t\,, \qquad (6)$$

where

$Q_2$ = convection-induced heat generation, W,

h = surface heat transfer coefficient, W/(m $^2$·K),

A = surface heat transfer, $m^2$, and

△t= cell temperature difference, ºC.

## 3. Phase change materials (PCMs)

### *3.1. Classification and function of PCMs*

PCMs are capable of storing/releasing the latent heat during solidification/melting phases. Furthermore, PCMs are able to maintain a constant operation temperature given their high latent heat.

According to phase change temperature range, PCMs can be divided into high-temperature range with melting points ranging from 120ºC–850ºC and a low-temperature range from 0–120ºC. Generally, solar power generation, low-temperature engines, and low-power electricity stations perform at higher temperatures. While the latter is normally used in recycling waste heat recovery, solar energy storage and battery thermal management fields. PCMs are categorized into four groups based on physical substance changes during phase transition: solid–solid PCM (SSPCM), solid–liquid PCM (SLPCM), solid–gas PCM (SGPCM), and liquid–gas PCM (LGPCM). SSPCMs possess the unique advantages of small volume change, low subcooling, non-corrosion, high thermal efficiency, long lifespan but low latent heat, and high cost. SLPCM can be observed in eutectic, organic, and inorganic forms. The explicit classifications of SLPCM are summarized in Fig. 5. At present, SSPCM and SLPCM, as heat dissipation media, are mainly applied in the BTMS area. In contrast, SGPCM and LGPCM are rarely used due to their largely varying gas production volumes. Paraffin (PA), an organic PCM, has been widely applied in the battery thermal safety field due to its appropriate melting temperature range, high

latent heat (Table 5), stable and chemically inert properties, self-nucleation, minimal super cooling effect, and cost-effective advantages.

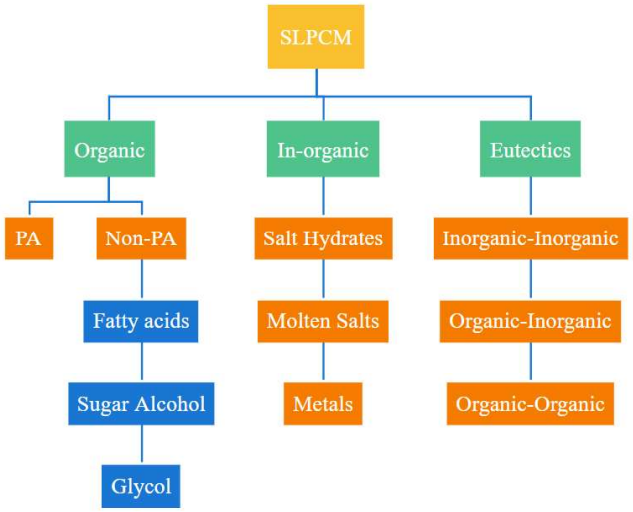


**Fig. 5.** Classification of SLPCM [36].

**Table 5**

Thermophysical properties of selected straight chain alkanes.

| Molecular formula | Molecular weight | Melting point/°C | Latent heat/J • $g^{-1}$ |
|---|---|---|---|
| $C_{16}H_{34}$ | 226 | 16.7 | 236.81 |
| $C_{17}H_{36}$ | 240 | 21.4 | 171.54 |
| $C_{18}H_{38}$ | 254 | 28.2 | 242.67 |
| $C_{19}H_{40}$ | 268 | 32.6 | - |
| $C_{20}H_{42}$ | 282 | 36.6 | 246.86 |
| $C_{21}H_{44}$ | 296 | 40.2 | 200.83 |
| $C_{22}H_{46}$ | 310 | 44.0 | 251.04 |
| $C_{23}H_{48}$ | 324 | 47.5 | 234.30 |
| $C_{24}H_{50}$ | 338 | 50.6 | 248.95 |
| $C_{25}H_{52}$ | 352 | 53.5 | - |
| $C_{26}H_{54}$ | 366 | 56.3 | 255.22 |
| $C_{27}H_{56}$ | 380 | 58.8 | 234.72 |

In terms of the energy storage efficiency, an ideal PCM normally has the following merits [54,55]: 1) suitable phase change temperature; 2) higher latent heat; 3) stable performance; 4) prominent thermal conductivity coefficient; 5) small volume expansion rate; 6) non-poisonous, non-corrosion, environmentally friendly, non-combustive, and non-explosive; and 7) low cost and excellent processability. The

application of composite PCMs, which are largely based on the power battery exterior shape, is elaborated in Fig. 6.

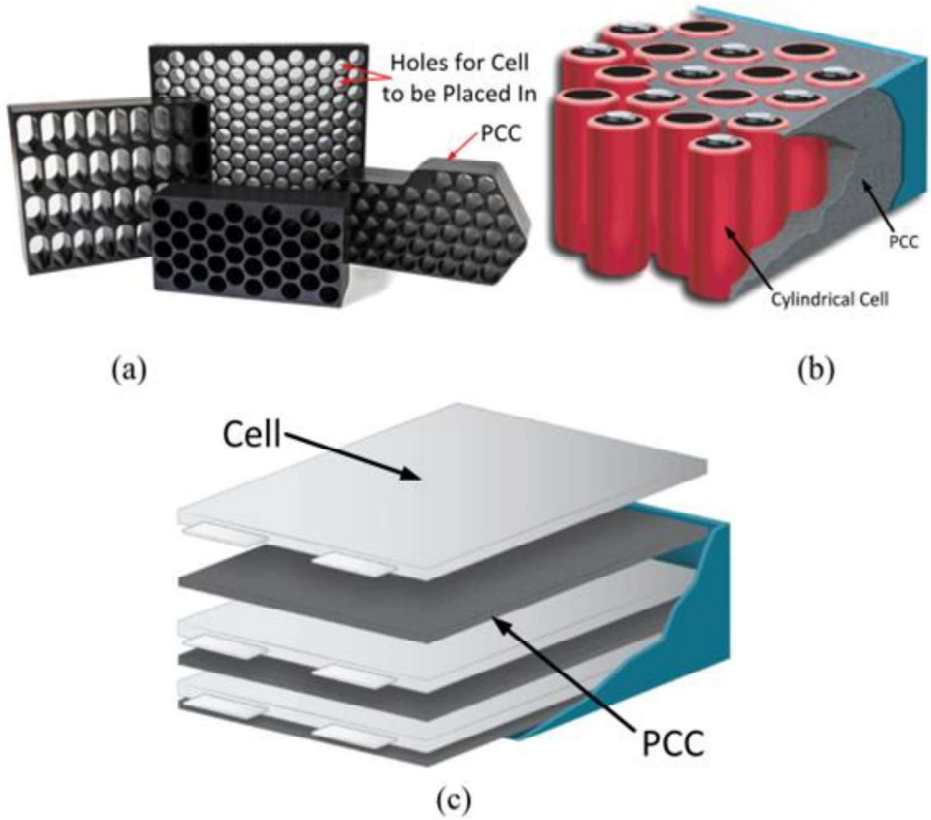


**Fig. 6.** Application forms of the composite PCMs in power systems: (a) fabricated PCM matrix; (b) PCC with cylindrical cells; and (c) PCC plates with prismatic cells [56,57].

Although remarkable latent heat and appropriate phase-changing temperature of PA, the relatively low thermal conductivity coefficient (0.1–0.3 W/m·K) will reduce the cooling efficiency and heat transfer rates, which further restricts the application of PA-based PCM in BTMS [58]. In addition to poor thermal conductivity, leakage issue in the molted form, mechanical strength, flame retardant as well as electrical insulation performances are very essential for power lithium-ion batteries modules/packs safety considering the practical applications. The improvement of the aforementioned characteristics, which will be expounded in the following sections, is also of vital significance for the optimization of BTMS from the macro view and the research of PCM modification from the micro perspective.

### *3.2. Enhanced pivotal properties of PCM*

#### *3.2.1. Thermal conductive performance*

One drawback of PCM is the unacceptably inherent low thermal conductivity which prolongs heat storage and releasing time. To address this issue, adding the high thermally conductive additives to the base PA such as metal mesh [59,60], metal foam [61-65], metallic oxide powders [66,67], expanded graphite (EG) [68-70], carbon fiber [71-73], nanoparticles [74-76], and graphene and carbon nanotube (CNT) [77-79] is the most promising solution. Additionally, the addition of fins, such as radial fins [80] and axial fins [81], is regarded as an effective pathway to solving low thermal conductivity issues. The most commonly used fabrication approaches of preparing the above high-conductive composite PCMs, but not limited to, are shown as follows: physical mixing and dispersing, and compression methods [82,83], vacuum impregnation method [84], chemical impregnation method [85], and self-absorption method [86]. Wu et al. [87] reported on the composite PCMs preparation and thermal conductivity enhancements following a traditional physical mixing. Their experimental results presented an increased thermal conductivity from 0.268 W/(m·K) to 7.654 W/(m·K) following the addition of 20% EG. Wu et al. [88] employed mechanical compression methods to produce copper mesh (CM)/PA/EG composite PCMs for a rectangular $LiFePO_4$ power battery pack (16 V/12 Ah) BTMS (Fig. 7). Their results exhibited a thermal conductivity coefficient of 7.65 W/(m·K), which was 30-fold that of pure PA (0.26 W/(m·K)), indicating a lower discharge temperature rising rate and faster rest temperature difference-decreasing rate. Zhang et al. [89] applied aluminium nitride (AlN) as the high thermal conductive additive via traditional physical mixing and dispersive techniques to produce PA/EG/epoxy resin composite PCMs (Fig. 8). These modules (3.2 V/33 Ah) were comprised of 30 18650-type $LiFePO_4$ cells, which exhibited increased thermal conductivity coefficients from 0.2 W/(m·K) for pure PA to 4.331 $W \cdot m^{-1} \cdot K^{-1}$ for the composite, suggesting enhanced heat conduction performance. Sheng et al. [90] examined

PA-based composite PCM-strengthened honeycomb carbon fibers, which enhanced their thermal energy storage using vacuum impregnation technology. As shown in Fig. 9, the carbon scaffolds, composite PCMs preparatory methods and detailed optical sample images were described. The composite PCMs exhibited a high thermal conductivity of 1.73 W/(m·K) at a carbon filler content of 12.8% as well as good shape stability. Cao et al. [91] reported on enhanced PCM performance via three-dimensional (3D) printing with prickly honeycomb carbon fibers for improved rectangular ternary lithium-ion battery thermal management. The composite were prepared through mechanical hot compression technique (Fig. 10), and the thermal conductive property came to the highest value of 5.723 W/(m·K). Arshad et al. [92] studied the thermal conductivity changing rules of metallic-oxide ($TiO_2$, $Al_2O_3$ and CuO)-based mono and hybrid nanocomposite PA-based PCMs for thermal management systems by conventional mixing and stirring method. According to the results, the thermal conductive performance was largely temperature-dependent and the samples with $Al_2O_3$ and CuO hybrid additives exhibited a thermal conductivity of 0.48 W/(m·K) at 35ºC. Heyhat et al. [93] examined the battery thermal management of a 18650 lithium-ion cell with thermal energy storage composites of PCM, metal foam, fins, and nanoparticles (Fig. 11). According to the results, a porous-PCM composition exhibited the highest heat transfer effect compared with the nano-PCM and fin-PCM samples, exhibiting a 4ºC–6ºC battery mean temperature reduction compared with pure PCM. Qu et al. [94] reported on the thermal conductivity of PA-based shape-stabilized PCM with hybrid EG-multiwalled CNT (EG-MWCNT) and EG-carbon nanofiber (EG-CNF) fillers. Hybrid carbon nano (CN)-additive fillers PA-high density polyethylene (HDPE) SSPCMs exhibited increased thermal conductivities by 60% and 21.2%, respectively, compared with the single CN additive EG. In addition, the PA-HDPE/EG-MWCNT composite PCMs presented better thermal conductivity properties compared with PA-HDPE/EG-CNF. Kiani et al. [95] carried out the increased thermal conductive property analysis of copper-foam enhanced PCMs when utilized in the lithium-ion BTMS. The porous structure largely affected the conductive heat distribution, producing an effective thermal conductivity

of 11.98 W/(m·K). Similarly, Zheng et al. [96] optimized a lithium-ion BTMS by generating a fin-enhanced PCM system. Compared with finless systems, this enhanced PCM/fin system more effectively cooled the power system. Ping et al. [97] lowered the prismatic battery module surface temperature by 36.4% compared with the system with pure PCM by producing a fin-enhanced PCM cooling system. Wang et al. [98] combined PCM and fins for the enhanced cooling efficiency of the battery packs. This coupled structure was able to withstand a high heat density and extend the PCM operation time. Weng et al. [99] added a specific branch-structure fin PCM BTMS with heat transfer channels. Inspired by the $LiFePO_4$ battery module (16 V/12 Ah), Wu et al. [100] produced a rectangular stabilized PCM/EG composite plate coupling with heat pipe (HP) (Fig. 12), which enhanced the PA/EG composite thermal conductivity from 0.268 to 7.654 W/(m·K). The composite PCMs with enhanced thermal conductivity maintained higher temperature within 50ºC and lowered the temperature fluctuation under the cycling conditions. Nomura et al. [101] introduced a high thermal conductivity PCM with a metal-stabilized carbon-fiber network prepared by a hot-pressing method. The results indicated improved thermal conductivity with increasing indium volume fraction. Samimi et al. [102] investigated enhancement dependence on PA carbon fiber loading on thermal conductivity, which exhibited minimum and maximum thermal conductivity enhancements of 85% and 155%, respectively (average of 105%). The participation of high conductive promoters in PCM were expected to improve the thermal conductivity coefficient, leading to a higher heat transfer/dissipation rate. However, the addition of fillers could generally result in lowered latent heat due to lowered PA substrate mass [103,104]. For example, Li et al. [105] loaded EG and silica gel into PA to produce a composite PCM, wherein the experimental results exhibited PA, PA/EG, and PA/EG/$SiO_2$ latent heats of 275 J/g, 131.9 J/g, and 112.8 J/g, respectively. Notably, excessive additives can affect the fluidity and uniformity of the whole PCM, thereby resulting in agglomeration and significantly lowering the composite heat storage capacity and thermal conductivity properties [106]. Therefore, in the selection of additives, an appropriate mass ratio is vital for the overall performance of the composite to achieve the optimal balance

between thermal conductivity and latent heat.

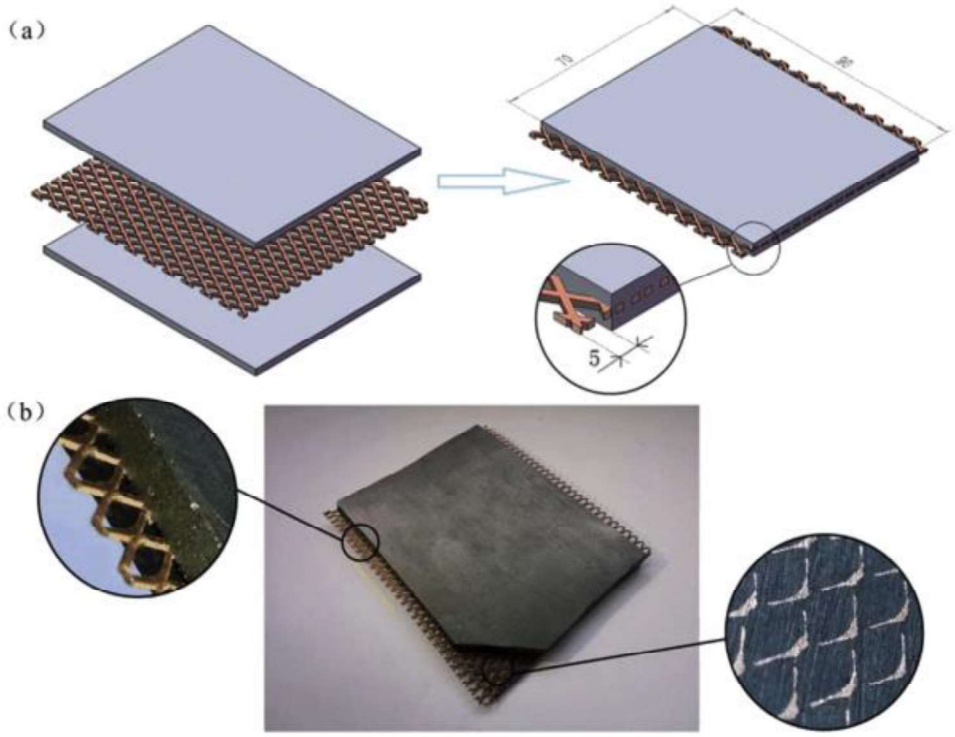


**Fig. 7.** Promoted thermal-conductive PA/EG composite PCMs [88].

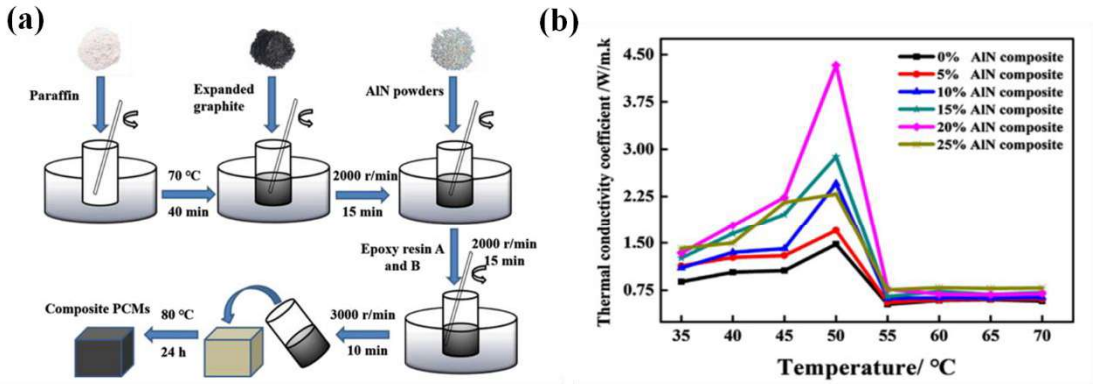


**Fig. 8.** PA/EG/epoxy resin composite PCMs with AlN as additives: (a) specific preparation process and (b) thermal conductivity property changes [89].

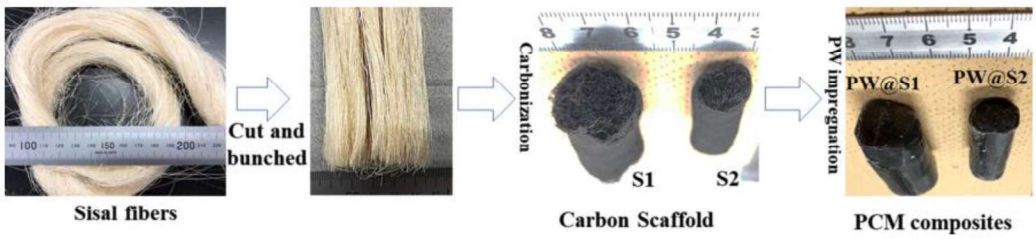


**Fig. 9.** Sisal-derived carbon scaffold and PA-based composite PCMs construction [90].

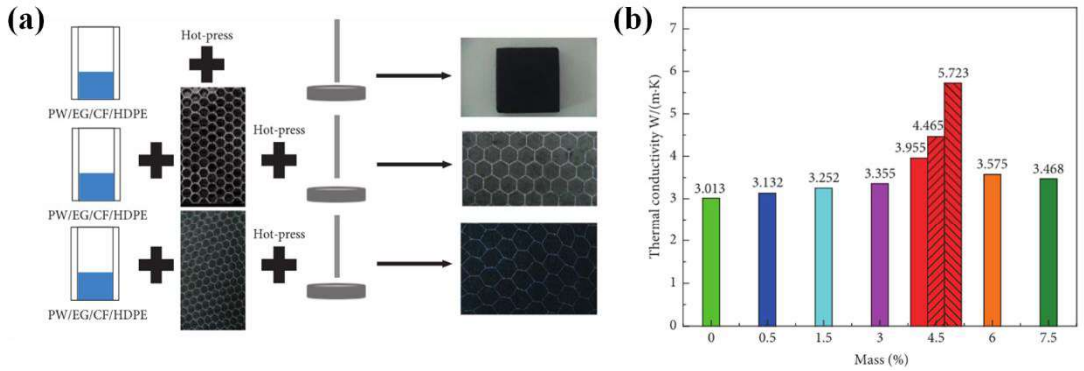


**Fig. 10.** PA/EG/carbon fiber/ HDPE composite PCMs: (a) specific preparation procedures and (b) thermal conductivity coefficient changes with different carbon fiber mass fractions [91].

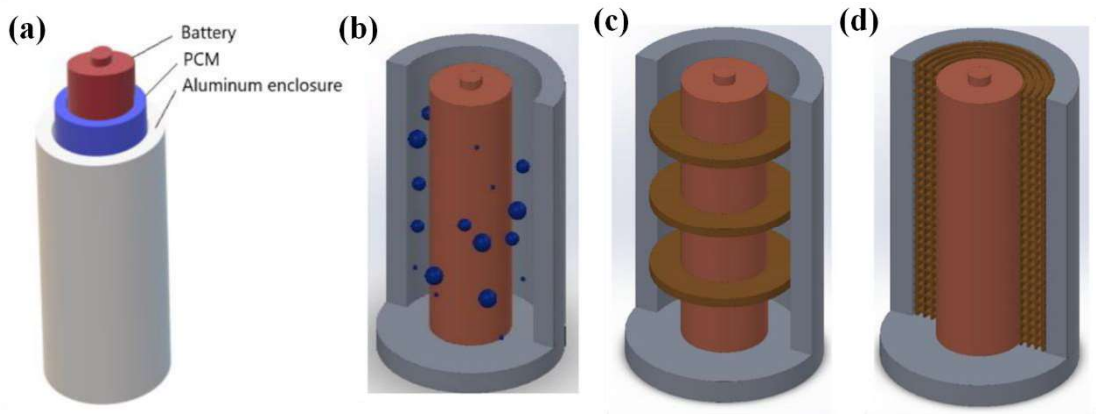


**Fig. 11.** Schematics of BTMS units with (a) pure PCM, (b) PCM/nanoparticles, (c) PCM/fins, and (d) PCM/metal foam [93].

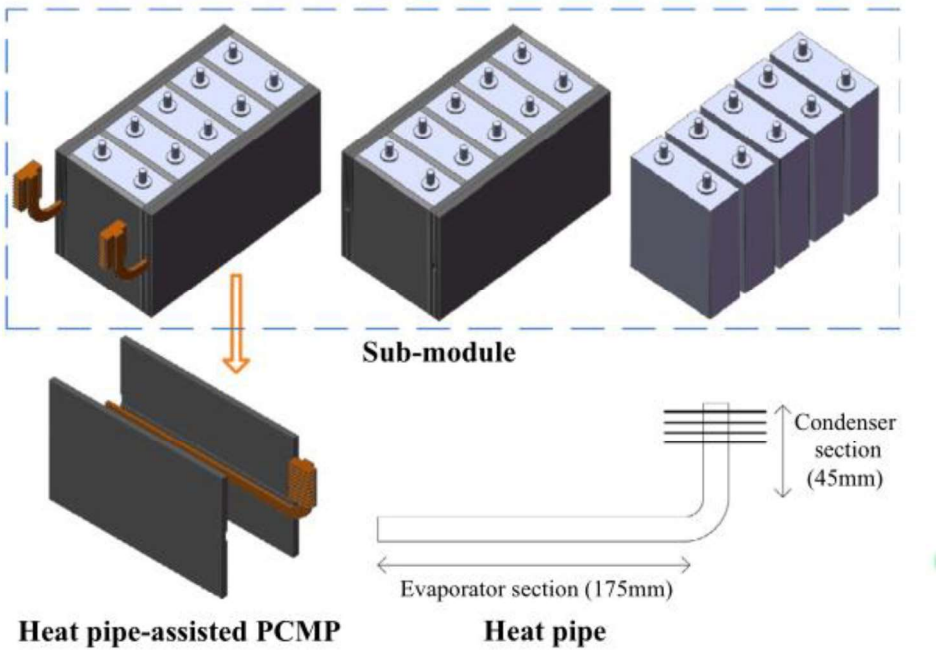

**Fig. 12.** PA/EG BTMS coupling with HP for the square batteries modules [100].

*3.2.2. Structural stability*

Regarding the PA-based PCM, much research work has been done to improve the thermal conductivity through various effective approaches. However, structural stability problems, such as the execution of long-term/harsh working EV/HEV cycles, poor mechanical properties, phase change component precipitation/leakage, and composite PCM matrix deformation (mechanical molding- or repeated melting/solidifying-induced PA/EG module cracking) (Fig. 13) [107,108] were generally ignored in practical applications, thereby severely restricting the utilization in the BTMS. Hence, the generation of a robust and strong PCM is beneficial for the BTMS. Three potential methods can be applied to address the aforementioned issues: (1) traditional packaging of closed tanks or containers; (2) shape-stabilized PCM construction, and (3) microencapsulated phase change materials (MicroPCM) (Fig. 14). The conventional solution produces a relatively complex structure that requires additional cost and weight, resulting in reduced lithium-ion battery module/pack energy density. One particular strategy, namely, the generation of specific shape-stabilized PCM with pure PA and supporting matrices, can address these issues. Shape maintenance and the leakage elimination of form-stable composite PCM during phase change periods can be achieved through the use of supporting polymer substrates such as HDPE, low-density polyethylene (LDPE) [109-111], polyethylene, and epoxy resin [112-115] as well as plastic/metallic skeletons and carbonaceous additives. In particular, Chen et al. [116] impregnated styrene-b-(ethylene-co-butylene)-b-styrene (SEBS) /PA/HDPE form-stable PCMs into metal foam to generate novel PCC for thermal energy storage. According to their experimental results, composite PCMs only exhibited 2.39% PA loss in PA from seepage after a 15 h thermal cycle test. Rao et al. [106] produced PA-based composite PCMs coupling with copper particles and copper foam, which improved the

mechanical strength. Pan et al. [117] enhanced the mechanical properties of a BTMS by applying cut copper fiber sintered with skeleton/PA composite PCMs. MicroPCM are tiny capsules with specific core-shell structure, such that the PCM core surrounded by the shell prevents PCM leakage during phase transition, finally enhancing the heat transfer area and controlling PCM volume change. At present, microencapsulated technology has been applied in organic and inorganic PCMs. In this part, the advances of the form-stable and microcapsule PA-based composite PCMs were mainly discussed.


**Fig. 13.** Structural stability problems of PCM matrix during preparation and testing.

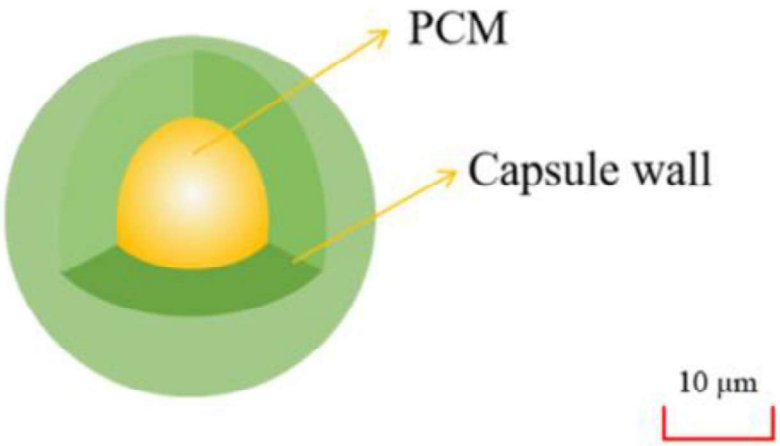


**Fig. 14.** Schematic diagram of MicroPCM.

Inspired by the epoxy matrix, Wang et al. [118] produced a novel-shaped stabilized PA/EG composite PCM (Fig. 15), which produced uniformly distributed PA in the polymer matrices without any leakage due to the flexible encapsulated scaffold

structure and highly tight network morphology caused by epoxy resin. Lv et al. [119] developed a PA/EG composite PCM with LDPE-enhanced coupled with low fins for a hybrid BTMS. The results indicated enhanced mechanical properties, less melted PA, and lowered PCM leakage following the introduction of LDPE. The composite PCM exhibited an improved bending strength, impact strength, and shore hardness that were 15.4-, 1.1-, and 3.5-fold higher than those of PA/EG, respectively (Fig. 16). According to Zhang et al. [120], enhanced AlN power was observed with PA/EG/epoxy resin composite PCMs. The 20 wt% AlN-enhanced composite PCMs exhibited an increased tensile strength, bending strength, and shock strength of 164.2%, 67.6%, and 38.1%, respectively. In addition, 4.59% lower precipitation rates were observed (Fig. 17). Similarly, Lv et al. [110] enhanced the battery thermal management by producing novel nanosilica-enhanced PCM with anti-leakage and anti-volume-changes advantages. Their nanosilica pores were able to readily absorb liquid PA, thus lowering composite PCM module PA leakage, inhomogeneity, and volume changes. Grosu et al. [121] reported that hierarchical macro-nanoporous metals were able to minimize leakage for high-thermal conductivity shape-stabilized PCM in BTMS. According to the results, the hierarchical trimodal macro-nanoporous metal (copper) exhibited superior antileakage due to enhanced nanopore capillary forces. With respect to the MicroPCM, Liu et al. [122] prepared and characterized sodium thiosulfate pentahydrate/silica MicroPCM for thermal energy storage. The testing data demonstrated a maximum MicroPCM encapsulation ratio of 94.65%, showing great potential for use in thermal energy storage applications. Tao et al. [123] developed a composite PCMs possessing a dual-level packaging structure (Fig. 18). PCM shape-stability was a result of its dual-level packaging design given the porosity of graphite and epoxy resin. As such, Xiao et al. [124] enhanced the battery thermal management by customizing a SSPCM design with a cross-linked polymeric structure and ultra-high thermal stability. The results indicated the strengthened volume stability and heat tolerance (up to 250$^{o}$C) while also minimizing deformation and leakage for practical BTMS application (Fig. 19).

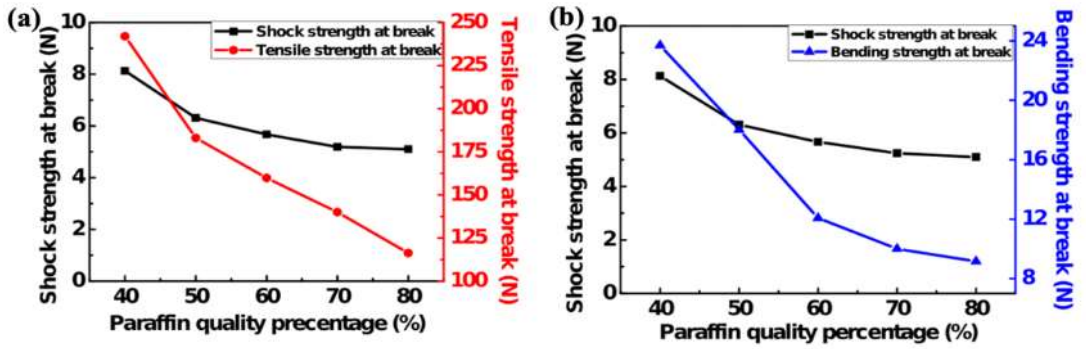


**Fig. 15.** Mechanical strengths variations: (a) shock and tensile strengths at break and (b) shock and bending strengths at break [118].

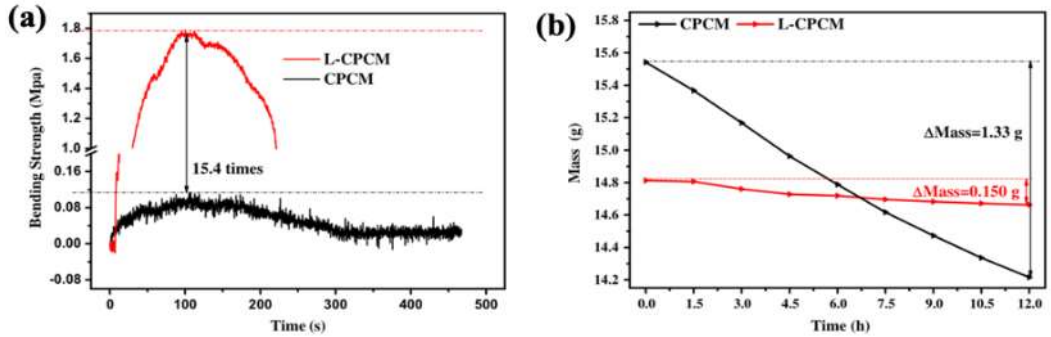


**Fig. 16.** Bending strength and leakage variations: (a) bending strength and (b) mass changes with time [119].

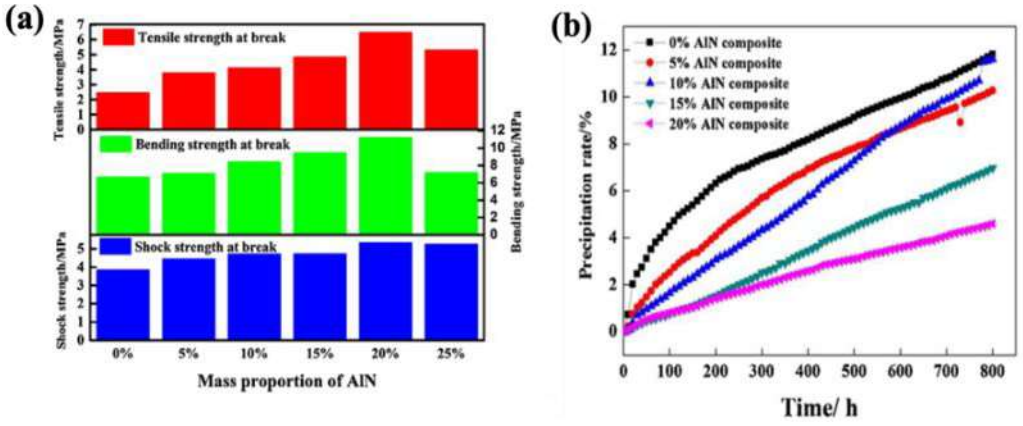


**Fig. 17.** Mechanical strength variations of different proportions of AlN powders in PCC: (a) tensile, bending strength, and shock strength at break and (b) leakage rate changes with testing time [120].

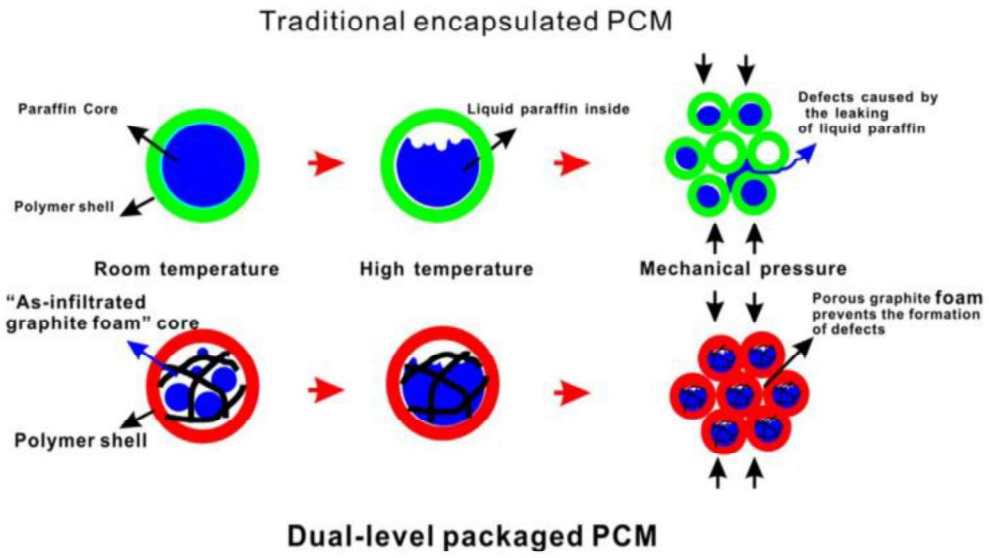


**Fig. 18.** Structure schematic of dual-level packaged PCMs at higher temperatures [123].

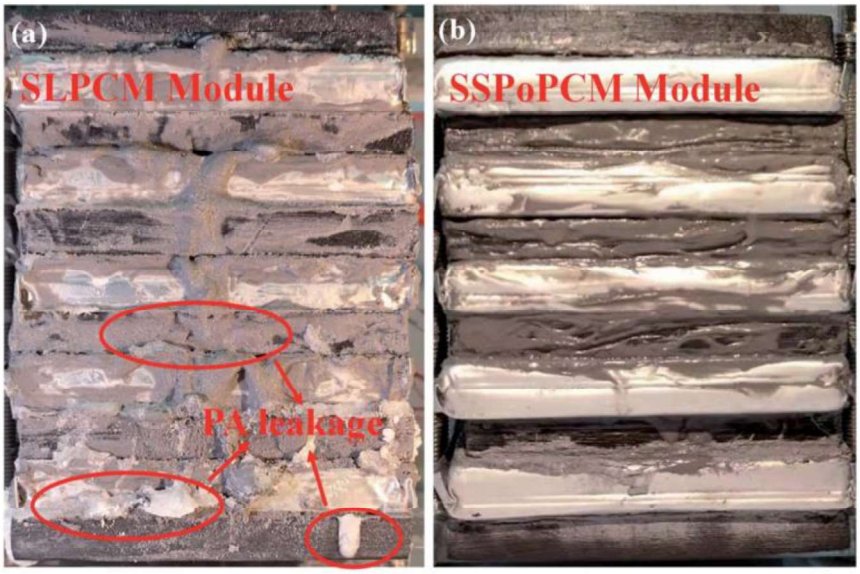


**Fig. 19.** Digital photographs of the PCC: (a) SLPCM and (b) solid-solid polymer PCM (SSPoPCM) modules after cycling [124].

### *3.2.3. Flame retardant property*

Based on the above analysis in Section 3.2.2, the development of form-stable composite PCMs can inevitably enhance the mechanical strength and relieve any leakage phenomenon. However, composite PCMs combining pure PA with polymeric substrate are inflammable at higher temperatures given their particular chemical compositions. Having an overall power system, especially for EVs/HEVs, with flame retardant PA-based composite PCM is essential for thermal safety. As such,

minimizing flammability can be achieved by incorporating PCM with flame retardant additives or insulating flame retardant interface materials. Particularly, halogen-free flame retardants are widely employed to address life safety and environmental pollution concerns. The methods to increase the flame retardant property of PA-based composite were systematically summarized in the section. Previous literature on PA-based MicroPCMs and form-stabilized (FS) products for thermal energy storage are presented in Table 6 [125].

**Table 6**

Literature reviews on fire-retardant PCC applications

| PCM | Type | Form/shell | Fire retardant | Result | Reference |
|---|---|---|---|---|---|
| PA | MicroPCM | Gelatin and Na-alginate | Clay-nano particle shell material, introduced during microencapsulation | Ignition time of treated textile increased by 25%–50 % | [126] |
| PA | MicroPCM | Polymetacrylic acid-*co*-ethyl methacrylate | PCM-diethyl ethylphosphonate (DEEP), introduced during microencapsulation | 6–9% increase in treated foam limiting oxygen index (LOI) | [127] |
| PA or fatty acid | MicroPCM | Melamine-formaldehyde resin, gelatin, polyurea, polyurethane, urea-formaldehyde resin, and combinations | Boric acid, sodium carbonate, and sodium silicate applied on the surface of the microcapsule after microencapsulation | NA | [128] |
| PA | FS | HDPE | Nine $Mg(OH)_2$, $Al(OH)_3$, ammonium polyphosphate (APP), PER, and EG formulations | NA | [129] |

| | | | | | |
|---|---|---|---|---|---|
| PA | FS-PCM | HDPE | 15-20-25 APP+PER+melamine (2:1:1) wt%; EG | NA | [130] |
| PA | FS-PCM | HDPE | APP, PER, Fe | 40%–56% lower heat release rate (HRR) | [131] |
| PA | FS-PCM | HDPE | APP, EG, zinc borate | HRR decreased by 60% | [132] |
| PA | FS-PCM | HDPE | APP, EG, zinc borate | HRR decreased by 60%–68% | [133] |
| *n*-Octadecane | Nano encapsulated | Melamine-formaldehyde | Phosphorus–nitrogen containing diamine (PNDA) | Peak heat release rate (PHRR) decreased by 32.8%<br>Total heat release (THR) decreased by 30.3%<br>Total smoke rate (TSR) decreased by 18.6% | [134] |
| *n*-Octadecane | Nano encapsulated | Poly(methylmethacrylate) | Diethyl bis(2-hydroxyethyl acrylate)amino methylphosphonate | pHRR decreased by 39.7% | [135] |

| | | | | | |
|---|---|---|---|---|---|
| | | | | Total heat release (THR) decreased by 18.4%<br>TSR decreased by 12.2%<br>LOI increased from 19.5% to 25.1% | |
| PA | Shape stabilized | - | Acrylic resin/EG; alkyd resin/EG; and epoxy resin/EG | pHRR decreased by 62%–84% | [136] |
| PA | Shape stabilized | HDPE and styrene-butadiene-styrene copolymer | Organomontmorillonite, EG | pHRR decreased by up to 72.7% | [137] |
| Paraffin chlorinated paraffin | FS-PCM | HDPE | EG, antimony trioxide | pHRR decreased up to ~50% | [138] |
| PA (70%) | FS-composite | Olefin block | Acrylic resin/EG, glass fibers | pHRR decreased by 58.8% | [139] |
| PA | FS-PCM | ER | PEPA-TMA | pHRR decreased by 45%, LOI reached 29.8% | [131] |

Zhang et al. [120] produced an FS flame retardant PCC comprising PA, EG, APP, red phosphorus (RP), and epoxy resin for power BTMS. The proposed composite

PCMs exhibited an APP/RP ratio of 23/10 for its optimum flame retardant performance based on macro- and micro-level investigations. Kazanci et al. [125] applied the halogen-free flame retardants ortho-phosphoric acid and pentaerythritol onto PA and a polystyrene shell to generate fire-resistant MicroPCMs (Fig. 20), which enhanced the flame retardancy and thermal energy storage. Huang et al. [139] combined modified glass fibers with FS PCM as a means to increase flame retardancy. It was indicated that the modified glass fibers could further improve the flame retardancy of PCM, thereby achieving a V-0 burning rating. Accompanied with the results of the cone calorimeter test, the PHRR of the flame retardant FS composite PCMs dropped by 58.8%. In addition, the combustion rate significantly slowed down due to the formation of modified glass fiber-induced carbon layer protection. Weng et al. [140] designed a flame-retarded aerogel felt/PCM coupling structure for the power battery module. Their experimental data demonstrated that the aerogel felt effectively inhibited the combustion flame and delaying battery TR. Ma et al. [141] improved the flame retardant curing agent PEPA-TMA by applying this to the high-performance flame retarded PA/epoxy resin FS PCM. The PCM fulfilled the UL 94 V-0 test requirements at an intumescent flame retardant (IFR) loading of 24 wt%, which enhanced the charring capacity and flame retardancy. Li et al. [142] applied a char forming agent (CFA) and the flame retardant APP to mixed PA/polypropylene (PP) PCMs. The combination of the CFA and APP largely enhanced the charring ability, such that PCM passed the UL-94 V-0 rating with an APP/CFA loading of 30%. The PCMs exhibited promoted flame retardancy given the obvious decrease in PHRR, THR, and SPR. Zhang et al. [143] investigated metal-thermal interactions as well as PA/IFR flame retardancy. According to their results, PA/IFR system exhibited a higher char yield with the metal, thereby improving the flame retarded performance and IFR flame retardant efficiency of PA. Zhang et al. [144] enhanced the IFR flame retardant efficiency through the generation of a flame retardant shape-stabilized PCM that was composed of PA, HDPE, EG, and IFR, as evinced by their presented flame retardant mechanism for PCM. Zhang et al. [145] examined the dependence of the chlorinated

paraffin (CP) and antimony trioxide (AT) thermal properties on EG, to which the results indicated more high-temperature PA/HDPE/CP/AT hybrid char residue, indicating improved CP/AT flame retardant efficiency following EG participation. Song et al. [146] prepared and examined EPDM-, PA-, nano-magnesium hydroxide-, and RP-based flame retardants form stable PCMs. Their results showed that the addition of nano-MH and RP increased the amount of char residuals at 700°C, thereby improving the flame retarding property. The thermal safety of power system was significantly dependent on the flame retarded PA-based composite PCM. However, focus has been placed on PA-based PCM thermal conductivity enhancements instead of its structural stability and flame retardancy. Hence, in the development of PCM, these previously dismissed properties should be of concern in consideration of practical utilization .

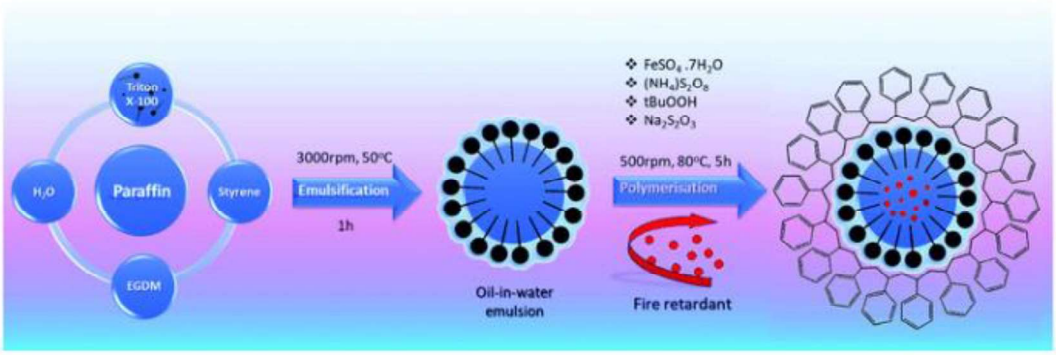


**Fig. 20.** PA-based MicroPCM production using fire-resistant additives [125].

## 4. Application of PCM in BTMS

### *4.1. Pure PCM thermal management system*

After analyzing the main property (thermal conductivity, structural stability, and flame retardancy) promotion methods of PCMs in Chapter 3, the application of enhanced PCMs in BTMSs and thermal safety will be summarized in this section. In general, the BTMS undergoes the PCM cooling method given its low cost, simplicity, and high cooling efficiency. The PCM-based BTMS has been increasingly used due to

its distinguished abilities to control the temperature and stretch the temperature distribution without the need for additional energy (passive cooling). For example, Karimi et al. [147] reported on the cooling performance of a typical cylindrical lithium-ion battery that was enhanced by applying PA-based PCM composites with a metal matrix and nanoparticles, wherein significant maximum temperature reductions of up to 70% were observed. Similarly, Kizilel et al. [148] investigated the BTMS cooling performance with PA/EG composite PCMs within the lithium-ion battery module, to which the results performed a constant maximum temperature around 45°C. The PCM pack exhibited a lowered capacity recession rate of 50% even at an ambient temperature of 45°C and a discharge rate of 2.08C-high rate (10 A). In addition, the above-mentioned design produced a lower compact pack volume for the enhanced complex cooling system, which in turn lowered the total large power weight for application, thus enhancing the lithium-ion pack energy density. Wang et al. [149] amended the typical 18650 battery module with three types of PCMs, namely, PCM 1 (pure PA), PCM 2 (EG 20%, PA 80%), and PCM 3 (EG 3%, ER 47%, PA 50%) (Fig. 21). According to the experimental results, the module for PCM 2 showed its peak temperature at 1C, 3C, and 5C discharge rates, which respectively decreased by 10%, 12%, and 20%, respectively. The PCM 3-based battery module exhibited an 8.36% lower maximum temperature as compared to that with PCM 2 following 30 continuous charging–discharging cycles. Wang et al. [150] reported on enhanced power cell cooling performances, specifically 26650, 42110, and square cells, following the application of copper foam (CF) onto PCM compared with those only using pure air cooling. The results suggested improvements in temperature-controlling capacity, wherein the peak temperature of the 26650, 42110, and square battery of CF/PCM-BTMS was well-maintained below 44.37ºC, 51.45ºC, and 50.69ºC for periods longer than those using pure PCM or air. Hussain et al. [65] produced nickel foam-PA composite, which significantly lowered the PCM surface temperature. In particular, a 31% and 24% temperature reduction were observed at a discharge rate of 2C compared with using natural air convection and pure PCM. Khateeb et al. [151] employed an aluminum foam-PCM composite onto a 13.2 Ah battery pack, which

exhibited a 5ºC lower temperature compared with pure PCM. In comparison, Wang et al. [152] reported on the 11.7ºC lower battery surface temperature at a discharge rate of 2C following the utilization of aluminum foam-PA composites. Zhang et al. [153] maintained the temperature of a cylindrical 42110-type lithium-ion battery module (36 V/20 Ah) by applying a PA-based PCM composite matrix coupled with CF (Fig. 22). The results indicated significant improvements in the thermal conductivity, which in turn maintained the module peak temperature and maximum temperature difference to be 50ºC and within 3ºC, respectively. Li et al. [154] applied CF-PCM composites to characterize the 10 Ah cell surface temperature, to which 29% and 12% lower temperature was respectively observed compared with the use of air convection and pure PCM mode at a discharge rate of 1C. Qu et al. [155] employed CF-enhanced PCM to investigate the passive thermal management of square lithium-ion batteries. The experimental results presented 17ºC and 30ºC lower battery surface temperatures following the addition of PCM/CF at discharge rates of 1C and 3C, respectively. Previous studies have also reported on various PA/EG composites [156-159]. Particularly, Somasundaram et al. [156] applied a PA/EG matrix to investigate the heat dissipation performance employing a thermo-electrochemical model, which exhibited a 18ºC lower temperature at a discharge rate of 5C. Sabbah et al. [157] experimentally investigated and simulated the PCM cooling system thermal performance under harsh conditions, particularly at a 6.66C discharge rate and 40ºC, to which a 5% lower peak temperature was observed at a discharge current of 10.0 A. Ling et al. [158] investigated various PA and PCM performances through the participation of PA/EG composites with BTMS. In particular, PA offered the best battery operating temperature given its melting point of 44ºC. In addition, a constant temperature could be achieved at higher composite densities and higher EG mass fractions. Fathabadi et al. [159] utilized PA/EG composites in a passive PCM cooling system, to which their results determined that the PCM could control the maximum operation temperature below 60ºC. Samimi et al. [88] used a composite PA-based PCM with carbon fiber in the battery module, to which their experimental data indicated a reduction of 15ºC. Zhang et al. [160] carried out the relative experiment

testing of 42110-type $LiFePO_4$ battery module (48 V/10 Ah) with PA/EG composites under different ambient temperature conditions (Fig. 23). The practical loading test was also applied to battery pack consisting of four aforementioned modules, to which the results exhibited the ability to control the PCM cooling system peak temperature under 42ºC and maintain a 5ºC maximum temperature difference. The peak temperature was maintained within 50ºC even under intense pulse discharge current condition. Azizi and Sadrameli [147] reported on the high-temperature $LiFePO_4$ battery pack thermal management following the application of a PCM and aluminum wire mesh plate composite. A 19%, 21%, and 26% maximum temperature reduction was observed at discharge rates of 1C, 2C, and 3C, respectively. Wilke et al. [161] applied a composite PCM to postpone lithium-ion battery pack TR propagation, which lowered the max temperature by at least 60°C. Rao et al. [162] studied the temperature reduction and distribution in the battery pack using PA/CF. At a discharge rate of 5C and under ambient temperatures of 29ºC and 33ºC, the battery module exhibited maximum temperatures of 40.89ºC and 42.33ºC as well as local temperature differences of 3.24ºC and 4.08ºC, respectively. Moraga et al. [163] employed multiple PCM layers for the lithium-ion polymer battery module (Fig. 24). A 20.9ºC and 23.2ºC lower maximum temperature was observed following the application of two different composite PCM designs compared with the module without PCM. Nashei et al. [164] investigated a battery pack with three PCM shells with varying thermo-physical specifications, to which the results deemed the three-layer cases as optimal (lowest battery maximum temperature after 7200 s discharge) given that higher PCM thermal conductivity allowed for closer battery placement. Al-Hallaj et al. [165] produced a PCM-based system prototype for a passive cooling system for lithium-ion batteries in EVs/HEVs. The produced system could be applied in lieu of active cooling systems without the need for additional components. Similarly, Al-Hallaj et al. [166] reported on a uniform discharge temperature profile using PCM in batteries. Talluri et al. [167] enhanced a 3.7 V/16 Ah pouch cell through the addition of a PCM cooling system (Fig. 25), of which the experimental results of a single battery indicated prominent battery temperature control. Lazrak et al. [168]

designed an innovative practical BTMS based on PCM with copper dutch weave enhanced and investigated the cooling effect, to which a 5ºC lower temperature increase and enhanced distribution were observed. Rao et al. [169] numerically and experimentally examined the PCM thermal management of ageing $LiFePO_4$ power battery, wherein the results indicated that PCM with a 45ºC lower melting point effectively dissipated heat to produce a maximum temperature below 50ºC, which significantly lowered the unit temperature difference before PCM melting. Weng et al. [140] coupled aerogel felt with flame-retarded PCM to minimize TR thermal propagation (Fig. 26). PCM-EG prevented flame combustion and lowered the battery module peak temperature, whereas the aerogel felt significantly delayed the battery TR. Ouyang et al. [170] monitored the thermal failure propagation of PCM, wherein the module wrapped with PCM exhibited failure propagation behavior given the low conductivity and diffusivity of traditional PCM. Wang et al. [171] reported on the relationship of PCM and TR, the effect on cell module failure propagation for those using PA and graphene-enhanced PA, and various battery module burning behaviors. The graphene-enhanced PA module more easily propagated given the strong heat transfer between adjacent cells. In comparison, the presented PCM modules could not effectively prevent TR propagation. Wilke et al. [161] investigated single cell TR entrance via nail penetration and its effect on PCM thermal management for propagation prevention. According to the results, only packs without PCM fully propagated compared with those with PCC (Fig. 27). Although the application of traditional rigid PCM matrix/block and plates in BTMS exhibited excellent heat dissipation performance, they undoubtedly increased the weight and volume of the power system, further decreasing the energy density. Hence, considering the lightweight goal, the innovative forms of PCM, such as curved and flexible PCMs, are attracting more and more attention [172-177]. Wu et al. [175] applied olefin block copolymer (OBC), EG, and PCM highly thermally conductive and flexible PCM (Fig. 28). Furthermore, they evaluated the thermophysical properties and applied structural stability composite PCMs in the battery modules. The produced flexible composite film effectively managed the thermal performance by lowering the commercial

lithium-ion battery working temperature by at least 12ºC, even at higher discharge rates. Wu et al. [178] applied OBC, PA, and EG into thermally induced flexible PCM for innovative battery thermal management, to which the experimental results exhibited a flexible PCM-based BTMS maximum temperature of 43.4°C at a discharge rate of 2.5C, which was 28.8°C lower than that without PCM. Lower temperature fluctuation and long-term PCM latent heat were observed even under dynamic stress and charge–discharge cycles. Huang et al. [179] developed a flexible composite PCM containing styrene butadiene styrene (SBS), PA, and EG. This composite PCM was then applied to the lithium-ion polymer pouch battery module (Fig. 29) to examine the maximum temperature and temperature difference. The maximum temperature was contained below 46°C and a temperature difference within 4°C was observed during the 5C discharge process. Zhao et al. [180] tested the gradient PCMs embedded thin heat sinks, specifically the power battery pack cooling and temperature uniformity, to which a 11.2% lower maximum battery temperature and a 78.3% lower temperature standard deviation were observed at 600 s. Zhang et al. [120] monitored an 18650 ternary battery module, particularly the cooling performance of air-cooled, pure PA, and composite flame-retarded PCM with AlN (Fig. 30). The fire retardant PCMs exhibited promoted battery module cooling and temperature maintenance, leading to a 44.7% lower peak temperature and 30.1% lower maximum temperature difference within 1.36ºC at a 3C discharge rate for 25ºC. The temperature was maintained within 5ºC even at a 45ºC high-temperature condition. It is known that with the increase of energy density of lithium-ion power batteries, a single BTMS cannot meet the heat dissipation requirement. In addition, after long, uninterrupted lithium-ion battery charging–discharging cycles, the heat that is stored inside the PCM must be diffused in time through secondary heat dissipation to maintain the high transfer efficiency and robust PCM BTMS. Thus, the present research investigated the use of hybrid heat dissipation systems such as PCM/air, PCM/liquid, PCM/HP, and PCM/TE.

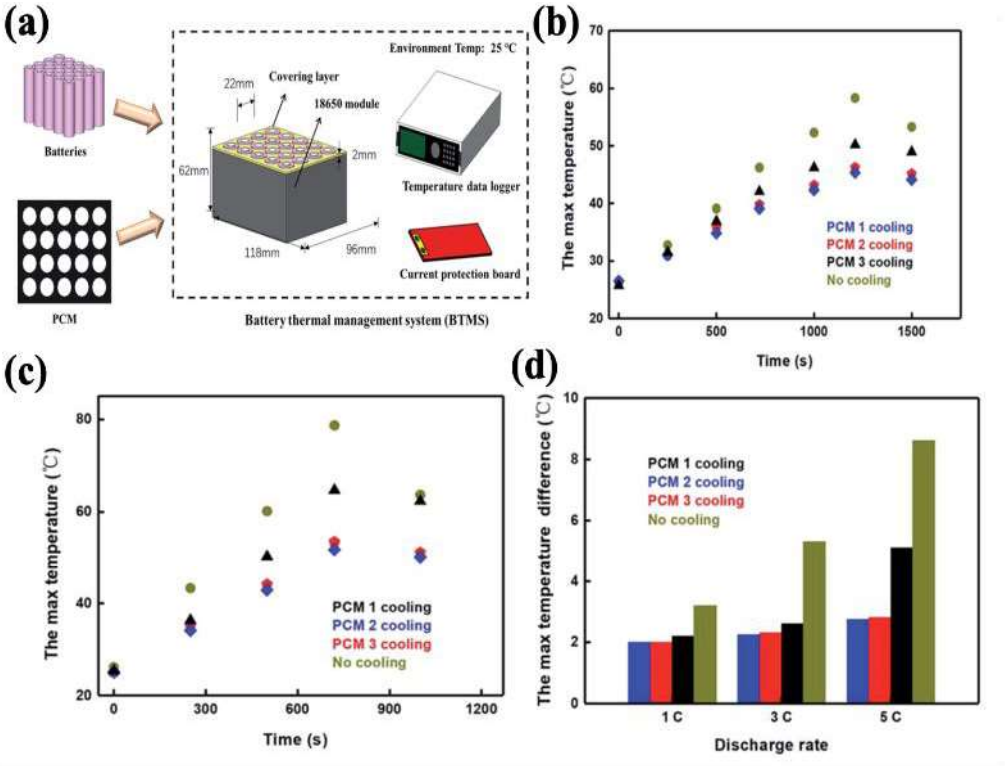


**Fig. 21.** Three kinds of composite PCMs in the 18650 cell: (a) battery module composed of selected cells and PCMs, (b) maximum temperature comparison at a discharge rate of 3.0C, (c) maximum temperature comparison at a discharge rate of 5.0C, and (d) maximum temperature difference comparison [149].

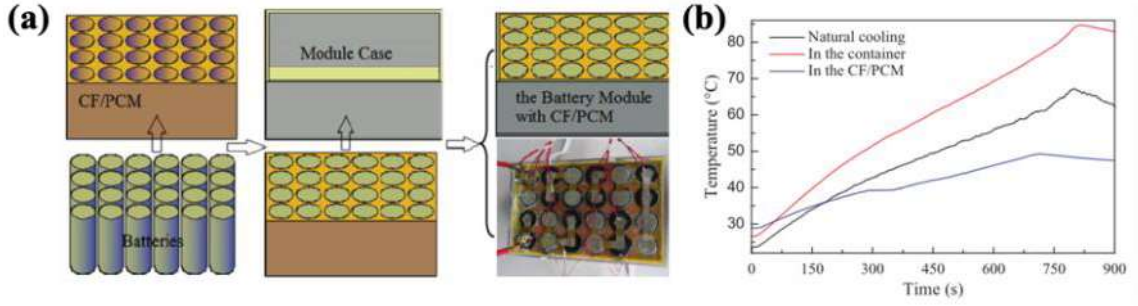


**Fig. 22.** Application of PCM/CF composites in cylindrical 42110-type battery module: (a) PCM/CF battery module and (b) comparison of maximum temperature at a 5C cell discharge with various cooling methods [153].

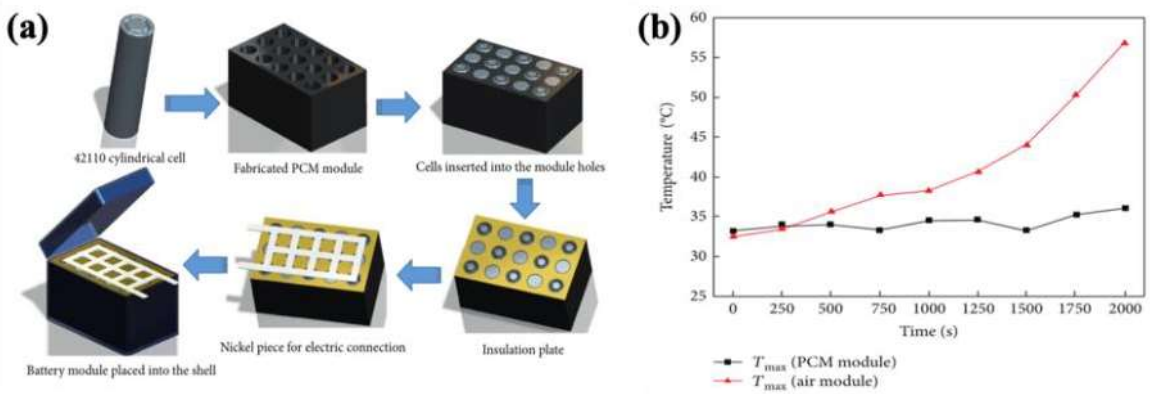


**Fig. 23.** Application of PA/EG composite in cylindrical 18650-type battery module: (a) battery module assembly schematic and (b) comparison of air-cooling module and PCM cooling module maximum temperature test data [160].

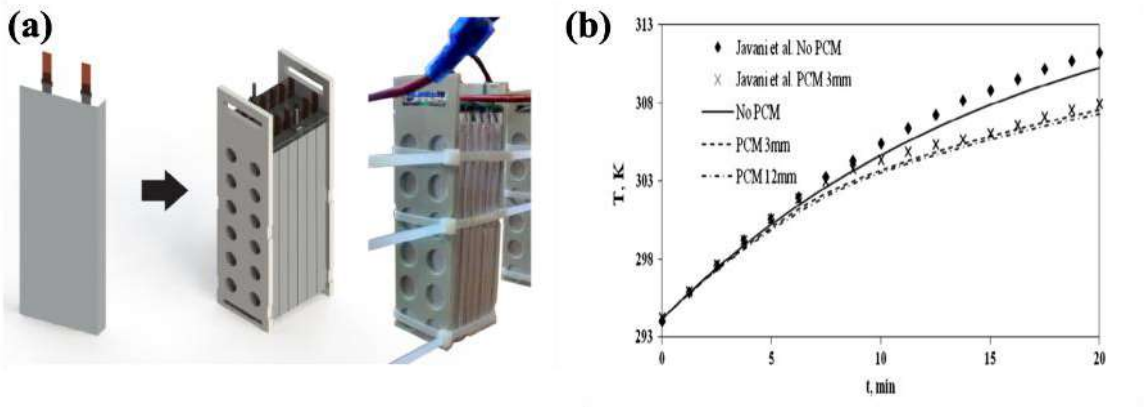


**Fig. 24.** Polymer battery module with PA/EG composite: (a) PCM assembly in battery module, and (b) transient comparison of average battery temperature with and without PCM [163].

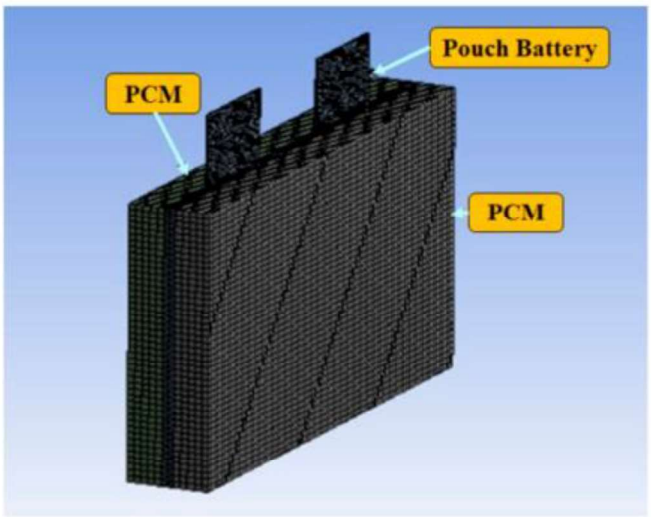


**Fig. 25.** Proposed single lithium-ion polymer pouch BTMS [167].

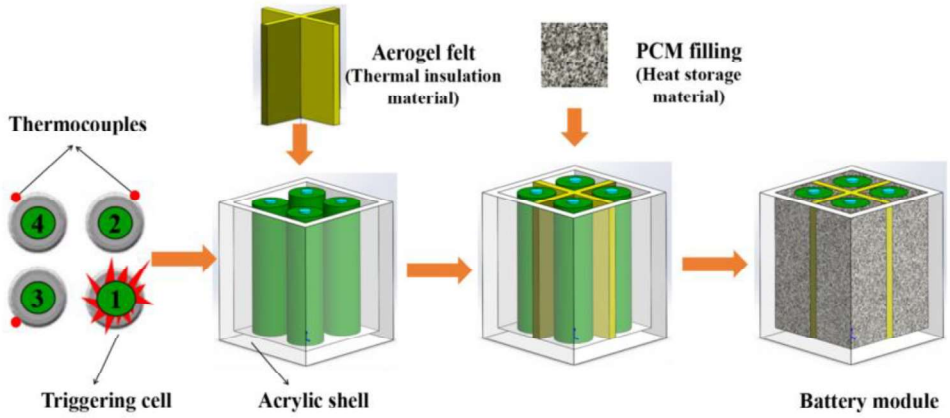


**Fig. 26.** Structure and assembly of designed flame retarded PA/aerogel felt battery module [140].

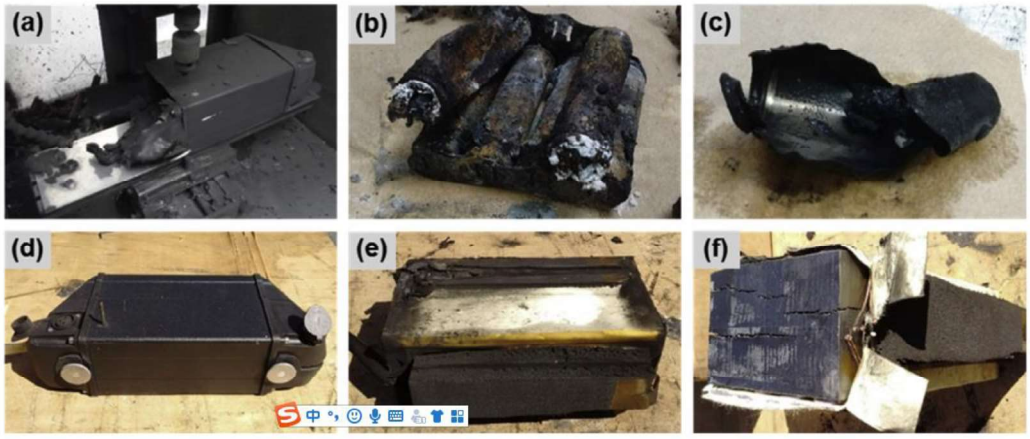


**Fig. 27.** Autopsy images: (a–c) battery pack without PCM and (d–f) battery pack with PCM [161].

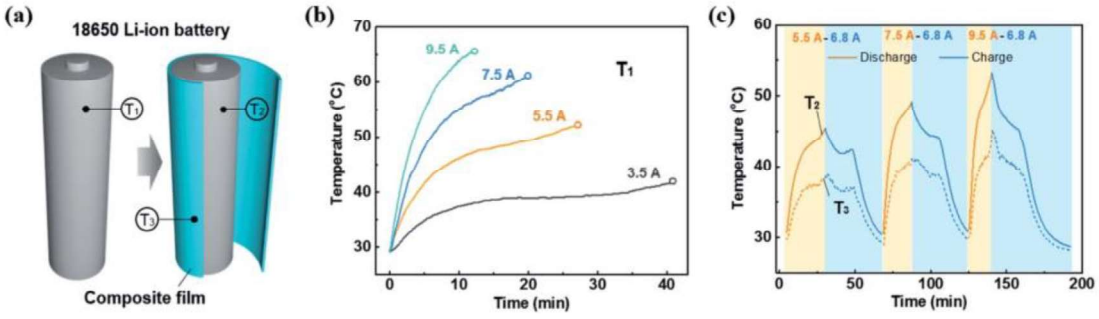


**Fig. 28.** Battery temperature management: (a) commercial 18650 lithium-ion cells with/without composite film wrapped, (b) cell surface temperature evolution at various discharging currents, and (c) temperature evolution of battery monomer wrapped with composite film [175].

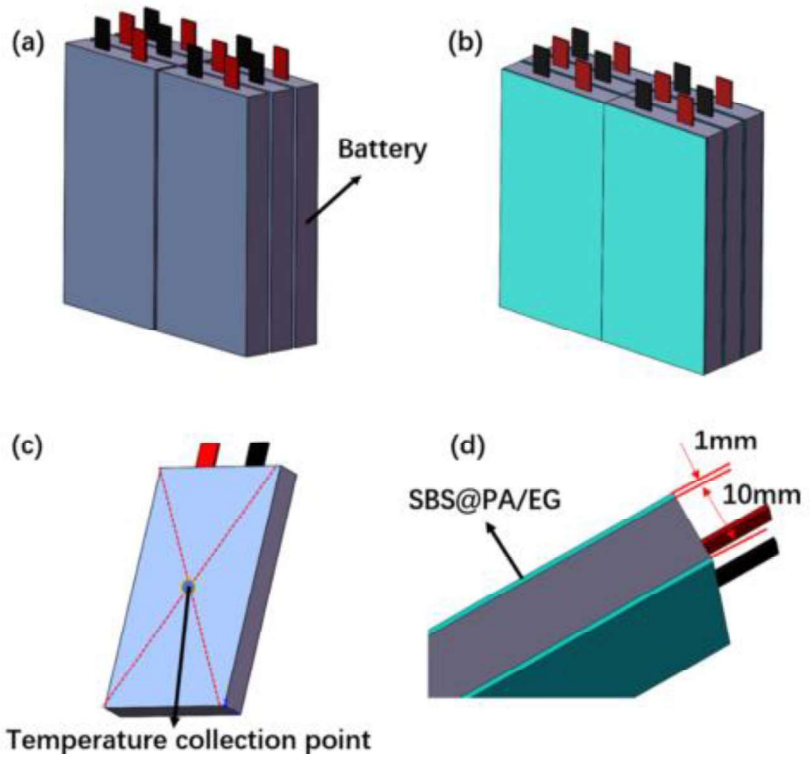


**Fig. 29.** Diagram of battery modules with flexile PCM BTMS: (a) battery module without a BTMS, (b) battery modules with flexible PCM on both sides of each monomer, (c) temperature testing point arrangement, and (d) schematic diagram of the monomer with flexible SBS/PA/EG placed [179].

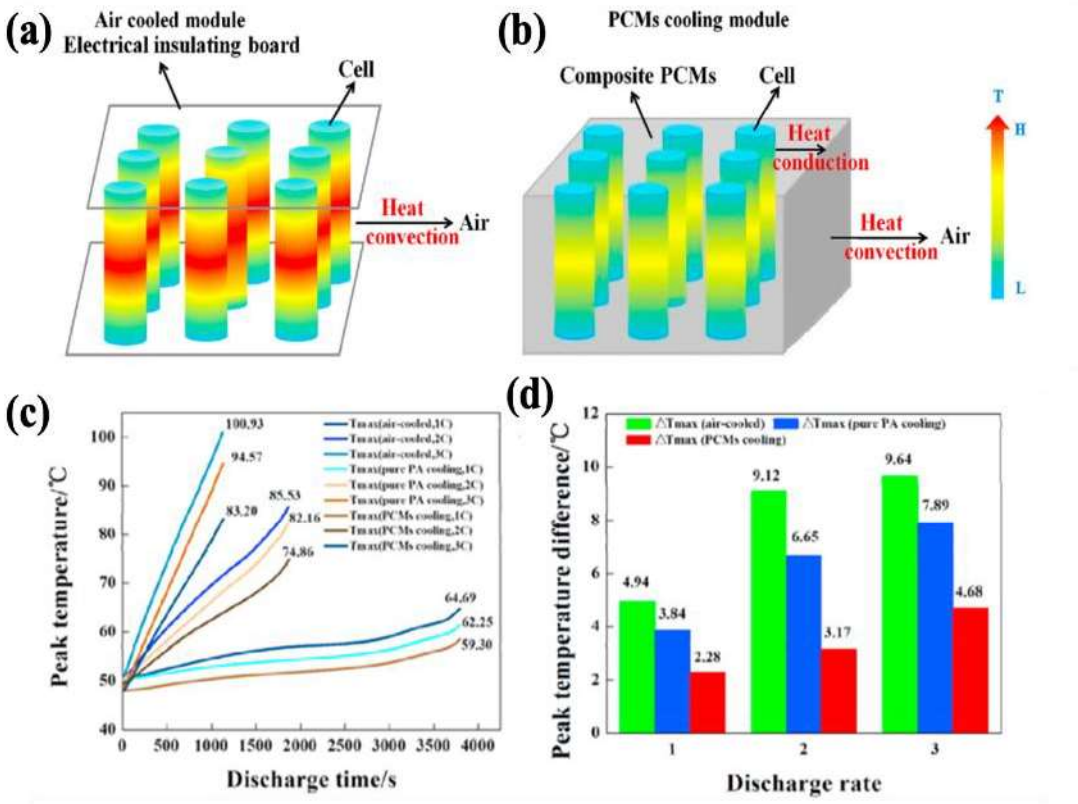


**Fig. 30.** Various BTMS cooling effects: (a) air cooling mode, (b) PCM heat dissipation mode, (c) comparison of peak temperatures (45°C) and (d) maximum temperature difference (45°C) [120].

### *4.2. Hybrid PCM thermal management system*

The available latent heat escapes following phase change, resulting in temperature regulation failure as well as subsequent BTMS failure, particularly under abusive and stressful conditions. PCM systems have high thermal energy storage capacity but lack of long-term thermal stability. As such, a secondary heat dissipation strategy must be applied to actual battery packs for heat storage capacity recovery, especially following harsh, repetitive processes. This approach enhances PCM thermal efficiency and safety, particularly in hybrid PCM systems that are coupled with traditional air cooling, liquid cooling, TE cooling, and HP cooling.

#### *4.2.1. PCM/air cooling system*

The hybrid PCM/air cooling system is regarded as the most common pathway

aiming to diffuse the heat in PCMs. Lv et al. [181] applied serpentine CPCM (S-CPCM) plates with forced air cooling to produce a PCM cooling structure, which commonly has the block-shaped CPCM (B-CPCM) (see Fig. 31). The high shape stability S-CPCM plates exhibited a higher surface area and more air flow channels as compared to the B-CPCM module, enhancing the overall secondary heat dissipation capability. The produced S-CPCM module exhibited a much lower maximum temperature compared with that of the B-CPCM module (51.9 vs. 54.2ºC) during repetitive charging–discharging cycles. Jilte et al. [182] reported on BTMS with PCM with cell-to-cell air cooling, to which the results presented constant cell temperature uniformity (within 0.05°C) at a rate of 2C and within 0.12°C at a discharge rate of 4C. The proposed cell-to-cell cooling layout exhibited a less than 5°C maximum cell temperature rise even at ambient condition and an air supply temperature of 40°C. Fathabadi et al. [159] investigated the differences in natural and forced convection of combined PCM and air cooling. The system presented a battery temperature below 60°C at an ambient temperature range of 20°C to 55°C. Ling et al. [183] examined the air- and PCM-based battery cooling strategies of a battery module with 20 cells (18650 cylindrical), to which the results preferred the combination of an air flow- and PCM-based hybrid system that employed both passive and active cooling. Qin et al. [184] reported on a hybrid BTMS integrated forced-air convection and PCM (Fig. 32), to which the results indicated controlled maximum temperature difference and maximum temperature within the proposed optimum range even at a dynamic charge/discharge current rate of 4C. Xie et al. [185] integrated PCM with air cooling and maintained a maximum temperature within 50°C during 4C charging–discharging cycles. Jiang et al. [186] produced a lithium-ion EG/PA composite battery pack with tube-shell design, in which BTMS was combined with forced air cooling and minimized cell temperature rise and maintained maximum temperature difference of 1°C–2°C. Kermani et al. [187] embedded PCM in CF for hybrid thermal management in lithium-ion batteries for forced-air convection (Fig. 33). The steady-state lithium-ion battery module surface temperature was kept below the 60°C limit even at high constant current discharge of 5 W. As such, this hybrid BTMS can be applied in

battery thermal safety operations because it simultaneously employs active and passive systems. Lu et al. [188] integrated PCM and ventilation fans in a novel personal cooling system (PCS), which effectively ameliorated the heat stress of both hot-humid and hot-dry environments. Wu et al. [88] designed a PA/EG composite plate using enhanced CM and combined this with the air-forced cooling as the secondary auxiliary heat dissipation measure in a prismatic battery pack (Fig. 34). The as-constructed CM enhanced the mechanical strength and thermal conductivity of PA/EG plate, thereby enhancing its heat dissipation performance and temperature uniformity. Additionally, the exposed copper fins from the composite aided in heat dissipation and air flow disturbance, especially with forced air convection, thereby strengthening its heat transfer capability. Shi et al. [189] examined a PCM-air-cooling integrated BTMS, to which their experimental and theoretical results indicated the complete melting of the PCM while maintaining the battery temperature at a safe range due to air cooling. Situ et al. [190] applied novel double CM-enhanced PCM plates to develop an efficient, rectangular $LiFePO_4$ battery module thermal management system. The outstretched CM of the double CM-PCM plates and air-cooling coupled system lowered the internal battery temperature while also lowering the power consumption. Lv et al. [119] added low aluminum heat dissipation fins to a PCM/air-forced cooling composite cooling strategy (Fig. 35), wherein the as-constructed PCM-based battery module exhibited prominent heat dissipation performance. This cooling system maintained the battery pack temperature of 50°C and a 5°C temperature difference at an extremely high discharge rate of 3.5C. The relative work referring to the combination of PCM and air cooling could be found in the following literature [191-194]. In short, the hybrid PCM/air cooling strategy integrated passive PCM with active air cooling, giving full play to their respective advantages. PCM, as the direct heat dissipation medium directly contacting with power batteries, possessed the outstanding capacities of controlling the temperature and stretching the temperature distribution. Additionally, air cooling with low energy consumption, simple construction, and low cost quickly diffused the heat accumulated in the PCM, further improving the utilization efficiency and service life of the PCM.

For small-scale lithium-ion battery systems with low heat dissipation requirements, PCM/air cooling can be selected as the first choice when designing the composite BTMS. Nevertheless, for large-scale power battery systems with higher cooling demand, -producing an efficient PCM-based composite BTMS using PCM or other innovative cooling techniques is of great need due to the low air thermal conductivity, which efficiently increases the energy density and thermal safety demands.

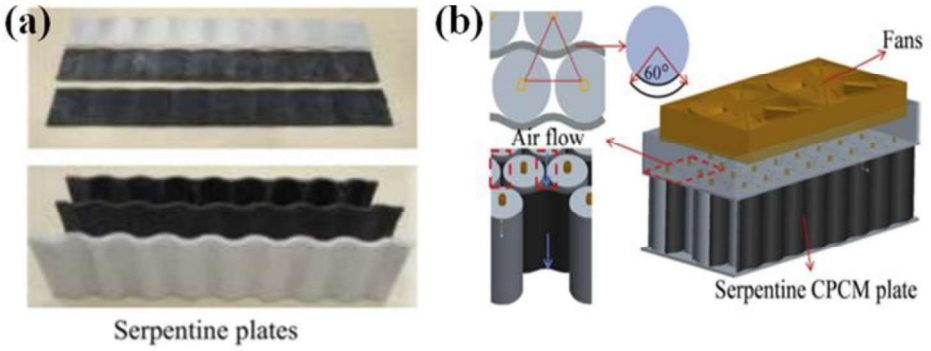


**Fig. 31.** S-CPCM coupled with forced air convection thermal management structure: (a) serpentine plates and (b) S-CPCM plates and air-forced cooling in the battery module [181].

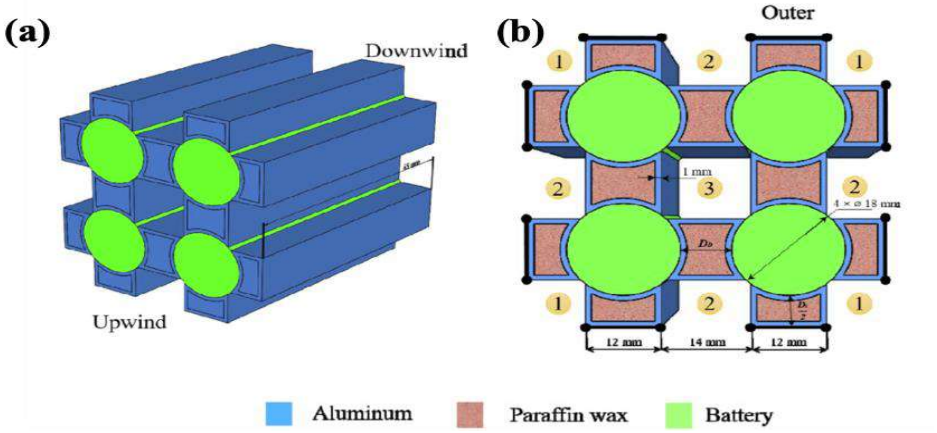


**Fig. 32.** Description of the proposed BTMS: (a) arrangement of air direction and channels and (b) top view of the introduced battery module [184].

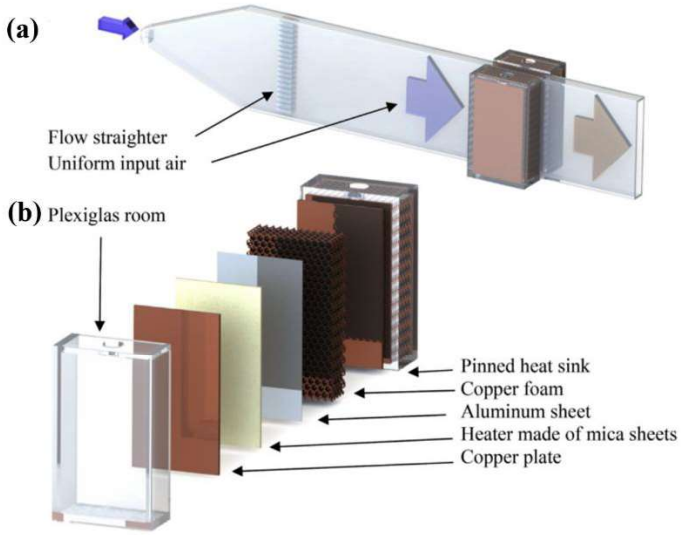


**Fig. 33.** Description of the proposed BTMS: (a) arrangement of air direction and channels and (b) composition of the battery module [187].


**Fig. 34.** Battery pack design with CM-PCM plate [88].

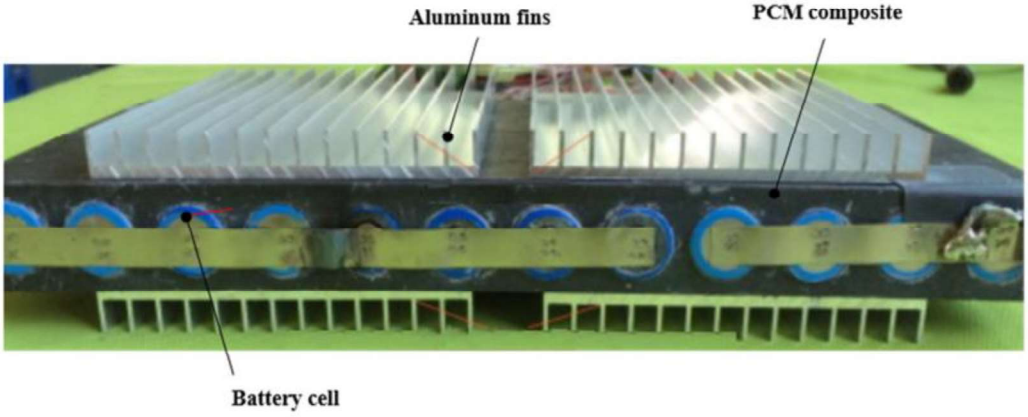


**Fig. 35.** LDPE-CPCM coupled battery pack employing PCM and air-forced cooling [119].

*4.2.2. PCM/liquid cooling system*

Generally speaking, cooling plates are the most commonly applied battery liquid cooling method, specifically the integrated PCM/liquid system, due to their flat metal plate shape with internal channels [195-198]. Zhao et al. [199] investigated liquid cooling-PCM in a battery module with 18650 lithium-ion cells, wherein the adjacent battery surfaces were largely dependent on the heat accumulation. Conjugated cooling effectively lowered the battery temperature ramp-up rate and steady-state battery temperature compared with single PCM or liquid cooling conditions. Similarly, Rao et al. [200] explored the cooling effect of PCM/mini-channel hybrid BTMS (Fig. 36) based on the water mass flow rate, phase change temperature, and PCM thermal conductivity coefficient. The novel BTMS exhibited a remarkable maximum temperature drop of 14.8°C compared with the PCM-based BTMS. Ling et al. [201] applied response surface methodology to optimize a hybrid BTMS that employed a PCM-liquid cooling strategy for lithium-ion batteries. The 20-cells module exhibited its maximum battery temperature of 37.0°C and a maximum temperature difference below 3°C during 1.5C discharge process. Hekmat et al. [202] characterized a lithium-ion battery module with PCM and cooling water pipes (Fig. 37), to which the hybrid cooling system presented a constant and lowest battery module temperature, indicating the superiority of hybrid BTMS. Hémery et al. [203] reported that a mixing BTMS, namely, a PCM and liquid cooling system, exhibited uniform temperature across the system during melting, though the wall temperature was maintained below 60°C. Bai et al. [204] applied an electrothermal model-based internal non-uniform heat source to explore the PCM/water cooling-plate thermal management of lithium-ion battery modules. The corresponding results implied the minimized TR following five continuous charging-discharging cycles. Kong et al. [205] optimized a PCM-controllable liquid cooling coupled BTMS at various ambient temperatures (Fig. 38) for commercial 21700 Li(NiMnCoAl)$O_2$ batteries, which exhibited good cooling efficiency at 30°C as well as maintained a maximum surface temperature of 41.1°C and battery pack temperature difference of 4°C after 3C discharge. Lopez et al. [206]

explored combined lithium-ion battery active (liquid heat exchanger)-passive (PCM) thermal management strategies, the results of which indicated the maximum and gradient module temperature dependence on the PCM properties and cell spacing. Song et al. [207] performed a thermal analysis to explore the conjugated cooling configurations of a battery module with PCM and liquid cooling technologies. According to the simulation results, the conjugated cooling effectively lowered both the battery temperature ramp-up rate and steady-state battery temperature compared with using single PCM or liquid cooling. Kshetrimayum et al. [208] applied an integrated PCM and micro-channel plate cooling system to characterize the heat propagation and TR of a nail-penetrated 18650-type battery module. The maximum cell temperature adjacent to the thermal abused cell was less than 363 K, which minimized TR spreading throughout all the battery cells. Cao et al. [209] experimentally and numerically explored the influence of liquid cooling-PCM hybrid thermal management system on temperature increase and temperature uniformity (Fig. 39). A higher cooling efficiency was observed from the high PCM mass fraction and cooling medium flow rate. Wu et al. [210] applied a hybrid liquid cooling- PCM system to optimize a light-weight battery module, which exhibited a 42.67% and 38.27% lowered maximum temperature and temperature difference, respectively, as compared to a single liquid-based cooling. Following optimization, the battery module temperature difference and thermal system weight were maintained at 3.7°C and 107.1 g, respectively, at a maximum temperature below 48.5°C at a 4C discharge rate. Ding et al. [211] numerically investigated a PCM/cooling plate hybrid system cooling performance under varying discharging conditions, the results of which suggested a relationship between the maximum temperature and physical PCM parameters. In particular, the maximum temperature difference was dependent a great deal on the cooling plate water flow direction. Li et al. [212] reported a PCM- and external liquid cooling-based battery module hybrid cooling system (Fig. 40), wherein double-sided liquid cooling better maintained the lowest battery temperature and within an acceptable temperature difference. In addition to the aforementioned studies, some work focused on the PCM/liquid integrated BTMS of power lithium-ion

batteries modules/packs [213-216]. In general, PCM-liquid cooling is largely employed as a mainstream development direction for EV BTMSs compared with the PCM/air-cooling method, particularly due to the cooling plate design, which is placed at the bottom of battery pack. However, Solving the leakage problem of cooling medium to prevent short circuit will eventually improve the thermal safety of the whole power system.

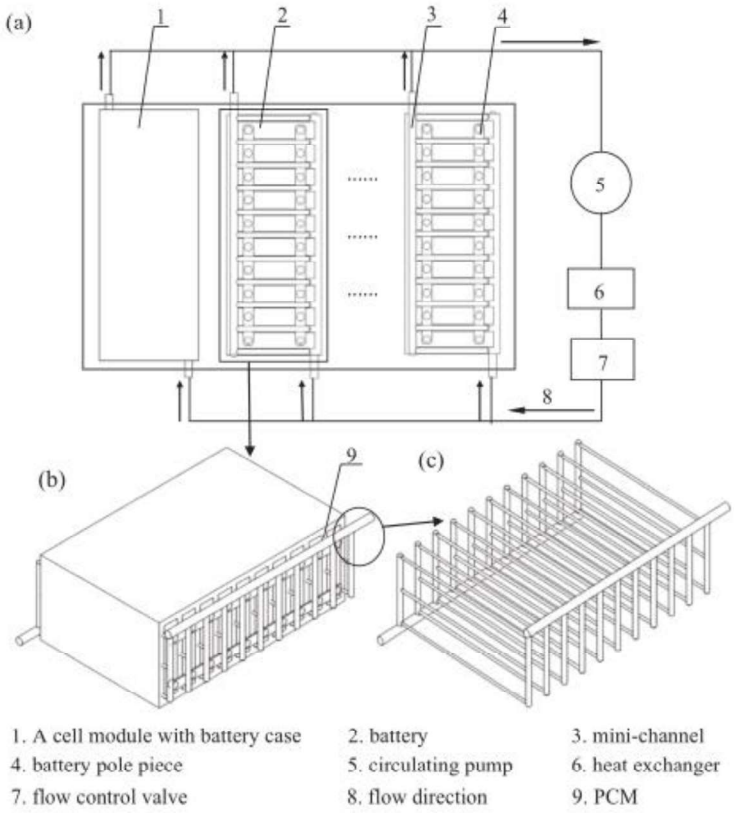


**Fig. 36.** Square lithium-ion battery pack diagram: (a) overall system, (b) a module without battery case, and (c) mini-channel structure [200].

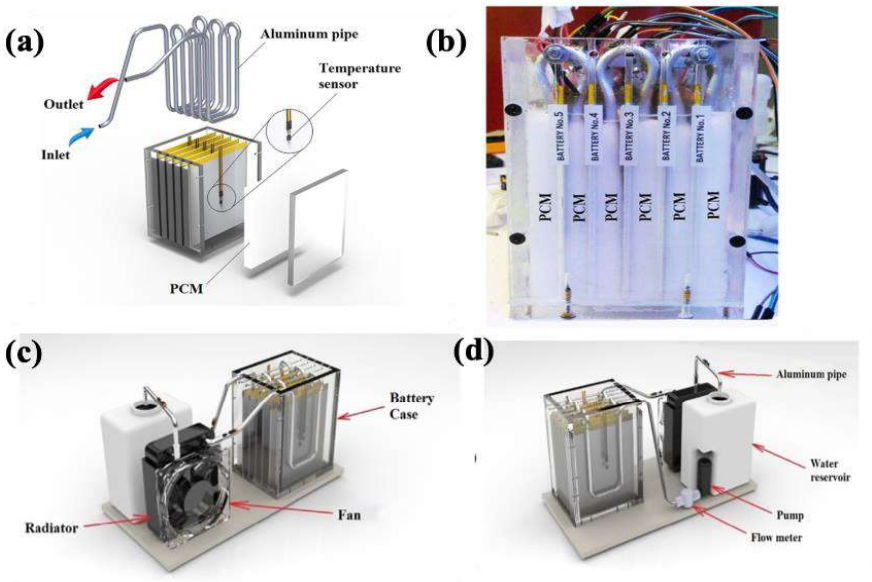


**Fig. 37.** Composite liquid/PCM cooling battery pack: (a) lithium-ion battery module and temperature sensors; (b) prismatic cells, cooling pipes, and PCM; (c) water circulation system and component frontal view; and (d) water circulation system and component back view [202].

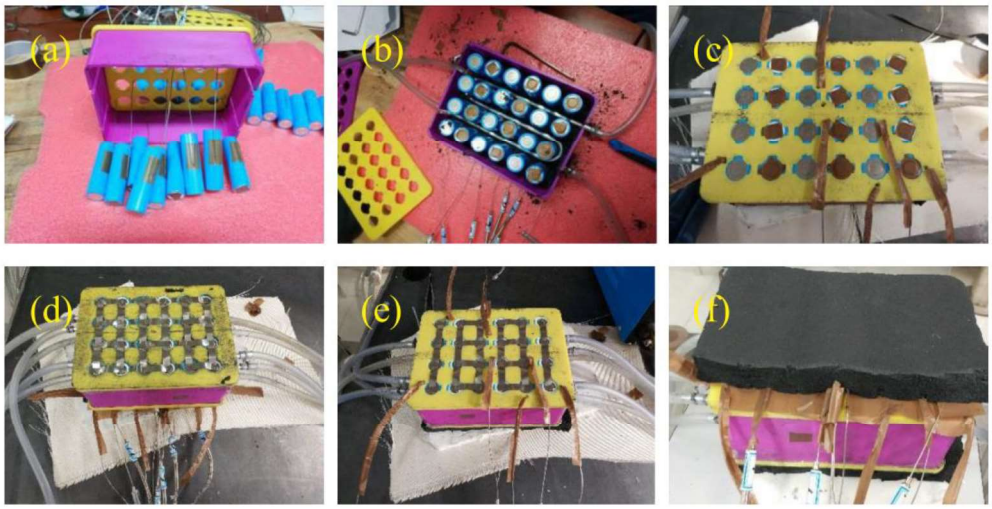


**Fig. 38.** Battery pack and coupled PCM-liquid-cooling system production [205].

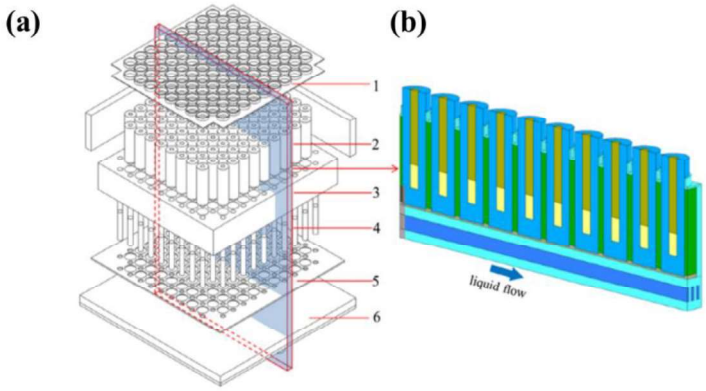

**Fig. 39.** Battery module with conjugated cooling configuration: (a) overall system: (1) heat spreading plate, (2) battery, (3) PCM, (4) thermal column, (5) insulation layer, (6) cold plate assembly, and (b) battery module numerical model [209].

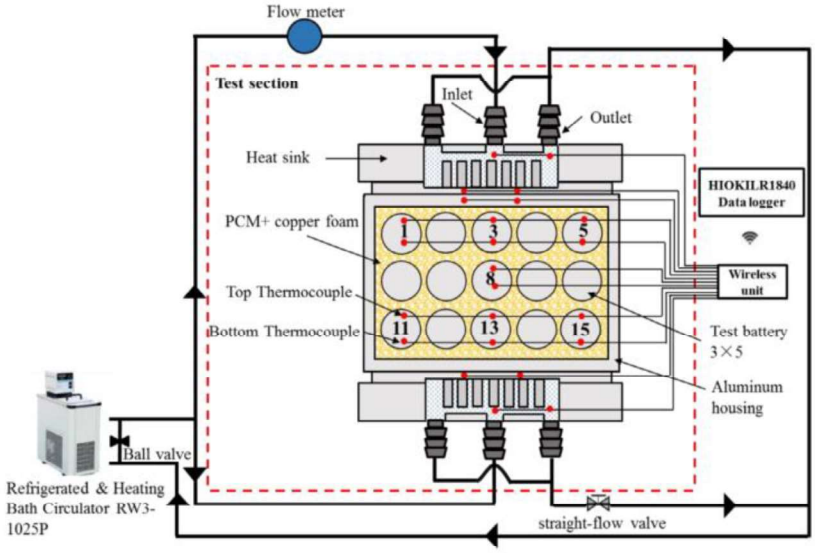


**Fig. 40.** Experimental system and thermocouple locations [212].

### *4.2.3. PCM/HP cooling system*

HPs are heat transferring devices that effectively operate without external pumped power, which allows efficient heat energy transport across longer distances due to high phase-change heat transfer speeds at all temperature differences. HPs are widely applied in thermal management systems due to their compact structure, flexible geometry, long lifetime, and low maintenance [217-219]. Finned HPs exhibit enhanced heat transfer, deeming them far superior compared with conventional bared HPs [220,221]. However, PCM-HP hybrids can exhibit low thermal conductivity and overheating issues. As such, Wu et al. [100] investigated the thermal performance of a HP-assisted PCM-based BTMS (Fig. 41), to which the highest battery temperature was maintained below 50°C at 5C discharge. Even under various cycling conditions, the aforementioned system still exhibit stable and lower temperature fluctuations. Chen et al. [222] designed a PCM/fin integrated structure for 18650-type Sanyo ternary and Sony $LiFePO_4$ (Fig. 42), and compared its cooling effect with that of air-cooled and pure PCM cooling. Undoubtedly，the PCM/fin additions maintained

the lowest temperature. Greco et al. [223] added HPs to a cylindrical cell using PA/porous-graphite-matrix graphite composite. Under similar conditions, the maximum system temperature decreased to 23.9°C compared with air-forced cooling. Wang et al. [224] characterized the thermal performance of PCM/oscillating HP (OHP)-based BTMS (Fig. 43). Compared with the single OHP-cooled and PCM/OHP-based hybrid heat dissipation strategy cooling effects, the designed hybrid BTMS efficiently cooled the system compared with that only using the HP-cooled system. Lei et al. [225] designed a PCM thermal storage-, HP-, and spray cooling-inspired lithium-ion battery thermal management approach (Fig. 44). The proposed design BTMS controlled temperature growth at an average surface temperature of 8°C at a 24 A discharging current and 40°C room temperature. The battery surfaces exhibited a maximum temperature difference below 2.6°C. Yuan et al. [226] evaluated the dependence of the lithium-ion BTMS performance enhancement on coupled PCM-HP. The designed BTMS exhibited 20°C lithium-ion battery heating at an ambient temperature below 0°C, such that the inner battery temperature difference efficiently reached 0°C. Zhao et al. [227] examined the cylindrical power battery pack PCM-HP thermal management performance (Fig. 45), wherein the developed coupled system maintained a peak temperature less than 50°C at a maximum temperature difference below 5°C for a longer period compared with air-based BTMS and PCM-based BTMS. Hata et al. [228] evaluated a PCM-HP battery-cooling system under a short-circuited condition (Fig. 46). According to the results, TR was observed at a battery temperature above 80°C, and PCM-HP maintained the lithium-ion battery temperature at about 80°C. Yanada et al. [229] applied PCM-HPs to characterize a lithium-ion battery cooling system for EVs, the results of which indicated that TR temperatures were attained after 708 s using the proposed cooling system compared with 104 s with no cooling device. Putra et al. [230] employed a passive battery cooling system that used beeswax PCM and HP (Fig. 47) for EVs, to which PCM-HP exhibited a maximal temperature decrease of 33.42°C. Chen et al. [231] applied a coupled PCM/HP cooling system on a power battery pack. Their experimental results indicated that it had positive cooling effect on the battery

pack to adopt PCM/HP coupled system, ensuring battery operations within the optimal temperature range and a more uniform temperature distribution. Zhang et al. [232] produced a HP-assisted separation type PCM-based BTMS using various current discharge rates and cycles. The proposed system exhibited a more suitable temperature and minimized temperature imbalances within the battery pack compared with other methods. Huang et al. [233] applied aluminum flat HP as the secondary heat dissipation approach of PCM-based cooling system for 18650-type battery modules (Fig. 48). Excellent temperature-control capacity was observed, the highest temperature of which was controlled at 50°C under a discharge rate of 3C with an approximately 3°C peak temperature difference. Other corresponding research studies concentrating on a PCM/HP hybrid system are reported in the literature [234-236]. The aforementioned studies confirmed the outstanding cooling efficiency, temperature-controlling, and temperature-balancing capacities of the PCM/HP composite BTMS. However, a small HP contact area and bulkiness given its evaporator and condenser sections hindered its integration, particularly with PCM. Thus, selection of the PCM/HP hybrid system is mainly dependent on the HP design scheme, which is based on the specific weight and size of the PCM mass and heat generation of the power batteries.

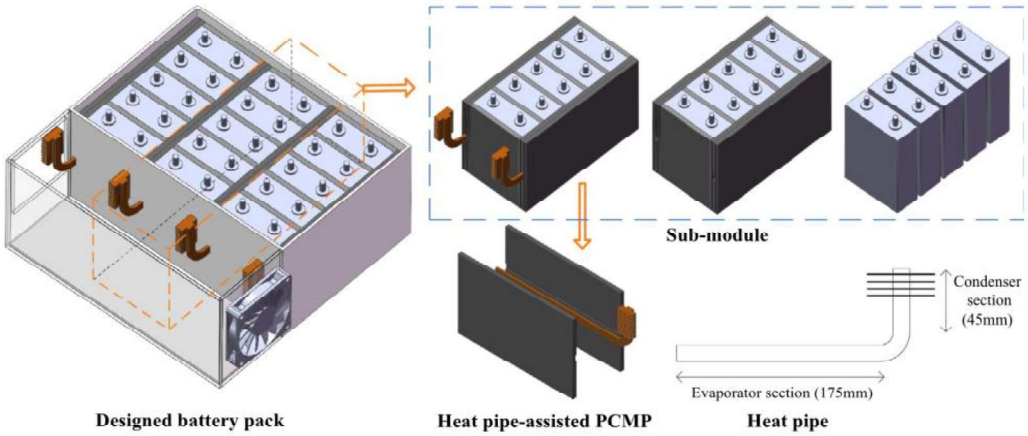


**Fig. 41.** Designed battery pack and sub-modules employing PCM/HP cooling strategies [100].

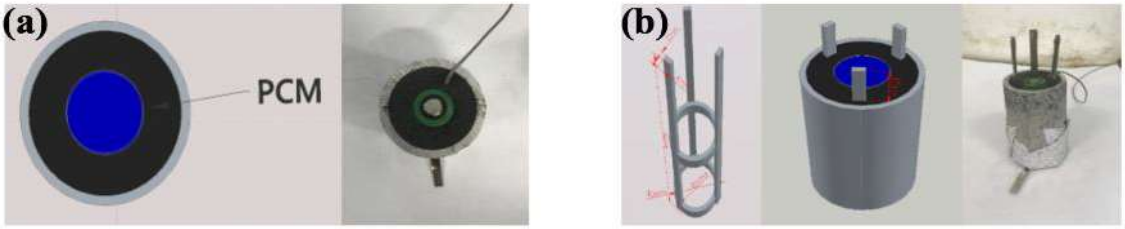


**Fig. 42.** 18650-type cell with PCM/fin structure: (a) PCM cooling and (b) heat dissipation fins and PCM-fin cooling [222].

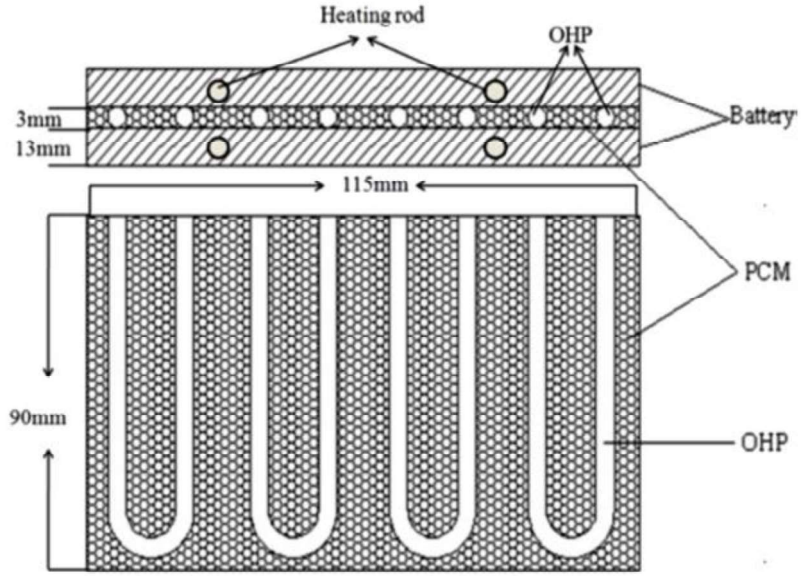


**Fig. 43.** PCM/OHP-based battery cooling system [224].

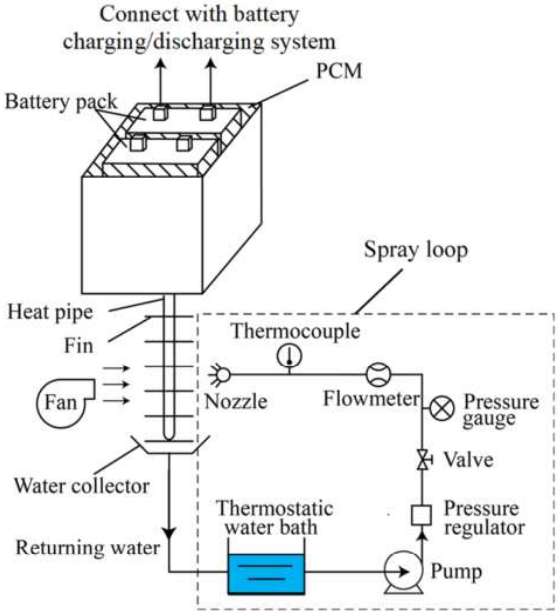


**Fig. 44.** Proposed PCM thermal storage-, HP-, and spray cooling-inspired BTMS design [225].

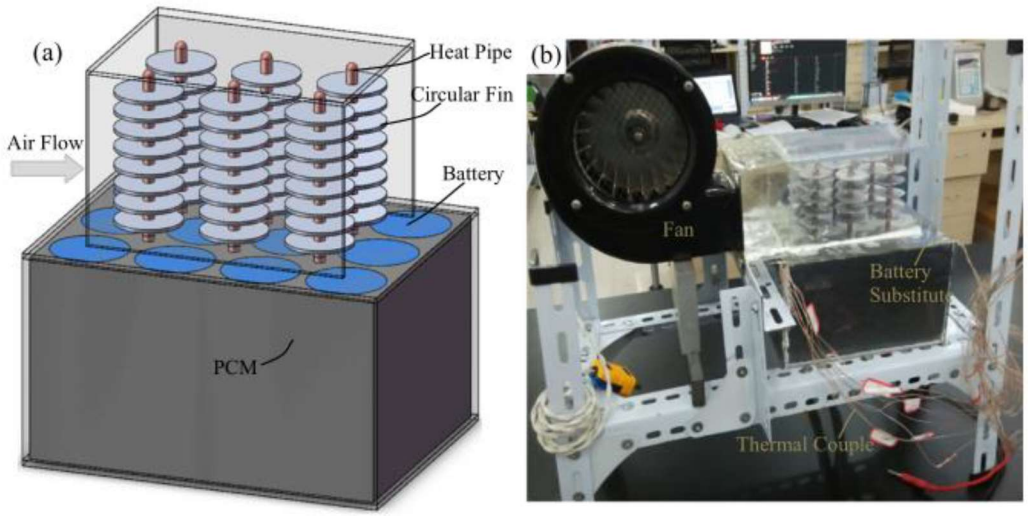


**Fig. 45.** Battery module with PCM/HP composite BTMS: (a) Designed scheme and (b) actual experimental setup [227].

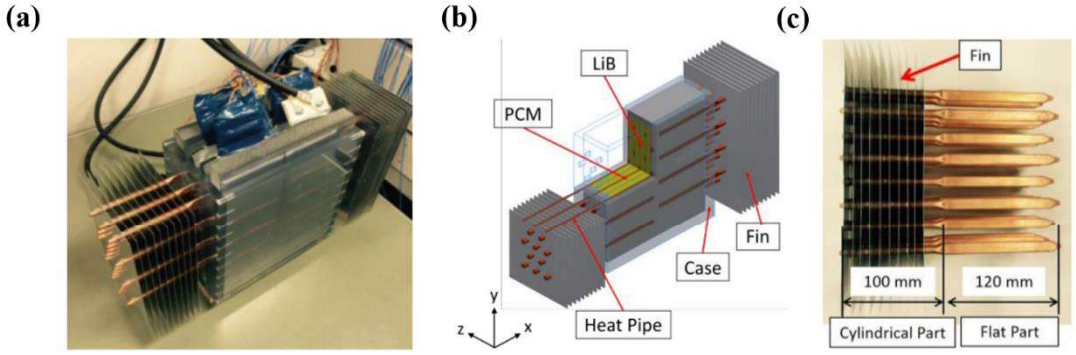


**Fig. 46.** Proposed PCM/HP hybrid cooling system: (a) overview, (b) schematic view, and (c) HPs with fins [228].

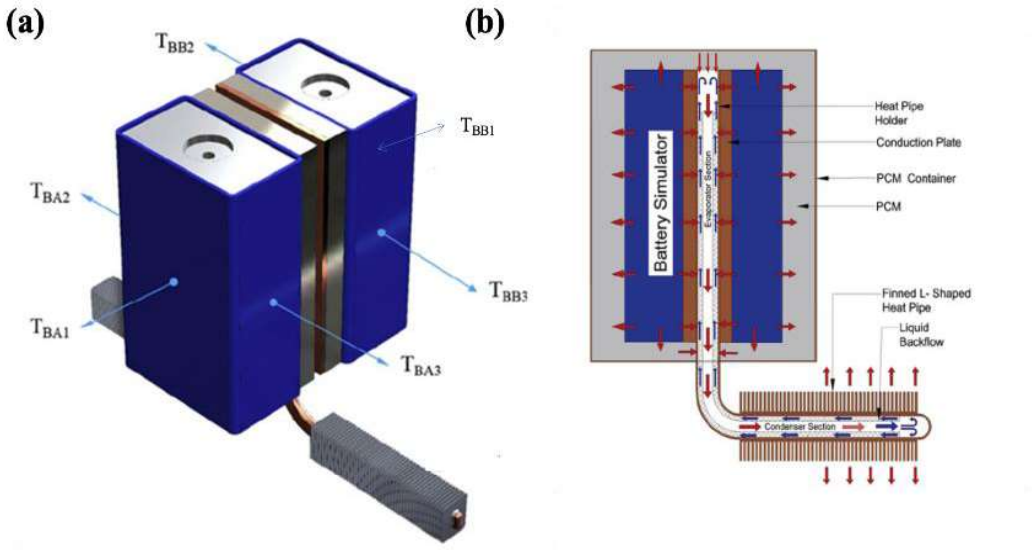


**Fig. 47.** Proposed hybrid PCM/HP cooling system for square batteries: (a) arrangement of power

batteries and thermocouples and (b) HP-PCM heat transfer/exchange [230].

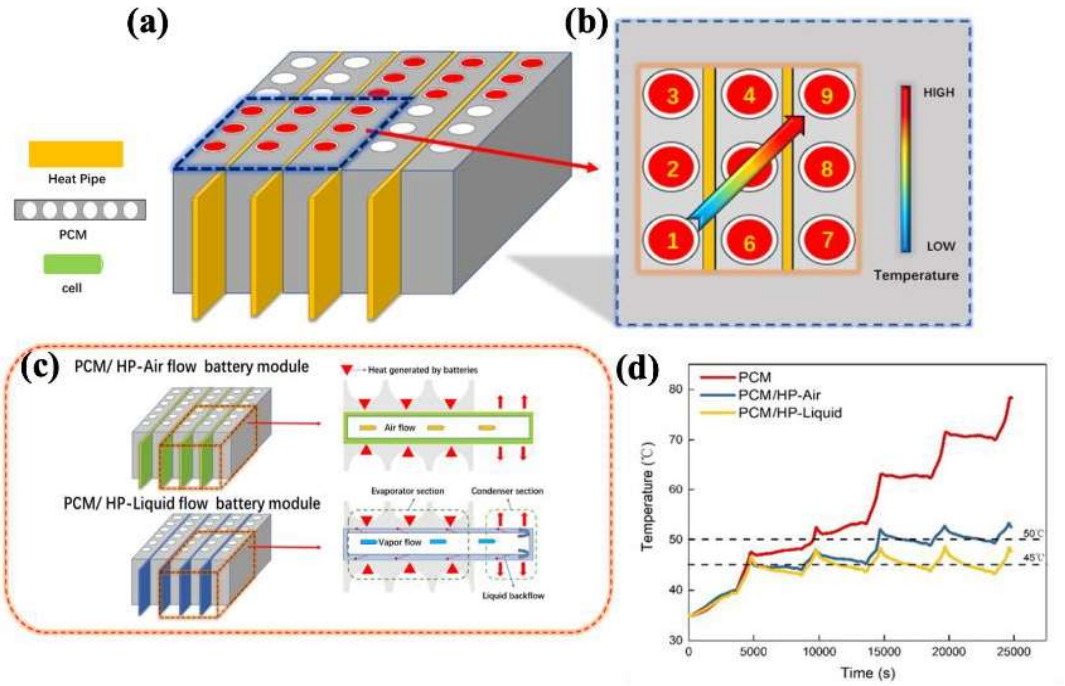


**Fig. 48.** Schematic of proposed hybrid PCM/HP cooling system: (a) designed battery module with integrated BTMS, (b) nine-cell sub-module rectangular region, (c) heat transfer mechanism, and (d) peak temperature variations [233].

### *4.2.4. PCM/TE cooling system*

TE modules or coolers (TECs) are active thermal components that convert electricity to thermal energy using the Peltier effect, which cools and heats various items (Fig. 49) [237-241]. TECs are enmeshed with p-type and n-type semiconductors alternately placed between two thin ceramic wafers. The Peltier effect generates a heat flux two-conductor junction, wherein the current passes through the circuit of matrices (Fig. 50) [242]. In general, TECs have the following merits: compact sizes, moderate weights, low maintenance requirements, wide operating temperature ranges, highly reliability, no mechanical moving parts, and long life-span [243-245]. However, they also exhibited low efficiencies and have additional power requirements, limiting their commercial applicability. TECs have been increasingly employed in BTMSs for improved performance [246-249]. Liu et al. [246] investigated the dependence of the

TE cooling system thermal management performance on the current. A battery temperature increase of about 3.5ºC could be maintained following discharge at equivalent current conditions and a semiconductor cooling unit working current of 3.5 A. In addition, an enhanced battery pack temperature difference of 5ºC was maintained. Riffat et al. [247] examined the thermal characteristics of a TEC module attached to the rectangular battery front, the results of which showed a 10ºC lower peak temperature at a 3C discharge rate following the utilization of TEC.

Alternatively, PCM and TE integration shows a promising potential in transforming a passive system to a semi-passive system as well as increasing the BTMS efficiency. Previous research has described the PCM/air, PCM/liquid, and PCM/HP-integrated BTMS, though few studies have reported on the PCM/TE composite system. Zhang et al. [250] employed a PCM and TE composite cooling sheet for power battery pack thermal management (Fig. 51). The battery surface temperature was maintained within a reasonable range at a high discharging rate. In addition, improved battery temperature uniformity and battery energy saving were observed. Manikandan et al. [251] presented a novel technique to enhance thermal performance of a TE cooler using PCM. They concluded that the temperature had a significant reduction. Jiang et al. [252] applied TE-PCM in a BTMS for a cylindrical cell (Fig. 52), which, was inferred to more efficiently control the temperature compared with natural convection and liquid cooling. The maximum battery temperature was maintained below 50ºC for up to 5335 s at a battery calorific value of 6 W compared with natural convection (930 s) and liquid cooling (1275 s). Cui et al. [253] investigated a concentrated PCM/TE cooling system, which maintained the operating temperature within the ideal working temperature range. Yin et al. [254] established an experimental platform containing three concentrated photovoltaic-PCM-TE hybrid subsystems, and demonstrated that the improved system could well maintain the system at the desired temperature. Song et al. [255] proposed a semiconductor TE device and PCMs for standby battery thermal management of an outdoor base station (Fig. 53), which exhibited a temperature difference below 5ºC for the limits of the thermal management temperature and PCM phase change

temperature. In addition, the maximum battery module temperature was maintained below 38.85 ºC after 1C discharging and 0.5C charging. The combined TE and PCM cooling method is expected to receive increasing attention in the future. However, based on the inherent property of TE cooling, when considering the application of TE and PCM in a BTMS, improving the lower efficiency of the Peltier process will benefit the removal of heat stored in PCM, further promoting PCM utilization efficiency and thermal safety performance.

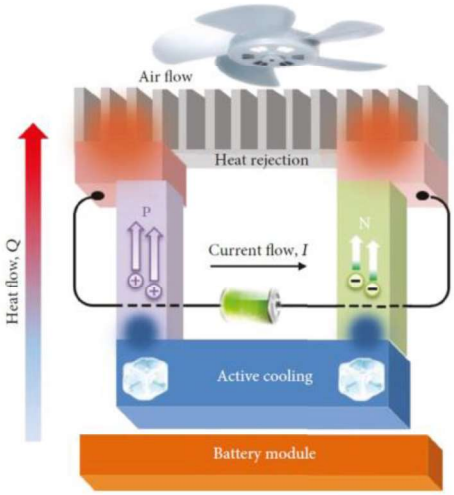


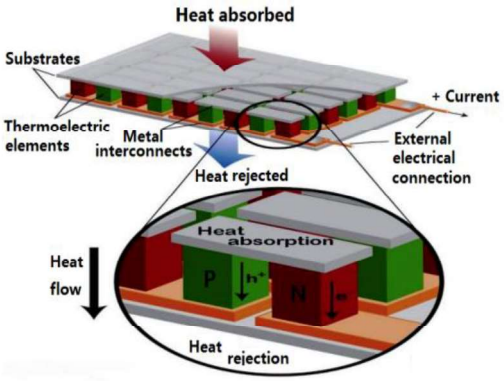


**Fig. 49.** Schematic of a TE module [237-241]. **Fig. 50**. Heat transfer principle of a TE chip [242].

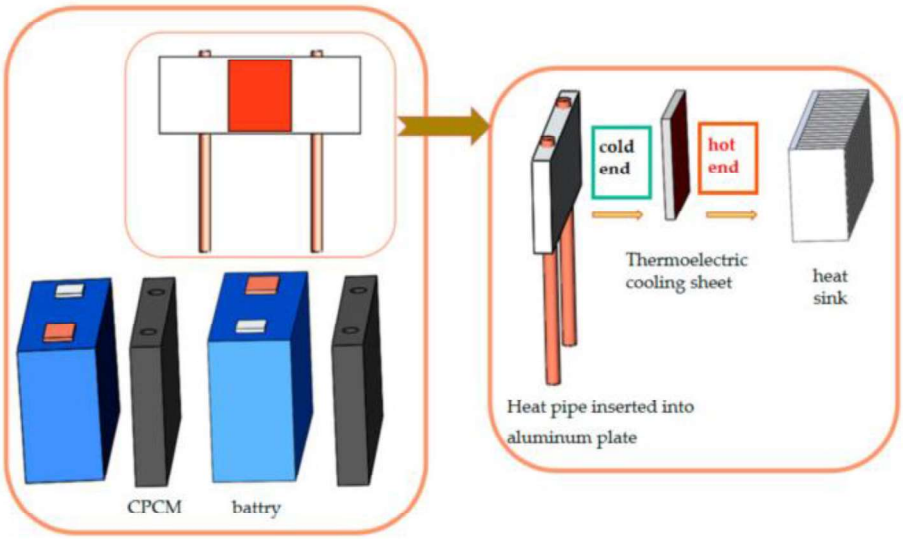


**Fig. 51.** TE sheet-PCM composite thermal management diagram [250].

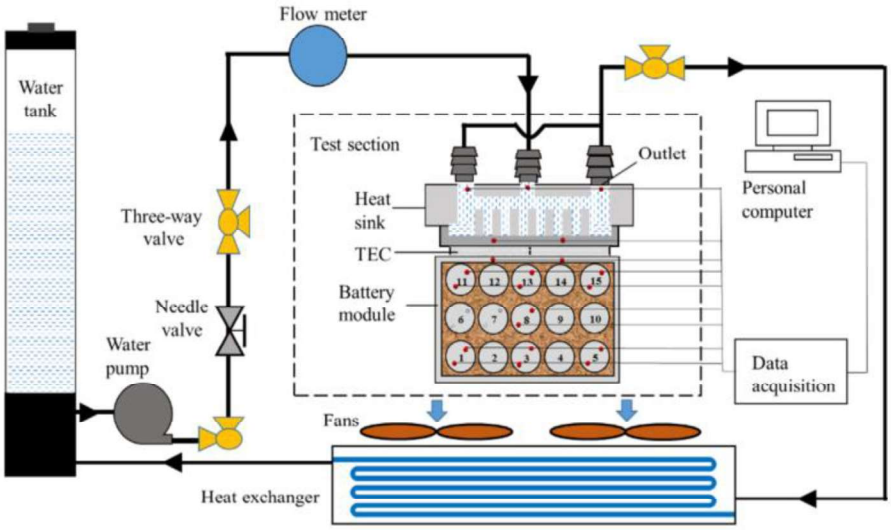


**Fig. 52**. PCM- and TE cooling-based battery module test setup [252].

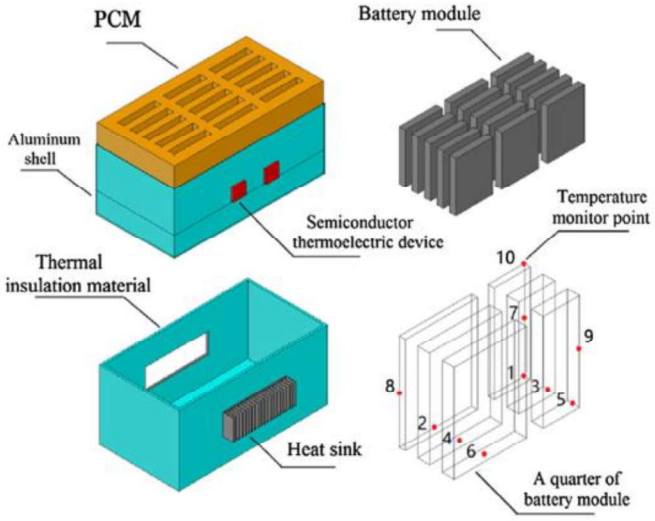


**Fig. 53.** Battery pack with TE semiconductor devices and PCMs [255].

### *4.3. Battery heating using PCM-based thermal management*

As is known, battery heating has been a major concern [256-258] under low temperature conditions. As an essential function of an effective BTMS, the common heating methods can be found in previous studies [259-261]. The battery performance and lifetime are largely dependent on low ambient temperatures, which can cause the increase of internal resistance, [262,263], solid electrolyte interphase (SEI) film formation, low reaction rate, electrode degradation, and electrolyte property decay [264-267]. Previous studies have focused on single cell-heating or single heating

method development for facile and non-standardized battery modules [268,269]. For example, Zhang et al. [268] employed metallic resistance heating on a cell, which exhibited a higher heating efficiency and thermo-consistency compared with those using the positive temperature coefficient heating method. Zhu et al. [269] applied alternating current (AC) pulse heating as the single heating method for large, laminated power lithium-ion batteries. Low-temperature thermal management is essential for safe and efficient lithium-ion battery pack operation in EVs. However, previous studies have focused on battery pack heat dissipation and have minimally reported on PCM-BTMS heating strategies under extremely cold conditions. Single and hybrid PCM-based BTMSs are generally employed for lithium-ion power system preheating at colder temperatures. Zhong et al. [270] examined a designed 18650-type battery module with a composite PCM cooling/resistance wire preheating coupling system (Fig. 54), the results of which indicated that the system efficiently preheated the batteries under colder temperature conditions. The coupling system raised the inner battery center temperature up to 40$^{o}$C within 300 s. Huo et al. [271] applied the lattice Boltzmann method to characterize PCM-based battery thermal management under ultra-low temperature conditions. The results indicated that raising the latent heat best preserved heat at lower temperatures. Lv et al. [272] reported on a PCM-BTMS hybrid with forced air convection heating or silicone plate heating (Fig. 55), wherein the closed-ended battery design optimized the forced-air-convection heating strategies and silicone plate heating at 90 W to provide the optimal heating performances. Fan et al. [273] explored battery heating under colder climate conditions, the results of which indicated that an external heating source allowed higher mass flow rate for enhanced heating. However, quickly raising the heating medium inlet temperature could result in heated batteries, which might exceed a maximum battery temperature of 40$^{o}$C. Ling et al. [274] compared the PCM thermal management performances of various lithium-ion battery packs at low temperatures. According to the results, highly thermally conductive PCM exhibited lower cell temperature variations, thus reducing the voltage differences. He et al. [275] coupled heating sheets and PCM to characterize the thermal management system of lithium

ion battery modules (Fig. 56), wherein the PCM-based battery modules maintained the temperatures for longer periods compared with the air-based ones. In addition, the PCM-based battery module exhibited a temperature difference of 2.82°C, whereas the air-based module was 14.49°C. Ghadbeigi et al. [276] examined the PCM-based BTMS performance under cold temperatures conditions, which was composed of PA and PA/EG composites, and compared their results to a battery module without PCM material. Rao et al. [277] produced a PCM- and air heating-based 3D module of power battery thermal management unit under cold temperatures, to which the air heating time was 6.4, 5.2, and 4.2 times that of PCM heating to allow the battery center temperature to reach 10ºC. Better PCM performance at shortened cold startup times were a result of the high PCM latent heat (Fig. 57). A lower temperature difference of 4.6°C from 9.9°C was observed at a five-fold higher PCM thermal conductivity. PCM-based BTMS research has focused on heat dissipation and cooling requirements, though power batteries undergo stressful and abusive conditions, particularly at higher discharge rates and operating or ambient temperatures. Nevertheless, the utilization of PCMs in heating the lithium-ion batteries at cold temperature has since been ignored. Notably, various operation and environmental conditions must be addressed, particularly extremely low temperatures, to allow equal battery heating and cooling. Hence, this study focused on the development of PCMs for low-temperature heating batteries. Future research should focus on lowering energy consumption while simultaneously improving the PCM-based BTMS battery heat transfer efficiency to promote the integrated power system thermal safety.

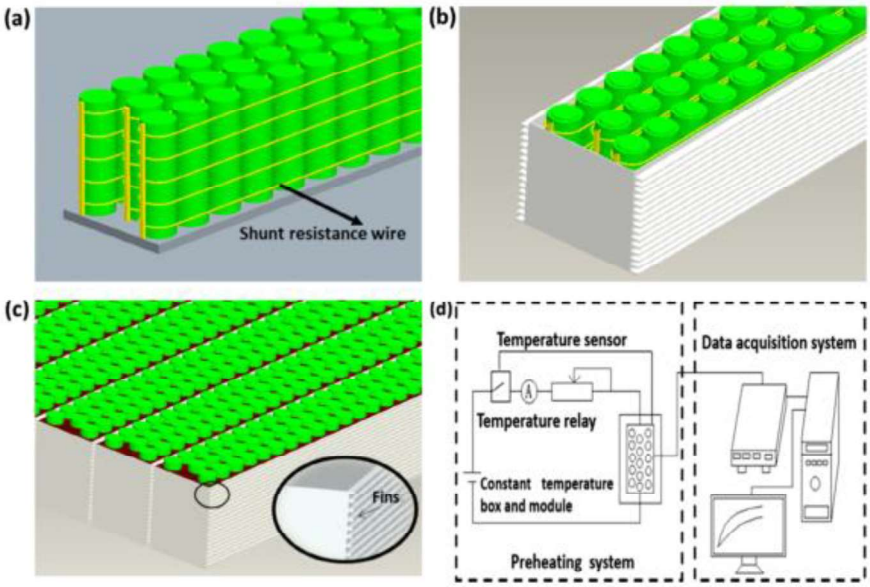


**Fig. 54** Battery module design: (a) resistance wire wrapped around batteries, (b) batteries within the module shell, (c) battery pack composed of battery modules, and (d) preheating experimental setup [270].

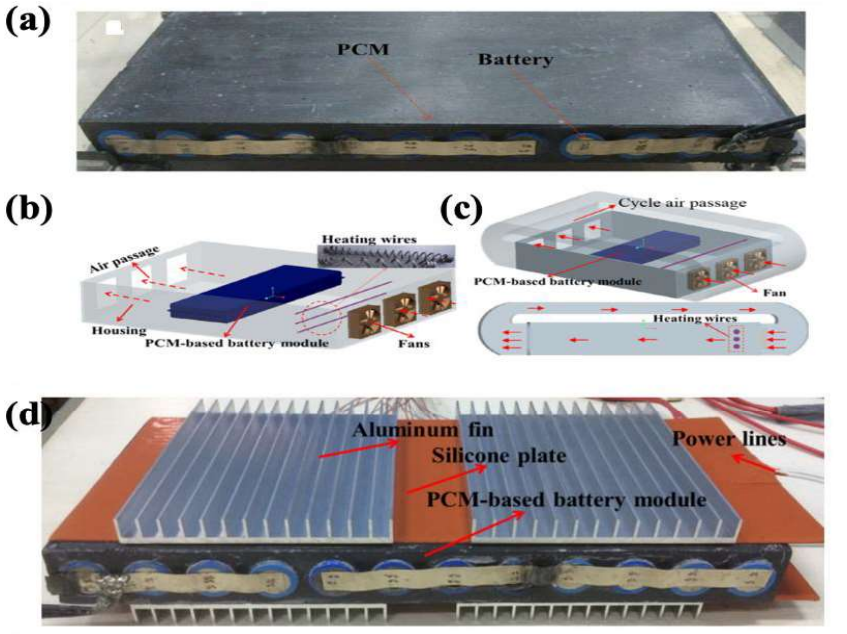


**Fig. 55.** PCM battery module heating strategies: (a) standardized PCM-based battery module, (b) forced air convection heating strategy, (c) optimized forced air convection heating strategy, and (d) silicone plate heating strategy [272].

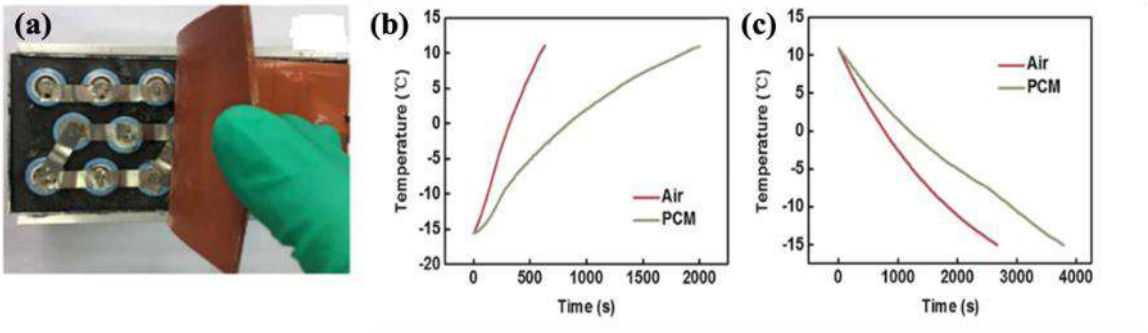


**Fig. 56.** Battery module heating system coupled with PCM and heating sheet: (a) battery module with heat sheet, (b) average air-based battery module surface temperature with two heat sheets at 50°C, and (c) average PCM-based battery module surface temperature with two heat sheets at 50°C [275].

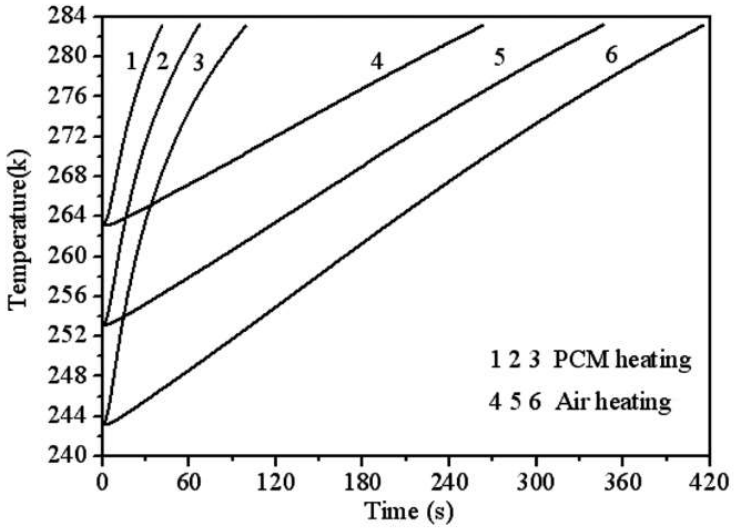


**Fig. 57.** Comparison of temperature responses of PCM and air heating [277].

### *4.4. Opportunities and challenges of PCM-BTMS*

In general, the PCM cooling system is widely applied for battery thermal management given its excellent temperature control and equalization. As known, maintaining a high-energy power lithium-ion battery system density can increase the EVs and HEVs driving ranges. Thus, a high-efficiency BTMS can be produced by lowering the system weight and improving the energy density.

Traditional PCM modules, especially those with bulky PCM blocks and matrices, inevitably increased the weight and volume of the whole power system, thereby significantly reducing the energy density. To solve the mentioned problem, the development of innovative forms and new lightweight PCMs and PCM-BTMSs is of crucial concern. In addition, current research on PCM cooling systems is still in the experimental phase compared with traditional mature air cooling and liquid cooling. The developed battery packs with PCM function are also at the sample level, and have not been promoted for practical EV application. Optimizing the PCM thermophysical parameters and PCM BTMS particularly the performance optimization, structure design, weight, cost, space, energy consumption, and cooling efficiency, can speed up PCM-based battery module industrialization. The heat dissipation demand of high-density power batteries must be addressed, which a single PCM heat dissipation system cannot fulfill. At this time, the more efficient PCM-based hybrid cooling systems integrating the passive PCM and active cooling technologies will inevitably become the future development trend. Within the composite cooling system, the active and passive have separate advantages based on their essential attributes. The complementary system will efficiently remove the heat accumulated in the PCM heat dissipation medium, improving the heat storage/heat release efficiency of PCM and furthering its utilization efficiency and cycle life for the overall performance and safety.

Different PCM-based hybrid BTMS approaches, which include PCM/air cooling, PCM/liquid cooling, PCM/HP, and PCM/TE cooling, have varying merits and disadvantages, such as space availability, cost, weight, integration degree, and service life. As such, the development of a rational design and installation of an appropriate thermal management system must address demands of heat dissipation of practical loading conditions.

## 5. Conclusions and future directions in the field

### *5.1. Conclusions*

Lithium-ion batteries are limited by their temperature dependence, which can result in temperature increase and non-uniformity. Applicable PCM-based cooling systems must be able to lower the maximum temperature while maintaining a homogeneous cell temperature distribution. However, low thermal conductivities, combustion performance of organic PCM, structural instability caused by the leakage, and deformation or collapse have restricted the development of PCM-BTMSs. This study first reviewed and classified mainstream lithium-ion batteries, to which the lithium-ion battery heat generation/transfer mechanisms were characterized. Then, considering the practical application and security attributes of PCM, the current research situation and performance promotion solutions to the low thermal conductivity, structural instability, and combustion characteristics were illustrated. Following that, the design scheme, cooling efficiency, and advantages and disadvantages of current BTMS that employ PCM as heat transfer medium for EVs/HEVs were objectively evaluated and analyzed. Lastly, the current challenges and opportunities referring to PCM and BTMS employing PCM were concretely expounded. Based on the above study, the following conclusions were drawn:

(1) In terms of lithium-ion power batteries, three main kinds of products are applied in electrified-driven vehicles according to the external shape and appearance: cylindrical, prismatic, and pouch. For standard and typical cylindrical cells (especially 18650-type), the battery module/pack is the most commonly used type of assembly as it improves the temperature consistency among thousands of cells and controls the temperature. Different from cylindrical cells, prismatic cells possess a higher heat dissipation efficiency due to their larger contact area. Enough space should be considered when applying the prismatic cells to the EVs/HEVs. The special structure of the pouch cell enables a decrease in weight and increase in the high-energy densities and packaging efficiency, though this may result in additional mechanical destroy and swelling. Owing to the difference of various chemical compositions of lithium batteries, those with higher energy

density (such as NCM811/C, NCM/SiC) may exhibit higher potential safety risks due to their electrode materials, especially under abusive conditions (electric abuses, thermal abuses, and mechanical abuses). These abnormalities shorten the battery lifespan and may result in TR. Hence, an efficient BTMS is crucial and necessary for lithium-ion battery modules/packs.

(2) The PCM thermal conductivity significantly influences the overall power system heat transfer efficiency. However, in consideration of the practical application of PCM, only improving the thermal conductivity coefficient by adding the high thermal conductive fillers (such as metallic powers/foam, carbon-based foams) is insufficient. Continuous battery module charging/discharging cycles can result in PCM structure damage to some extent due to the intrinsic property of organic PCM. Therefore, the structural stability and flame retardancy of PCM is predicted to be a research hotpot. The development of form-stabilized and flame retarded composite PCMs are very urgent. It is noting that the heat latent and melting point, as the fundamental parameters of PCM, should not be decreased while adding the functional additives to PCM. When selecting the appropriate composite PCM for a battery system, a high-thermal conductive, robust, and excellent flame retarded composite PCM is suitable and helpful for enhancing the system security.

(3) A PCM cooling system has been confirmed to have remarkable temperature-reducing and temperature-stretching capacities through experimental and simulation methods. For power lithium-ion battery systems with higher heat dissipation standards, a single PCM-BTMS is not enough. Hybrid PCM-based systems that are coupled with traditional air cooling, liquid cooling, HPs, and TE are more efficient choices, and are predicted to be the inevitable trend of high-energy density battery systems. A secondary cooling strategy such as active auxiliary measures can eliminate stored PCM heat while maintaining the high PCM heat transfer efficiency and utilization life. Further, in addition to the cooling performance of PCMs at high temperature condition, the heating methods of PCMs in extreme low temperature have been reviewed through the combination of resistance wires, heating sheet, and so on.

(4) To maintain the higher energy density of lithium-ion battery systems, a lightweight and creative form of PCM is a very effective solution. Although PCM and PCM-based cooling systems have been verified and confirmed through many experimental and simulation research work, these ideas are still in the laboratory phase given that many technical issues must first be solved prior to application in practical EVs/HEVs. In the end, the developed PCM-based cooling system must be compact, integrated, efficient, lightweight, has low energy consumption, and be secure. Every PCM-based heat dissipation system has its obvious advantages and disadvantages. Hence, we need to rationally choose the suitable BTMS according to the practical factors such as the heat generation, cooling demand, space, weight, and cost.

### *5.2. Future recommendation*

Based on the above review and analysis，the following research perspectives are highlighted as the future development of PCM-based BTMS:

(1) Considering the high energy density, lightweight and continuous driving range requirements of EVs/HEVs, ternary lithium-ion power batteries have been regarded as one of the mainstream technology routes. It is worth noting that the participation of PCM in the power battery module/pack can not significantly reduce the energy density of the system. Simultaneously, excellent heat dissipation efficiency and high safety performance should be maintained. Hence, composite PCM with flexible, processable, high thermal conductivity and latent heat, flame retardant and electrical insulation properties will become the focus of future research. The key point is that a good proportion and balance point should be discovered for the physical property parameters of the composite PCM so as to ensure the superior comprehensive properties.

(2) As a functional material, the thermal conductivity and latent heat of PCM will directly affect the heat dissipation efficiency. PA is the most widely used organic PCM in BTMS due to its merits. Nevertheless, how to overcome the precipitation problem

under uninterrupted high temperature cycles without obviously decreasing the thermal physical performance parameters will be the key consideration in the future. Considering the actual operating conditions of EVs/HEVs (climbing, accelerating, starting, collision, etc.), it is critical to improve the mechanical strength of PCM to avoid collapse, cracks and damage phenomenon. MicroPCM is a recommended solution to the aforementioned problem. However, realizing the application of MicroPCM in power battery modules/packages needs to be further explored;

(3) If the temperature increase of power battery modules/packages is only controlled by PCM after long-term continuous high-rate charge-discharge cycles, the heat storage capacity of PCM will inevitably decline and cannot be recovered in time. Therefore, secondary heat dissipation is needed to improve the PCM durability, ultimately the utilization efficiency. Consequently, hybrid PCM-based BTMS will be one of the research hotspots in the future. Especially considering the current integrated CTP (cell to pack) and CTC (cell to chassis) technologies, the coupling of PCM and liquid cooling plate will be the most promising technical solution to achieve industrial application in the future.

(4) Low temperature rapid preheating is also one of the main functions of the BTMS. At present, referring to PCM-based BTMS, the research of preheating technology is less than that of heat dissipation system. A high-efficiency, cost-effective and safe rapidly heating system needs to be developed in the future.

(5) Different BTMS employing PCM have their merits and drawbacks. Up to now, the corresponding research focuses on the measurement of heat dissipation effect, performance evaluation and structure optimization, lacking quantitative data on economy, environmental benefit, maintenance, system complexity and weight. The aforementioned future research directions will be concerned by the researchers in the following work.

In a word, this work aimed to fully address the pivotal PCM thermophysical performances and security features to serve as a reference. In addition, the PCM-BTMS cooling performances were discussed and compared with actual BTMS

application, which will be benefit for accelerating the industrialization of this innovative cooling strategy.

## Credit author statement

Jiangyun Zhang: Conceptualization, Writing- Original draft preparation, Funding acquisition. Dan shao: Writing-review &editing. Liqin Jiang: Writing-review & editing. Guoqing Zhang: Writing-review & editing, Funding acquisition. Hongwei Wu: Conceptualization, Writing-review & editing, Funding acquisition. Rodney Day: Writing-review & editing. Wenzhao Jiang: Writing-review & editing.

## Acknowledgement

This research was financially supported by Guangdong Key Laboratory of Battery Safety（Grant No. 2019B121203008）, the National Natural Science Foundation of China (Grant No. 51906047, Grant No. 21875046, No.51803036), Science, the UK-China Newton Fund Researcher Links Workshop (Grant No. 2020-RLWK12-10349) and Technology Program of the State Administration for Market Regulation of China（Grant No. 2020MK127）. The authors ensure that permission is attained for all copyrighted graphics, images, tables and/or figures. Note that for any figures, graphics or images published elsewhere by the author or others.

## References

[1] Ren DS, Feng XN, Liu LS, et al. Investigating the relationship between internal short circuit and thermal runaway of lithium-ion batteries under thermal abuse condition. Energy Storage Mater 2021;34:563-73.

[2] M.T. Jamal-abad, A. Zamzamian, M. Dehghan. Experimental studies on the heat transfer and pressure drop characteristics of Cu water and Al water nanofluids in a spiral coil, Exp Therm Fluid Sci 2013;47:206-12.

[3] A. Mahmoudzadeh Andwari, A. Pesiridis, S. Rajoo, et al. A review of Battery Electric Vehicle technology and readiness levels, Renew Sust Energ Rev 2017;78:414-30.

[4] J. Lo. Effect of temperature on lithium-iron phosphate battery performance and plug-in hybrid electric vehicle range, Waterloo, 2013 Ph.D. thesis.

[5] S. Goutam, J.M. Timmermans, N. Omar, et al. Comparative study of surface temperature behavior of commercial li-ion pouch cells of different chemistries and capacities by infrared thermography, Energies 2015;8(8):8175-92.

[6] Gan YH, He LF, Liang JL, et al. A numerical study on the performance of a thermal management system for a battery pack with cylindrical cells based on heat pipes, Appl Therm Eng 2020;179:115740.

[7] Liao ZH, Zhang S, Li K, et al. A survey of methods for monitoring and detecting thermal runaway of lithium-ion batteries, J Power Sources 2019;436:226879.

[8] Liu YJ, Dong F. What are the roles of consumers, automobile production enterprises, and the government in the process of banning gasoline vehicles? Evidence from a tripartite evolutionary game model. Energy 2022;238:122004.

[9] Marques Benvenutti LM, Ribeiro AB, Uriona M. Long term diffusion dynamics of alternative fuel vehicles in Brazil. J Clean Prod 2017;164:1571-85.

[10] Logan KG, Xi JDN. UK and China：Will electric vehicle integration meet Paris Agreement Targets? Transp Res Interdisc Perspect 2020;8:100245.

[11] Feng XN, Ouyang MG, Liu X, et al. Thermal runaway mechanism of lithium ion battery for electric vehicles:A review. Energy Storage Mater 2018;10:246-67.

[12] Chombo PV, Laoonual YP. A review of safety strategies of a Li-ion battery. J Power Sources 2020;478:228649.

[13] Liu CC , Xu DJ, Weng JW, et al. Phase change materials application in battery thermal management aystem: a review, Materials 2020;13:1-37.

[14] D. Shepardson, S. Shivdas, U.S. safety board probes fatal Tesla accident in Florida, 2018. https://www.reuters.com/article/us-tesla-crash/two-killed-in-tesla-car-crash-in-florida-police-idUSKBN1IA205. (Accessed 20 June 2019).

[15] ChinaAutoWeb, 2019. https://chuneng.bjx.com.cn/news/20190415/974755.shtml. (Accessed 15 April 2019).

[16]ChinaAutoWeb,2020.http://www.escn.com.cn/news/show-1044296.html.(Accessed 21 May 2020).

[17]ChinaAutoWeb,2020.https://www.360kuai.com/pc/9eae098fbd08da9f0?cota=3&kuai_so=1&sign=360_57c3bbd1&refer_scene=so_1. (Accessed 6 November 2020).

[18]ChinaAutoWeb,2020.http://jx.chinadaily.com.cn/a/202011/10/WS5faa22efa3101e7ce972e721.html. (Accessed 10 November 2020).

[19]ChinaAutoWeb, 2020. https://xueqiu.com/6146194392/164070684. (Accessed 24 November 2020).

[20] Feng XN, Zheng SQ, Ren DS, et al. Investigating the thermal runaway mechanisms of lithium-ion batteries based on thermal analysis database, Appl Energ 2019;246:53-64.

[21] Ren DS, Feng XN, Lu LG, et al. An electrochemical-thermal coupled overcharge-to-thermal-runaway model for lithium ion battery, J Power Sources 2017;364:328-40.

[22] Mohammed AH, Esmaeeli R, Aliniagerdroudbari H, et al. Dual-purpose cooling plate for thermal management of prismatic lithium-ion batteries during normal operation and thermal runaway, Appl Therm Eng 2019;160:114106.

[23] Liu JW, Li H, Li WY, et al. Thermal characteristics of power battery pack with liquid-based thermal management, Appl Therm Eng 2020;164:114421.

[24] Wiriyasart S, Hommalee C, Sirikasemsuk S, et al. Thermal management system with nanofluids for electric vehicle battery cooling modules, Case Stud Therm Eng 2020;18:100583.

[25] Al-Hallaj S, J. R. Selman, et al. A novel thermal management system for EV batteries using phase change material (PCM), J. Electrochem. Soc 2000;147:3231-6.

[26] Lan W, Shang BF, Wu RK, et al. Thermally-enhanced nanoencapsulated phase change materials for latent functionally thermal fluid, Int J Therm Sci 2021;159:106619.

[27] Wu WX, Wu W, Wang SF. Thermal optimization of composite PCM based large-format lithium-ion battery modules under extreme operating conditions, Energ Convers Manage 2017;153:22-33.

[28] Cicconi P, Kumar P, Varshney P. A support approach for the modular design of Li-ion batteries: A test case with PCM, J Energy Storage 2020;31:101684.

[29] Libeer W, Ramos F, Newton C, et al. Two-phase heat and mass transfer of phase change materials in thermal management systems, Int J Heat Mass Tran 2016;100:215-23.

[30] Lv YF, Yang XQ, Zhang GQ. Durability of phase-change-material module and its relieving effect on battery deterioration during long-term cycles, Appl Therm Eng 2020;179:115747.

[31] Righetti G, Savio G, Meneghello R, et al. Experimental study of phase change material (PCM) embedded in 3D periodic structures realized via additive manufacturing, Int J Therm Sci 2020;153:106376.

[32] Rehman T, Ali HM, Janjua MM, et al. A critical review on heat transfer augmentation of phase change materials embedded with porous materials/foam, Int J Heat Mass Tran 2019;135:649-73.

[33] Malik M, Dincer L, Rosen MA. Review on use of phase change materials in battery thermal management for electric and hybrid electric vehicles, Int J Energ Res 2016;40:1011-31.

[34] Jaguemont J , Mierlo JV. A comprehensive review of future thermal management systems for battery-electrified vehicles, J Energy Storage 2020;31:101551.

[35] Liu CC , Xu DJ, Weng JW, et al. Phase change materials application in battery thermal management aystem: a review, Materials 2020;13:1-37.

[36] Chen JW, Kang SY, E JQ, et al. Effects of different phase change material thermal management strategies on the cooling performance of the power lithium ion batteries: A review, J power sources 2019;442:227228.

[37] Panasonic, Lithium Ion Batteries, (2007).

[38] G. Zubi, R. Dufo-López, M. Carvalho, G. Pasaoglu, The lithium-ion battery: State of the art and future perspectives, Renew Sust Energ Rev 2018;89:292-308.

[39] Situ WF, Yang XQ, Li XX, et al. Effect of high temperature environment on the performance of $LiNi_{0.5}Co_{0.2}Mn_{0.3}O_2$ battery, Int J Heat Mass Tran 2017;104:743-8.

[40] Hu SK, Cheng GH, Cheng MY, et al. Cycle life improvement of $ZrO_2$-coated spherical $LiNi_{1/3}Co_{1/3}Mn_{1/3}O_2$ cathode material for lithium ion batteries, J Power Sources 2009;188:564-9.

[41] Nie M, Xia YF, Wang ZB, et al. Effects of precursor particle size on the performance of $LiNi_{0.5}Co_{0.2}Mn_{0.3}O_2$ cathode material, Ceram. Int 2015;41:15185-92.

[42] Du QX, Tang ZF, Ma XH, et al. Improving the electrochemical properties of high-energy cathode material $LiNi_{0.5}Co_{0.2}Mn_{0.3}O_2$ by Zr doping and sintering in oxygen, Solid State Ionics 2015;279:11-7.

[43] Wong D, Shrestha B, Wetz DA, et al. Impact of high rate discharge on the aging of lithium nickel cobalt aluminum oxide batteries, J Power Sources 2015;280:363-72.

[44] Zhao R, Zhang SJ, Gu JJ, et al. Modeling the electrochemical behaviors of charging Li‐ion batteries with different initial electrolyte salt concentrations, Int J Energ Res 2016;40:1085-92.

[45] Dong T, Wang YW, Peng P, et al. Electrical-thermal behaviors of a cylindrical graphite-NCA Li-ion battery responding to external short circuit operation, Int J Energ Res 2019;43:1444-59.

[46] Wang C, Zhang GQ, Meng LK, et al. Liquid cooling based on thermal silica plate for battery thermal management system, Int J Energ Res 2017;41:2468-79.

[47] Xie Y, He XJ, Hu XS, et al. An improved resistance-based thermal model for a pouch lithium-ion battery considering heat generation of posts, Appl Therm Eng 2020;164:114455.

[48] Ghalkhani M, Bahirael F, Nazri GA, et al. Electrochemical-thermal model of pouch-type lithium-ion batteries, Electrochim Acta 2017;247:569-87.

[49] Xiao M, Choe SY. Theoretical and experimental analysis of heat generations of a pouch type $LiMn_2O_4$/carbon high power Li-polymer battery, J Power Sources 2013;241:46-55.

[50] An ZJ, Jia L, Ding Y, et al. A review on lithium-ion power battery thermal management technologies and thermal safety, J Therm Sci 2017;26:391-412.

[51] Chakraborty A, Kunnikuruvan S, Dixit M, et al. Review of computational studies of NCM cathode materials for Li-ion batteries, Isr J Chem 2020;60:850-62.

[52] Lv PZ, Liu XJ, Qu J, et al. Recent advances of thermal safety of lithium ion battery for energy stroage. Energy Storage Mater 2020;31:195-220.

[53] Wang Y, Gao Q, Zhang TS, et al. Advances in integrated vehicle thermal

management and numerical simulation. Energies 2017;10:1636.

[54] Mitran RA , Lonita S, Lincu D, et al. A review of composite phase change materials based on porous silica nanomaterials for latent heat storage applications, Molecules 2021;26:1-45.

[55] Rao ZH, Wang SF. A review of power battery thermal energy management, Renew Sust Energ Rev 2011;15:4554-71.

[56] Sabbah R, Kizilel R, Selman JR, et al. Active (air-cooled) vs. passive (phase change material) thermal management of high power lithium-ion packs: Limitation of temperature rise and uniformity of temperature distribution, J Power Sources 2008;182:630-8.

[57] Kizilel R, Sabbah R, Selman JR, et al. An alternative cooling system to enhance the safety of Li-ion battery packs, J Power Sources 2009;182:1105-12.

[58] Chen ZQ, Gao DY, Shi J. Experimental and numerical study on melting of phase change materials in metal foams at pore scale, Int J Heat Mass Tran 2014;72:646-55.

[59] Gulfam R, Zhang P, Meng ZN. Advanced thermal systems driven by paraffin-based phase change materials-A review, Appl Energ 2019;238:582-611.

[60] Yang ST, Ling C, Fan YQ, et al. A review of lithium-ion battery thermal management system strategies and the evaluate criteria, Int J Electrochem Sc 2019;14:6077-107.

[61] Tauseef R, Ali HM, Janjua MM, et al. A critical review on heat transfer augmentation of phase change materials embedded with porous materials/foams. Int J Heat Mass Tran 2019;135:649-73.

[62] Wang YN, Wang ZK, Min HT, et al. Performance investigation of a passive battery thermal management system applied with phase change material, J Energy Storage 2021;35:102279.

[63] Zhang S, Feng DL, Shi L, et al. A review of phase change heat transfer in shape-stabilized phase change materials (ss-PCMs) based on porous supports for thermal energy storage, Renew Sust Energ Rev 2021;135:110127.

[64] Lu MY, Zhang XL, Li J, et al. Research progress on power battery cooling technology for electric vehicles, J Energy Storage 2020;27:101155.

[65] Abid Hussain, Tso CY, Chao Christopher YH. Experimental investigation of a passive thermal management system for high-powered lithium ion batteries using nickel foam-paraffin composite, Energy 2016;115:209-18.

[66] Nazarychev VM, Glova AD, Volgin IV, et al. Evaluation of thermal conductivity of organic phase-change materials from equilibrium and non-equilibrium computer simulations: Paraffin as a test case. Int J Heat Mass Tran 2021;165:120639.

[67] Asker M, Genceli H. Numerical Study on Solidification of Phase Change Materials Embedded with Metal Foam. European Mechanical Science 2021;5:1-5.

[68] Drissi S, Ling TC, Mo KH. Thermal efficiency and durability performances of paraffinic phase change materials with enhanced thermal conductivity-A review. Thermochim Acta 2019;673:198-210.

[69] Li Z, Sun WG, Wang G, et al. Experimental and numerical study on the effective thermal conductivity of paraffin/expanded graphite composite. Sol Energ Mat Sol C 2014;128:447-55.

[70] Luo JF, Yin HW, Li WY, et al. Numerical and experimental study on the heat transfer properties of the composite paraffin/expanded graphite phase change material. Int J Heat Mass Tran 2015;84:237-44.

[71] Kim J, Oh J, Lee H. Review on battery thermal management system for electric vehicles, Appl Therm Eng 2019;149:192-212.

[72] Kaviyarasu S, Rajakumar S. Review on battery thermal management system using phase change material. International Research Journal of Modernization in Engineering Technology and Science 2020;02:797-814.

[73] Zhang P, Meng ZN, Zhu H, et al. Experimental and Numerical Study of Heat Transfer Characteristics of a Paraffin/Metal Foam Composite PCM. Energy Procedia 2015;75:3091-7.

[74] Tariq SL, Ali HM, Akram MA, et al. Nanoparticles enhanced phase change materials (NePCMs)-A recent review. Appl Therm Eng 2020;176:115305.

[75] Wang JF, Xie HQ, Guo ZX, et al. Improved thermal properties of paraffin wax by the addition of $TiO_2$ nanoparticles. Appl Therm Eng 2014;73:1541-7.

[76] Yuan KJ, Shi JM, Aftab W, et al. Engineering the thermal conductivity of

functional phase-change materials for heat energy conversion, storage, and utilization. Adv Funct Mater 2020;30:1904228.

[77] Malik M, Dincer I, Rosen M, et al. Experimental investigation of a new passive thermal management system for a Li-ion battery pack using phase change composite Material. Electrochim Acta 2017;257:345-55.

[78] Wang XL, Li B, Qu ZG, et al. Effects of graphite microstructure evolution on the anisotropic thermal conductivity of expanded graphite/paraffin phase change materials and their thermal energy storage performance. Int J Heat Mass Tran 2020;155:119853.

[79] Jiang GW, Huang JH, Fu YS, et al. Thermal optimization of composite phase change material/expanded graphite for Li-ion battery thermal management. Appl Therm Eng 2016;108:1119-25.

[80] Srivatsa PVSS, Baby R, Balaji C. Numerical investigation of PCM based heat sinks with embedded metal foam/crossed plate fins. Numer Heat Tr A-Appl 2014;66:1131-53.

[81] Yang X, Lu Z, Bai Q, Zhang Q, Jin L, Yan J. Thermal performance of a shell-and-tube latent heat thermal energy storage unit: role of annular fins. Appl Energ 2017;202:558-70.

[82] Khan Z, Khan ZA. An experimental investigation of discharge/solidification cycle of paraffin in novel shell and tube with longitudinal fins based latent heat storage system. Energ Convers Manage 2017;154:157-67.

[83] Wang Y, Wang SY, Wang JP, et al. Preparation, stability and mechanical property of shape-stabilized phase change materials. Energ Buildings 2014;77:11-16.

[84] Goli P, Legedza S, Dhar A, et al. Graphene-enhanced hybrid phase change materials for thermal management of Li-ion batteries. J Power Sources 2014;248:37-43.

[85] Xiao X, Zhang P, Li M. Preparation and thermal characterization of paraffin/metal foam composite phase change material. Appl Energ 2013;112:1357-66.

[86] Raza G, Shi Y, Deng Y. Expanded graphite as thermal conductivity enhancer for paraffin wax being used in thermal energy storage systems. 2016 13th Int Bhurban

Conf Appl Sci Technol 2016:1-12.

[87] Wu WX, Zhang GQ, Ke XF, et al. Preparation and thermal conductivity enhancement of composite phase change materials for electronic thermal management. Energ Convers Manage 2015;101:278-84.

[88] Wu WX, Yang XQ, Zhang GQ, et al. An experimental study of thermal management system using copper mesh-enhanced composite phase change materials for power battery pack. Energy 2016;113:909-16.

[89] Zhang JY, Li XX, Zhang GQ, et al. Characterization and experimental investigation of aluminum nitride-based composite phase change materials for battery thermal management. Energ Convers Manage 2020;204:112319.

[90] Sheng N, Rao ZH, Zhu CY, et al. Honeycomb carbon fibers strengthened composite phase change materials for superior thermal energy storage. Appl Therm Eng 2020;164:114493.

[91] Cao M, Huang JH, Liu ZQ. The enhanced performance of phase-change materials via 3D printing with prickly aluminum honeycomb for thermal management of ternary lithium batteries. Adv Mater Sci Eng 2020; 8167386.

[92] Arshad A, Jabbal M, Yan YY. Thermophysical characteristics and application of metallic-oxide based mono and hybrid nano composite phase change materials for thermal management systems. Appl Therm Eng 2020;181:115999.

[93] Heyhat MM, Mousavi S, Siavashi M. Battery thermal management with thermal energy storage composites of PCM, metal foam, fin and nanoparticle. J Energy Storage 2020;28:101235.

[94] Qu Y, Wang S, Zhou D, et al. Experimental study on thermal conductivity of paraffin-based shape-stabilized phase change material with hybrid carbon nano-additives. Renew Energ 2020;146:2637-45.

[95] Kiani M, Omiddezyani S, Houshfar E, et al. Lithium-ion battery thermal management system with $Al_2O_3$/AgO/CuO nanofluids and phase change material. Appl Therm Eng 2020;180:115840.

[96] Zheng NB, Fan RJ, Sun ZQ, et al. Thermal management performance of a fin-enhanced phase change material system for the lithium-ion battery. Int J Energ Res

2020;44:7617-29.

[97] Ping P, Peng R, Kong D, Chen G, Wen J. Investigation on thermal management performance of PCM-fin structure for Li-ion battery module in high-temperature environment. Energ Convers Manage 2018;176:131-46.

[98] Wang Z, Zhang H, Xia X. Experimental investigation on the thermal behavior of cylindrical battery with composite paraffin and fin structure. Int J Heat Mass Tran. 2017;109:958-70.

[99] Weng J, He Y, Ouyang D, Yang X, Zhang G, Wang J. Thermal performance of PCM and branch-structured fins for cylindrical power battery in a high-temperature environment. Energ Convers Manage 2019;200:112106.

[100] Wu WX, Yang XQ, Zhang GQ, et al. Experimental investigation on the thermal performance of heat pipe-assisted phase change material based battery thermal management system. Energ Convers Manage 2017;138:486-92.

[101] Nomura T, Zhu CY, Nan S, et al. High thermal conductivity phase change composite with a metal-stabilized carbon-fiber network. Appl Energ 2016;179:1-6.

[102] Samimi F, Babapoor A, Azizi M, et al. Thermal management analysis of a Li-ion battery cell using phase change material loaded with carbon fibers. Energy 2016;96:355-71.

[103] He JS, Yang XQ, Zhang GQ. A phase change material with enhanced thermal conductivity and secondary heat dissipation capability by introducing a binary thermal conductive skeleton for battery thermal management. Appl Therm Eng 2019;148:984-91.

[104] Xia GD, Cao L, Bi GL. A review on battery thermal management in electric vehicle application. J Power Sources 2017;367:90-105.

[105] Li JH, Huang JH, Cao M. Properties enhancement of phase-change materials via silica and Al honeycomb panels for the thermal management of $LiFePO_4$ batteries. Appl Therm Eng 2018;131:660-8.

[106] Rao ZH, Wen YP, Liu CZ, et al. Enhancement of heat transfer of microcapsulated particles using copper particles and copper foam. Particuology 2018;41:85-93.

[107] Zou DQ, Liu XS, He RJ, et al. Preparation of a novel composite phase change material (PCM) and its locally enhanced heat transfer for power battery module. Energ Convers Manage 2019;180:1196-202.

[108] Luo XH, Guo QG, Li XF, et al. Experimental investigation on a novel phase change material composites coupled with graphite film used for thermal management of lithium-ion batteries, Renew Energ 2020;145:2046-55.

[109] Huang YH, Cheng WL, Zhao R, Thermal management of Li-ion battery pack with the application of flexible form-stable composite phase change materials. Energ Convers Manage 2019;182:9-20.

[110] Lv YF, Situ WF, Yang XQ, et al. A novel nanosilica-enhanced phase change material with anti-leakage and anti-volume-changes properties for battery thermal management. Energ Convers Manage 2018;163:250-9.

[111]Wu WX, Wang SF. Form-stable and thermally induced flexible composite phase change material for thermal energy storage and thermal management applications. Appl Energ 2019;236:10-21.

[112] Lian QS, Li T, Sayyed AAAS, et al. Facile strategy in designing epoxy/paraffin multiple phase change materials for thermal energy storage applications. Acs Sustain Chem Eng 2018;6:3375-84.

[113] Su JF, Zhao YH, Wang XY, et al. Effect of interface debonding on the thermal conductivity of microencapsulated-paraffin filled epoxy matrix composites. Compos Part A-Appl S 2012;43:325-32.

[114] Naria EA, Miguel AAF, Andres SG, et al. Novel formulations of phase change materials epoxy composites for thermal energy storage. Materials 2018;11:1-18.

[115] Ma TT, Li LP, Wang QW, et al. High-performance flame retarded paraffin/ epoxy resin form-stable phase change material. J Mater Sci 2019;54:875-85.

[116] Chen P, Gao XN, Wang YQ, et al. Metal foam embedded in SEBS/paraffin/HDPE form-stable PCMs for thermal energy storage. Sol Energ Mat Sol C 2016;149:60-5

[117] Pan MQ, Zhong YJ. Experimental and numerical investigation of a thermal management system for a Li-ion battery pack using cutting copper fiber sintered

skeleton/paraffin composite phase change materials. Int J Heat Mass Tran 2018;126:531-43

[118] Wang ZY, Situ WF, Li XX, et al. Novel shape stabilized phase change material based on epoxy matrix with ultrahigh cycle life for thermal energy storage. Appl Therm Eng 2017;123:1006-12.

[119] Lv YF, Yang XQ, Li XX, et al. Experimental study on a novel battery thermal management technology based on low density polyethylene-enhanced composite phase change materials coupled with low fins. Appl Energ 2016;178:376-82.

[120] Zhang JY, Li XX, Zhang GQ, et al. Experimental investigation of the flame retardant and form-stable composite phase change materials for a power battery thermal management system. J Power Sources 2020;480:229116.

[121] Grosu Y,Zhao YQ, Giacomello A, et al. Hierarchical macro-nanoporous metals for leakage-free high-thermal conductivity shape-stabilized phase change materials. Appl Energ 2020;269:115088.

[122] Liu CZ, Wang C, Li YM, et al. Preparation and characterization of sodium thiosulfate pentahydrate/silica microencapsulated phase change material for thermal energy storage. RSC Adv 2017;7:7238.

[123] Tao ZC, Wang HB, Liu JQ. Dual-level packaged phase change materials thermal conductivity and mechanical properties. Sol Energ Mat Sol C 2017;169:222-5.

[124] Xiao CR, Zhang GQ, Li ZH, et al. Custom design of solid-solid phase change material with ultra-high thermal stability for battery thermal management. RSC Adv 2020;8:14624.

[125] Kazanci B, Cellat K, Paksoy H. Preparation, characterization, and thermal properties of novel fire-resistant microencapsulated phase change materials based on paraffin and a polystyrene shell. RSC Adv 2020;10:24134-44.

[126] Demirbag S, Aksoy SA. Encapsulation of phase change materials by complex coacervation to improve thermal performances and flame retardant properties of the cotton fabrics. Fiber Polym 2016;17:408-17.

[127] Qiu XL, Lu LX, Chen ZZ. Preparation and characterization of flame retardant

phase change materials by microencapsulated paraffin and diethyl ethylphosphonate with poly(methacrylic acid-*co*-ethyl methacrylate) shell. J Appl Polym Sci 2015;132(17) DOI: 10.1002/app.41880.

[128] Davis DA, Work DE, Riazzi TJ. Microencapsulation of a phase change material with enhanced flame resistance. *US Pat.* Application No. 12/575,507, 2010.

[129] Sittisart P, Farid MM. Fire retardants for phase change materials, Appl Energ 2011;88:3140-5.

[130] Fang GY, Li H, Chen Z, et al. Preparation and properties of palmitic acid/$SiO_2$ composites with flame retardant as thermal energy storage materials._Sol Energ Mat Sol C 2011;95:1875-81.

[131] Zhang P, Hu Y, Song L, et al. Synergistic effect of iron and intumescent flame retardant on shape-stabilized phase change material. Thermochim Acta 2009;487:74-9.

[132] Cai YB, Wei QF, Huang FL, et al. Thermal stability, latent heat and flame retardant properties of the thermal energy storage phase change materials based on paraffin/high density polyethylene composites. Renew Energ 2009;34:2117-23.

[133] Cai YB, Wei QF, Huang FL, et al. Preparation and properties studies of halogen-free flame retardant form-stable phase change materials based on paraffin/high density polyethylene composites. Appl Energ 2008;85:765-75.

[134] Du XS, Fang YL, Cheng X, et al. Fabrication and characterization of flame-retardant nanoencapsulated *n*-Octadecane with melamine-formaldehyde shell for thermal energy storage. ACS Sustain Chem Eng 2018;11:15541-9.

[135] Du XS, Wang S, Du ZL, et al. Preparation and characterization of flame-retardant nanoencapsulated phase change materials with poly(methylmethacrylate) shells for thermal energy storage. J Mater Chem A 2018; 6:17519-17529.

[136] Xu L, Liu X, An ZH, et al. EG-based coatings for flame retardance of shape stabilized phase change materials. Polym Degrad and Stabil 2019; 161: 114-20.

[137] Wang JP, Wang Y, Yang R, et al. Flame retardance property of shape-stabilized phase change materials. Sol Energ Mat Sol C 2015; 140:439-45.

[138] Wang BB, Sheng HB, Shi YQ , et al. Recent advances for microencapsulation of flame retardant. Polym Degrad and Stabil 2015; 113:96-109.

[139] Huang YH, Cheng YX, Zhao R, et al. A high heat storage capacity form-stable composite phase change material with enhanced flame retardancy. Appl Energ 2020; 262:114536.

[140] Weng JY, Ouyang DX, Yang XQ, et al. Alleviation of thermal runaway propagation in thermal management modules using aerogel felt coupled with flame-retarded phase change material. Energ Convers Manage 2019;200:112071.

[141] Ma TT, Li LP, Wang QW, et al. High-performance flame retarded paraffin/epoxy resin form-stable phase change material. J Mater Sci 2019;54:875-85.

[142] Li LP, Wang G, Guo CG. Influence of intumescent flame retardant on thermal and flame retardancy of eutectic mixed paraffin/polypropylene form-stable phase change materials. Appl Energ 2016;162:428-34.

[143] Zhang P, Song L, Lu HD, et al. The thermal property and flame retardant mechanism of intumescent flame retardant paraffin system with metal. Ind Eng Chem Res 2010;49:6003-9.

[144] Zhang P, Hu Y, Song L, et al. Effect of expanded graphite on properties of high-density polyethylene/paraffin composite with intumescent flame retardant as a shape-stabilized phase change material. Sol Energ Mat Sol C 2010;94:360-5.

[145] Zhang P, Song L, Lu HD, et al. The influence of expanded graphite on thermal properties for paraffin/high density polyethylene/chlorinated paraffin/antimony trioxide as a flame retardant phase change material. Energ Convers Manage 2010;51:2733-37.

[146] Song GL, Ma SD, Tang GY, et al. Preparation and characterization of flame retardant form-stable phase change materials composed by EPDM, paraffin and nano magnesium hydroxide. Energy 2010;35:2179-83.

[147] Karimi G, Azizi M, Babapoor A. Experimental study of a cylindrical lithium ion battery thermal management using phase change material composites. J Energy Storage 2016;8:168-74.

[148] Kizilel R, Lateef A, Sabbah R, et al. Passive control of temperature excursion

and uniformity in high-energy Li-ion battery packs at high current and ambient temperature. J Power Sources 2008; 183:370-5.

[149] Wang ZY, Li XX, Zhang GQ, et al. Thermal management investigation for lithium-ion battery module with different phase change materials. RSC Adv 2017; 7:42909.

[150] Wang ZY, Li XX, Zhang GQ, et al. Experimental study of a passive thermal management system for three types of battery using copper foam saturated with phase change materials. RSC Adv 2017; 7:27441.

[151] Khateeb SA, Amiruddin S, Farid M, et al. Thermal management of Li-ion battery with phase change material for electric scooters: experimental validation. J Power Sources 2005;142:345-53.

[152] Wang Z, Zhang Z, Jia L, et al. Paraffin and paraffin/aluminum foam composite phase change material heat storage experimental study based on thermal management of Li-ion battery. Appl Therm Eng 2015;78:428-36.

[153] Zhang GQ, Zhang YY, Rao ZH. Phase change materials coupled with copper foam for thermal management of lithium-Ion battery. Advanced Science, Engineering and Medicine 2012;4:484-7.

[154] Li WQ, Qu ZG, He YL, et al. Experimental study of a passive thermal management system for high-powered lithium ion batteries using porous metal foam saturated with phase change materials. J Power Sources 2014;255:9-15.

[155] Qu ZG, Li WQ, Tao WQ. Numerical model of the passive thermal management system for high-power lithium ion battery by using porous metal foam saturated with phase change material. Int J of Hydrogen Energ 2014;39:3904-13.

[156] Somasundaram K, Birgersson E, Mujumdar AS. Thermal-electrochemical model for passive thermal management of a spiral-wound lithium-ion battery. J Power Sources 2012;203:84-96.

[157] Sabbah R, Kizilel R, Selman JR, et al. Active (air-cooled) vs passive (phase change material) thermal management of high power lithium-ion packs: limitation of temperature rise and uniformity of temperature distribution. J Power Sources 2008;182:630-8.

[158] Ling Z, Chen J, Fang X, et al. Experimental and numerical investigation of the application of phase change materials in a simulative power batteries thermal management system. Appl Energ 2014;121:104-13.

[159] Fathabadi H. High thermal performance lithium-ion battery pack including hybrid active-passive thermal management system for using in hybrid/electric vehicles. Energy 2014;70:529-38.

[160] Zhang JY, Li XX, He FQ, et al. Experimental investigation on thermal management of electric vehicle battery module with paraffin/expanded graphite composite phase change material. Int J Photoenergy 2017;2929473.

[161] Wilke S, Schweitzer B, Khateeb S, et al. Preventing thermal runaway propagation in lithium ion battery packs using a phase change composite material: an experimental study. J Power Sources 2017;340:51-9.

[162] Rao ZH, Huo YT, Liu XJ, et al. Experimental Investigation of battery thermal management system for electric vehicle based on paraffin/copper foam. J Energy Inst, 2014.

[163] Moraga NO, Xamán JP, Araya RH. Cooling Li-ion batteries of racing solar car by using multiple phase change materials. Appl Therm Eng 2016;108:1041-54.

[164] Nashei R, Alamatsaz A, Salimpour MR. Using multi-shell phase change materials layers for cooling a lithium-ion battery. Therm Sci 2016;20:391-403.

[165] Al-Hallaj, S., Selman, J. R. Thermal modeling of secondary lithium batteries for electric vehicle/hybrid electric vehicle applications. J Power Sources 2002;110:341-8.

[166] Al-Hallaj, S., Selman, J. R. A novel thermal management system for electric vehicle batteries using phase-change material. J Electrochem Soc 2000;147:3231-6.

[167] Talluri T, Kim TH, Shin KJ. Analysis of a batterypack with a phase change material for the extreme temperature conditions of an electrical vehicle. Energies 2020;13:1-15.

[168] Lazrak A, Fourmigue JF, Robin JF. An innovative practical battery thermal management system based on phase change materials: numerical and experimental investigations. Appl Therm Eng 2018;128:20-32.

[169] Rao ZH, Wang SF, Zhang GQ. Simulation and experiment of thermal energy

management with phase change material for ageing $LiFePO_4$ power battery. Energ Convers Manage 2011;52:3408-14.

[170] Ouyang DX, Weng JW, Hu JY, et al. Experimental investigation of thermal failure propagation in typical lithium-ion battery modules. Thermochimica Acta 2019;676:205-13.

[171] Wang Z, Wang J, et al. Investigation of external heating-induced failure propagation behaviors in large-size cell modules with different phase change materials. Energy 2020;204:117946.

[172] Sun QR, Zhang HQ, Xue JJ, et al. Flexible phase change materials for thermal storage and temperature control. Chem Eng J 2018;353:920-9.

[173] Li WW, Cheng WL, Xie B, et al. Thermal sensitive flexible phase change materials with high thermal conductivity for thermal energy storage. Energ Convers Manage 2017;149:1-12.

[174] Qi XD, Shao YW, Wu HY, et al. Flexible phase change composite materials with simultaneous light energy storage and light-actuated shape memory capability. Compos Sci Technol 2019; DOI: 10.1016/j.compscitech.2019.107714.

[175] Wu WX, Wu W, Wang SF. An innovative battery thermal management with thermally induced flexible phase change material. Energ Convers Manage 2019;236:10-21.

[176] Zhang Q, He ZB, Fang XM, et al. Experimental and numerical investigations on a flexible paraffin/fiber composite phase change material for thermal therapy mask. Energy Storage Mater 2017;6:36-45.

[177] Cai ZD, Liu J, Zhou YX, et al. Flexible phase change materials with enhanced tensile strength, thermal conductivity and photo-thermal performance. Sol Energ Mat Sol C 2021;219:110728.

[178] Wu S, Li TX, Wu MQ, et al. Highly thermally conductive and flexible phasechange composites enabled by polymer/graphite nanoplatelet-based dual networks for efficient thermal management. J Mater Chem A 2020;8: 20011.

[179] Huang QQ, Li XX, Zhang GQ, et al. Thermal management of Lithium-ion battery pack through the application of flexible form-stable composite phase change

materials. Appl Therm Eng 2021;183: 116151.

[180] Zhao JT, Wu CH, Rao ZH. Investigation on the cooling and temperature uniformity of power battery pack based on gradient phase change materials embedded thin heat sinks. Appl Therm Eng 2020;174: 115304.

[181] Lv YF, Liu GJ, Zhang GQ, et al. A novel thermal management structure using serpentine phase change material coupled with forced air convection for cylindrical battery modules. J Power Sources 2020;468: 228398.

[182] Jilte RD, Kumar R, Ahmadi MH, et al. Battery thermal management system employing phase change material with cell-to-cell air cooling. Appl Therm Eng 2019;161: 114199.

[183] Ling ZY, Wang FX, Fang XM, et al. A hybrid thermal management system for lithium ion batteries combining phase change materials with forced-air cooling. Appl Energ 2015;148: 403-9.

[184] Qin P, Liao MR, Zhang DF, et al. Experimental and numerical study on a novel hybrid battery thermal management system integrated forced-air convection and phase change material. Energ Convers Manage 2019;195: 1371-81.

[185] Xie YQ, Tang JC, Shi F, et al. Experimental and numerical investigation on integrated thermal management for lithium-ion battery pack with composite phase change materials. Energ Convers Manage 2017;154: 562-75.

[186] Jiang GW, Huang JH, Liu MC, et al. Experiment and simulation of thermal management for a tube-shell li-ion battery pack with composite phase change material. Appl Therm Eng 2017;120: 1-9.

[187] Kermani MM, Houshfar E, Ashjaee M. A novel hybrid thermal management for Li-ion batteries using phase change materials embedded in copper foams combined with forced-air convection. Int J Therm Sci 2019;141: 47-61.

[188] Lu YH, Wei FR, Lai DD, et al. A novel personal cooling system (PCS) incorporated with phase change materials (PCMs) and ventilation fans: An investigation on its cooling efficiency. J Therm Biol 2015;52: 137-46.

[189] Shi S, Xie YQ, Li M, et al. Non-steady experimental investigation on an integrated thermal management system for power battery with phase change materials.

Energ Convers Manage 2017;138: 84-96.

[190] Situ WF, Zhang GQ, Li XX, et al. A thermal management system for rectangular $LiFePO_4$ battery module using novel double copper mesh-enhanced phase change material plates. Energy 2017;141: 613-23.

[191] Pielichowska K, Pielichowski K. Phase change materials for thermal energy storage. Prog Mater Sci 2014;65: 67-123.

[192] Du K, Calautit J, Wang ZH, et al. A review of the applications of phase change materials in cooling, heating and power generation in different temperature ranges. Appl Energ 2018;220: 242-73.

[193] Huang X, Alva G, Jia YT, et al. Morphological characterization and applications of phase change materials in thermal energy storage: A review. Renew Sust Energ Rev 2017;72: 128-45.

[194] Subramanian M, Hoang AT, B Kalidasan, et al. A technical review on composite phase change material based secondary assisted battery thermal management system for electric vehicle . J Clean Prod 2021;322:129079.

[195] Wu WX, Wang SF, Wu W, et al. A critical review of battery thermal performance and liquid based battery thermal management. Energ Convers Manage 2019;182:262-81.

[196] Huo YT, Rao ZH, Liu XJ, et al. Investigation of power battery thermal management by using mini-channel cold plate. Energ Convers Manage 2015;89:387-95.

[197] Qian Z, Li YM, Rao ZH. Thermal performance of lithium-ion battery thermal management system by using mini-channel cooling. Energ Convers Manage 2016;126:622-31.

[198] Liu HL, Shi HB, Shen H, et al. The performance management of a Li-ion battery by using tree-like mini-channel heat sinks: experimental and numerical optimization. Energy 2019;189:116150.

[199] Zhao YQ, Zou BY, Li C, et al. Active cooling based battery thermal management using composite phase change materials. Energy Procedia 2019;158: 4933-40.

[200] Rao ZH, Wang QC, Huang CL. Investigation of the thermal performance of phase change material/mini-channel coupled battery thermal management system. Appl Energ 2016;164: 659-69.

[201] Ling ZY, Cao JC, Zhang WB, et al. Compact liquid cooling strategy with phase change materials for Li-ion batteries optimized using response surface methodology. Appl Energ 2018;228: 777-88.

[202] Hekmat S, Molaeimanesh GR. Hybrid thermal management of a Li-ion battery module with phase change material and cooling water pipes: An experimental investigation. Appl Therm Eng 2020;166: 114759.

[203] Hemmery CV, Pra F, Robin JF, et al. Experimental performances of a battery thermal management system using a phase change material. J Power Sources 2014;270:349-58.

[204] Bai FF, Chen MB, Song WJ, et al. Thermal management performances of PCM/water cooling-plate using for lithium-ion battery module based on non-uniform internal heat source. Appl Therm Eng 2017;126:17-27.

[205] Kong DP, Peng RQ, Ping P, et al. A novel battery thermal management system coupling with PCM and optimized controllable liquid cooling for different ambient temperatures. Energ Convers Manage 2020;204:112280.

[206] Lopez CF, Jeevarajan JA, Mukherjee PP. Evaluation of combined active and passive thermal management strategies for lithium-ion batteries. J Electrochem Energy 2016;13:031007-10.

[207] Song LM, Zhang HY, Yang C. Thermal analysis of conjugated cooling configurations using phase change material and liquid cooling techniques for a battery module. Int J Heat Mass Tran2019;133:827-41.

[208] Kshetrimayum KS, Yoon YG, Gye HR, et al. Preventing heat propagation and thermal runaway in electric vehicle battery modules using integrated PCM and micro-channel plate cooling system. Appl Therm Eng 2019;159:113797.

[209] Cao JH, Luo MY, Fang XM, et al. Liquid cooling with phase change materials for cylindrical Li-ion batteries: An experimental and numerical study. Energy 2020;191:116565.

[210] Wu XY, Zhu ZH, Zhang HY, et al. Structural optimization of light-weight battery module based on hybrid liquid cooling with high latent heat PCM. Int J Heat Mass Tran 2020;163:120495.

[211] Ding B, Qi ZH, Mao CS, et al. Numerical investigation on cooling performance of PCM/cooling plate hybrid system for power battery with variable discharging conditions. J Therm Anal Calorim 2020;141:625-33.

[212] Li JW, Zhang HY. Thermal characteristics of power battery module with composite phase change material and external liquid cooling. Int J Heat Mass Tran 2020;156:119820.

[213] Jaguemon J, Omar N, Bossche PVD, et al. Phase-change materials (PCM) for automotive applications: A review. Appl Therm Eng 2018;132:308-20.

[214] An ZG, Chen X, Zhao L, et al. Numerical investigation on integrated thermal management for a lithium-ion battery module with a composite phase change material and liquid cooling. Appl Therm Eng 2019;163:114345.

[215] Wang FX, Cao JH, Ling ZY, et al. Experimental and simulative investigations on a phase change material nano-emulsion-based liquid cooling thermal management system for a lithium-ion battery pack. Energy 2020;207:118215.

[216] Mashayekhi M, Houshfar E, Ashjaee M. Development of hybrid cooling method with PCM and $Al_2O_3$ nanofluid in aluminium minichannels using heat source model of Li-ion batteries. Appl Therm Eng 2020;178:115543.

[217] Ali HM. Applications of combined/hybrid use of heat pipe and phase change materials in energy storage and cooling systems: A recent review. J Energy Storage 2019;26: 100986.

[218] Sharifi N, Faghri A, Bergman TL, et al. Simulation of heat pipe-assisted latent heat thermal energy storage with simultaneous charging and discharging. Int J Heat Mass Tran 2015;80: 170-9.

[219] Amini A, Miller J, Jouhara H. An investigation into the use of the heat pipe technology in thermal energy storage heat exchangers. Energy 2017;136: 163-72.

[220] Qu J, Ke ZQ, Zuo AH, et al. Experimental investigation on thermal performance of phase change material coupled with three-dimensional oscillating heat

pipe (PCM/3D-OHP) for thermal management application. Int J Heat Mass Tran 2019;129: 773-82.

[221] Behi H, Ghanbarpour M, Behi M. Investigation of PCM-assisted heat pipe for electronic cooling. Appl Therm Eng 2017;127: 1132-42.

[222] Chen MY, Zhang SY, Wang GY, et al. Experimental analysis on the thermal management of lithium-Ion batteries based on phase change materials. Appl Sci 2020;10: 7354.

[223] Greco A, Jiang X, Cao DP. An investigation of lithium-ion battery thermal management using paraffin/porous-graphite-matrix composite. J Power Sources 2015;278: 50-68.

[224] Wang QC, Rao ZH, Huo YT, et al. Thermal performance of phase change material/oscillating heat pipe-based battery thermal management system. Int J Therm Sci 2016;102: 9-16.

[225] Lei SR, Shi Y, Chen GY. A lithium-ion battery-thermal-management design based on phase-change-material thermal storage and spray cooling. Appl Therm Eng 2020;168: 114792.

[226] Yuan QQ, Xu XM, Tong GY, et al. Effect of coupling phase change materials and heat pipe on performance enhancement of Li-ion battery thermal management system. Int J Energ Res 2020; https://doi.org/10.1002/er.6165.

[227] Zhao JT, Lv PZ, Rao ZH. Experimental study on the thermal management performance of phase change material coupled with heat pipe for cylindrical power battery pack. Exp Therm Fluid Sci 2017;82: 182-8.

[228] HATA H, WADA SP, HIRATA K, et al. Performance evaluation of a battery-cooling system using phase-change materials and heat pipes for electric vehicles under the short-circuited battery condition. J Therm Sci Tech 2018; https://doi.org/10.1299/jtst.2018jtst0024.

[229] YAMADA T, KOSHIYAMA T, YOSHIKAWA M, et al. Analysis of a lithium-ion battery cooling system for electric vehicles using a phase-change material and heat pipes. J Therm Sci Tech 2017; 12:1-15.

[230] Putra N, Sandi AF, Ariantara B, et al. Performance of beeswax phase change

material (PCM) and heat pipe as passive battery cooling system for electric vehicles. Case Stud Therm Eng 2020; 21:100655.

[231] Chen YB, Cao HZ, Li HX, et al. Experimental study on coupled cooling system of PCM-heat pipe for vehicle power battery pack. Advances in Engineering Research 2015; https://doi.org/10.2991/eame-15.2015.127.

[232] Zhang WC, Qiu JY, Yin XX, et al. A novel heat pipe assisted separation type battery thermal management system based on phase change material. Appl Therm Eng; 2020;165: 114571.

[233] Huang QQ, Li XX, Zhang GQ, et al. Experimental investigation of the thermal performance of heat pipe assisted phase change material for battery thermal management system. Appl Therm Eng; 2018;141: 1092-100.

[234] Motahar S, Khodabandeh R. Experimental study on the melting and solidification of a phase change material enhanced by heat pipe. Int Commun Heat Mass; 2016;73: 1-6.

[235] Allen MJ, Sharifi N, Faghri A, et al. Effect of inclination angle during melting and solidification of a phase change material using a combined heat pipe-metal foam or foil configuration. Int J Heat Mass Tran 2015;80: 767-80.

[236] Robak CW, Bergman TL, Faghri A. Enhancement of latent heat energy storage using embedded heat pipes. Int J Heat Mass Tran 2011;54: 3476-84.

[237] Li XX, Zhong ZD, Luo JH, et al. Experimental investigation on a thermoelectric cooler for thermal management of a Lithium-ion battery module. Int J Photoenery 2019; 3725364.

[238] Elsheikh MH, Shnawah DA, Sabri MFM, et al. A review on thermoelectric Renew Energ: Principle parameters that affect their performance. Renew Sustain Energy Rev 2014;30: 337-55.

[239] He W, Zhang G, Zhang XX, et al. Recent development and application of thermoelectric generator and cooler. Appl Energ 2015;143: 1-25.

[240] Espinosa N, Lazard M, Aivala L, et al. Modeling a thermoelectric generator applied to diesel automotive heat recovery. J Electron Mater 2010;39: 1446-55.

[241] Zhao DL, Tan G. A review of thermoelectric cooling: Materials, modeling and

applications. Appl Therm Eng 2014;66: 15-24.

[242] Zhang WC, Xu KJ, Li LY, et al. Study on a battery thermal management system based on a thermoelectric effect. Energies 2020;11:1-15.

[243] Bell LE. Cooling, heating, generating power, and recovering waste heat with thermoelectric systems. Science 2008;321: 1457-61.

[244] Esfahanian V, Renani SA, Nehzati H, et al. Design and simulation of air cooled battery thermal management system using thermoelectric for a hybrid electric bus. Proceedings of the FISITA 2012 World Automotive Congress, Berlin, Heidelberg, 2013:463-73.

[245] Liu Y, Yang SC, Guo B, et al. Numerical analysis and design of thermal management system for lithium ion battery pack using thermoelectric coolers. Adv Mech Eng 2014;6: 852712.

[246] Liu ZY, Tang AK, Shan CX, et al. Assessing the impact of current control on the thermal management performance of thermoelectric cooling systems. Int J Energ Res 2014;1-14.

[247] Riffat SB, Ma XL. Improving the coefficient of performance of thermoelectric cooling systems: a review. Int J Energ Res 2004;28:753-68.

[248] Lyu Y, Siddique ARM, Majid SH, et al. Electric vehicle battery thermal management system with thermoelectric cooling. Energy Rep 2019;5:822-7.

[249] Zhang HY, Mui YC, Tarin M. Analysis of thermoelectric cooler performance for high power electronic packages. Appl Therm Eng 2010;30:561-8.

[250] Zhang CW, Chen SR, Gao HB, et al. Study of thermal management system using composite phase change materials and thermoelectric cooling sheet for power battery pack. Energies 2019;12: 1937.

[251] Manikandan S, Selvam C, Praful PS, et al. A novel technique to enhance thermal performance of a thermoelectric cooler using phase-change materials. J Therm Anal Calorim 2020;140: 1003-14.

[252] Jiang L, Zhang HY, Li JW, et al. Thermal performance of a cylindrical battery module impregnated with PCM composite based on thermoelectric cooling. Energy 2019;188: 116048.

[253] Cui TF, Xuan YM, Yin ES, et al. Experimental investigation on potential of a concentrated photovoltaic-thermoelectric system with phase change materials. Energy 2017;122: 94-102.

[254] Yin ES, Li Q, Li DH, et al. Experimental investigation on effects of thermal resistances on a photovoltaic-thermoelectric system integrated with phase change materials. Energy 2019;169: 172-85.

[255] Song WJ, Bai FF, Chen MB, et al. Thermal management of standby battery for outdoor base station based on the semiconductor thermoelectric device and phase change materials. Appl Therm Eng 2018;137: 203-17.

[256] Zhang JY, Li XX, Zhang GQ, et al. Experimental investigation on the essential cause of the degrading performances for an overcharging ternary battery. Int J Energ Res 2020;44:3134-47.

[257] Zhang JY, Yang XQ, Zhang GQ, et al. Investigation on the root cause of the decreased performances in the overcharged lithium iron phosphate battery. Int J Energ Res 2018;42:2448-55.

[258] Zhao X, Yin Y, Hu Y, et al. Electrochemical-thermal modeling of lithium plating/stripping of $Li(Ni_{0.6}Mn_{0.2}Co_{0.2})O_2$/carbon lithium-ion batteries at subzero ambient temperatures. J Power Sources 2019;418:61-73.

[259] Li Y, Wang CY. Heating strategies for Li-ion batteries operated from subzero temperatures. Electrochim Acta 2013;107:664-74.

[260] Jaguemont J, Boulon L, Dube Y. A comprehensive review of lithium-ion batteries used in hybrid and electric vehicles at cold temperatures. Appl Energ 2016;164:99-114.

[261] Peng XB, Chen SQ, Garg A, et al. A review of the estimation and heating methods for lithium-ion batteries pack at the cold environment. Energy Sci Eng 2019;7:645-662.

[262] Qiu JG, Yang XQ, Zhang GQ, et al. A study on structure-performance relationship of overcharged 18650-size $Li_4Ti_5O_{12}/LiMn_2O_4$ battery. J Therm Anal Calorim 2014;118:1413-8.

[263] Wu W, Wu W, Qiu X, et al. Low-temperature reversible capacity loss and aging

mechanism in lithium-ion batteries for different discharge profiles. Int J Energ Res 2019;43:243-53

[264] Zhao N, Li Y, Zhao X, et al. Effect of particle size and purity on the low temperature electrochemical performance of $LiFePO_4$/C cathode material. J Alloy Compd 2016;683:123-32.

[265] Zhao N, Zhi X, Wang L, et al. Effect of microstructure on low temperature electrochemical properties of $LiFePO_4$/C cathode material. J Alloy Compd 2015;645:301-8.

[266] Lei ZG，Zhang YW, Lei XG. Temperature uniformity of a heated lithium-ion battery cell in cold climate. Appl Therm Eng 2018;129:148-54.

[267] Jaguemont J, Boulon L, Venet P, et al. Lithium-ion battery aging experiments at subzero temperatures and model development for capacity fade estimation. IEEE Trans Veh Technol 2016;65:4328-43.

[268] Zhang JN, Sun FC, Wang ZP. Heating character of a $LiMn_2O_4$ battery pack at low temperature based on PTC and metallic resistance material. Energy Procedia 2017;105:2131-8.

[269] Zhu JG, Sun ZC, Wei XZ, et al. Experimental investigations of an AC pulse heating method for vehicular high power lithium-ion batteries at subzero temperatures. J Power Sources 2017;367:145-57.

[270] Zhong GJ, Zhang GQ, Yang XQ, et al. Researches of composite phase change material cooling/resistance wire preheating coupling system of a designed 18650-type battery module. Appl Therm Eng 2017;127:176-83.

[271] Huo YT, Rao ZH. Investigation of phase change material based battery thermal management at cold temperature using lattice Boltzmann method. Energ Convers Manage 2017;133:204-15.

[272] Lv YF, Yang XQ, Zhang GQ, et al. Experimental research on the effective heating strategies for a phase change material based power battery module. Int J Heat Mass Tran 2019;128:392-400.

[273] Fan RJ, Zhang CZ, Wang Y, et al. Numerical study on the effects of battery heating in cold climate. J Energy Storage 2019;26:100969.

[274] Ling ZY, Wen XY, Zhang ZG, et al. Thermal management performance of phase change materials with different thermal conductivities for Li-ion battery packs operated at low temperatures. Energy 2018;144:977-83.

[275] He FQ, Li XX, Zhang GQ, et al. Experimental investigation of thermal management system for lithium ion batteries module with coupling effect by heat sheets and phase change materials. Int J Energ Res 2018;42:3279-88.

[276] Ghadbeigi L, Day B, Lundgren K, et al. Cold temperature performance of phase change material based battery thermal management systems. Energy Rep 2018;4:303-7.

[277] Rao ZH, Wang SF, Zhang YL. Thermal management with phase change material for a power battery under cold temperatures. Energ Source Part A 2014;36:2287-95.

# Advanced thermal management system driven by phase change materials for power lithium-ion batteries: A review

Jiangyun Zhang[a,*], Dan Shao[d], Liqin Jiang[c], Guoqing Zhang[a], Hongwei Wu[b], Rodney Day[b], Wenzhao Jiang[a]

[a] *School of Materials and Energy, Guangdong University of Technology, Guangzhou, Guangdong 510006, China*

[b] *School of Physics, Engineering and Computer Science, University of Hertfordshire, Hatfield, AL10 9AB, United Kingdom*

[c] *Guangdong Zhuhai Supervision Testing Institute of Quality And Metrology, Zhuhai, 519000, China*

[d] *Guangdong Key Laboratory of Battery Safety, Guangzhou Institute of Energy testing, Guangzhou, Guangdong 511447, China*

The figures in this manuscript are as follows:

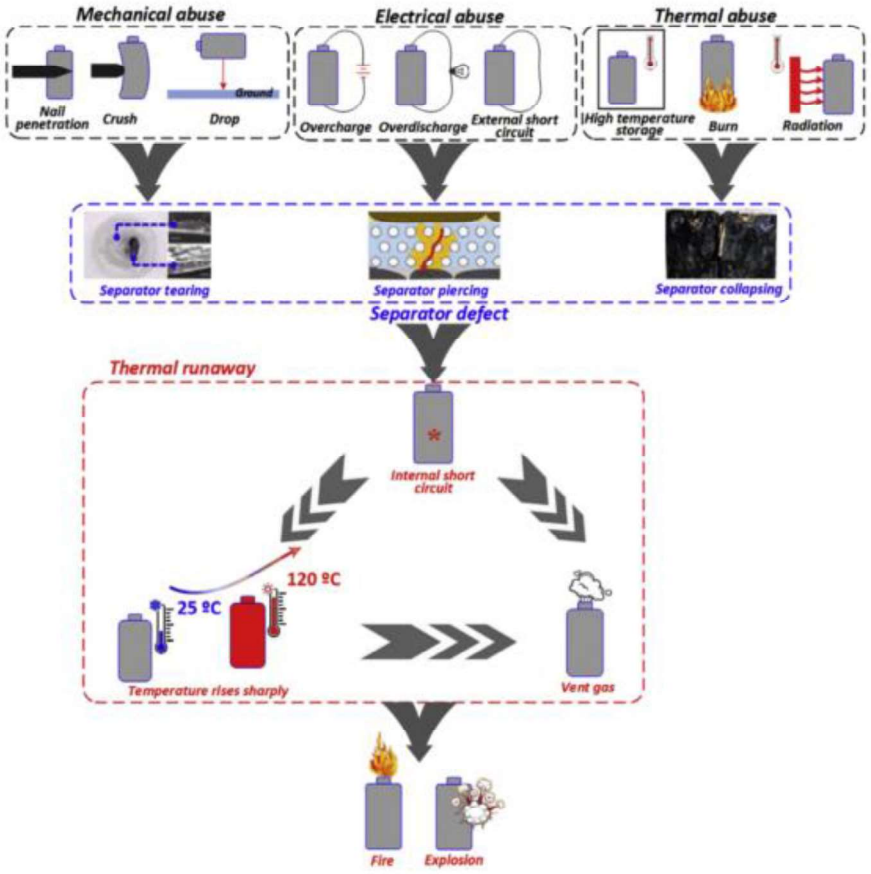


**Fig. 1.** Schematic of lithium-ion battery TR mechanism under different abusive conditions [7].

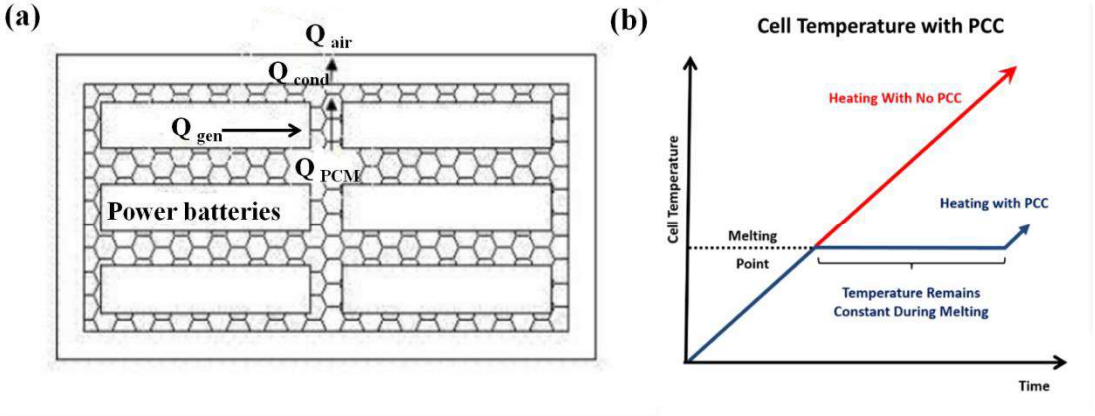


**Fig. 2.** Working principles of BTMS using PCM: (a) heat transfer mechanism of PCM-based cooling technology and (b) temperature-controlling and temperature-balancing theories of the phase change composite (PCC) BTMS [25,27].

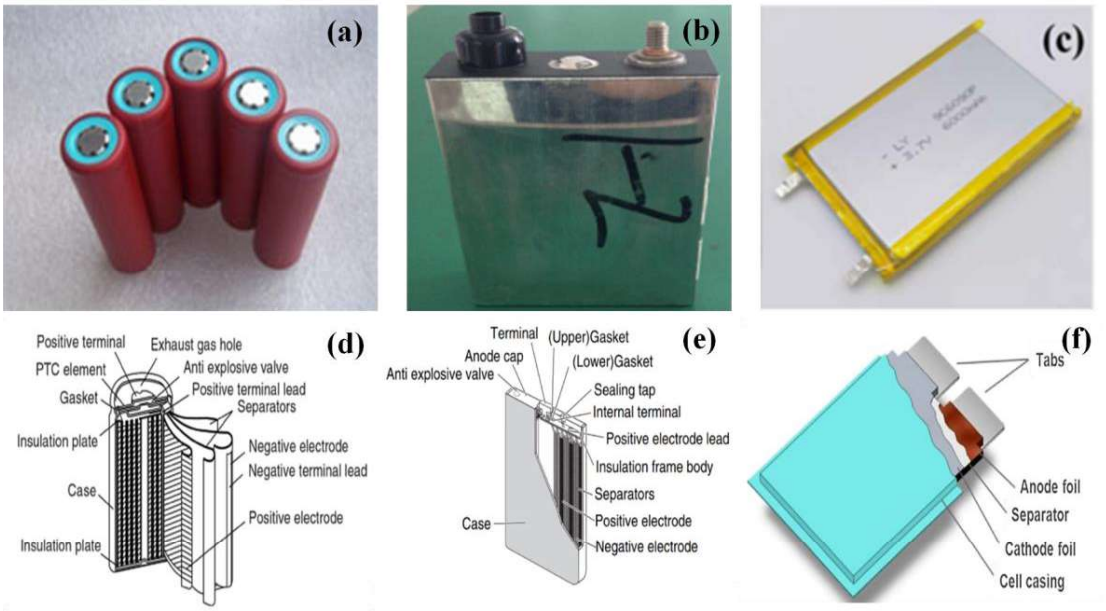


**Fig. 3.** Commonly used power lithium-ion batteries and their internal structure: (a) cylindrical cells, (b) rigid prismatic cells, (c) pouch cells, (d) cylindrical lithium-ion cell structure, (e) prismatic lithium-ion cell structure, and (f) lithium-ion cell pouch structure [37,38].

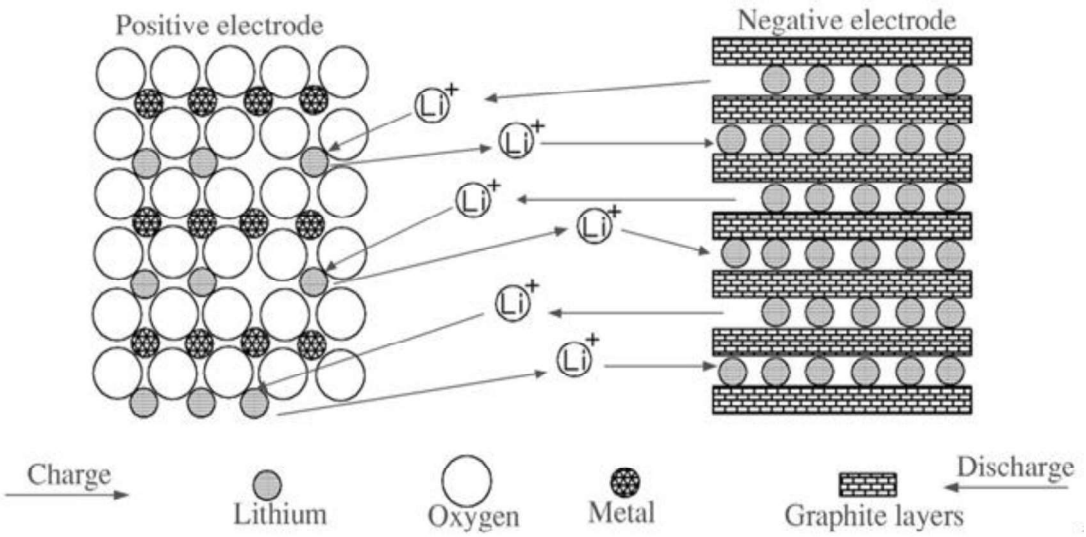


**Fig. 4.** Lithium-ion power battery working principle.

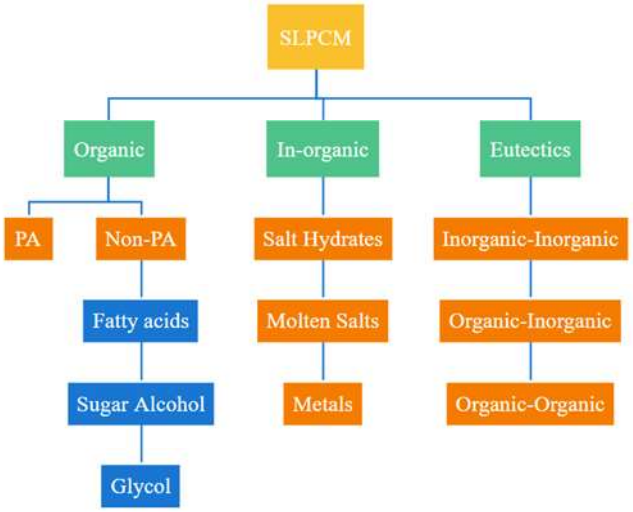


**Fig. 5.** Classification of SLPCM [36].

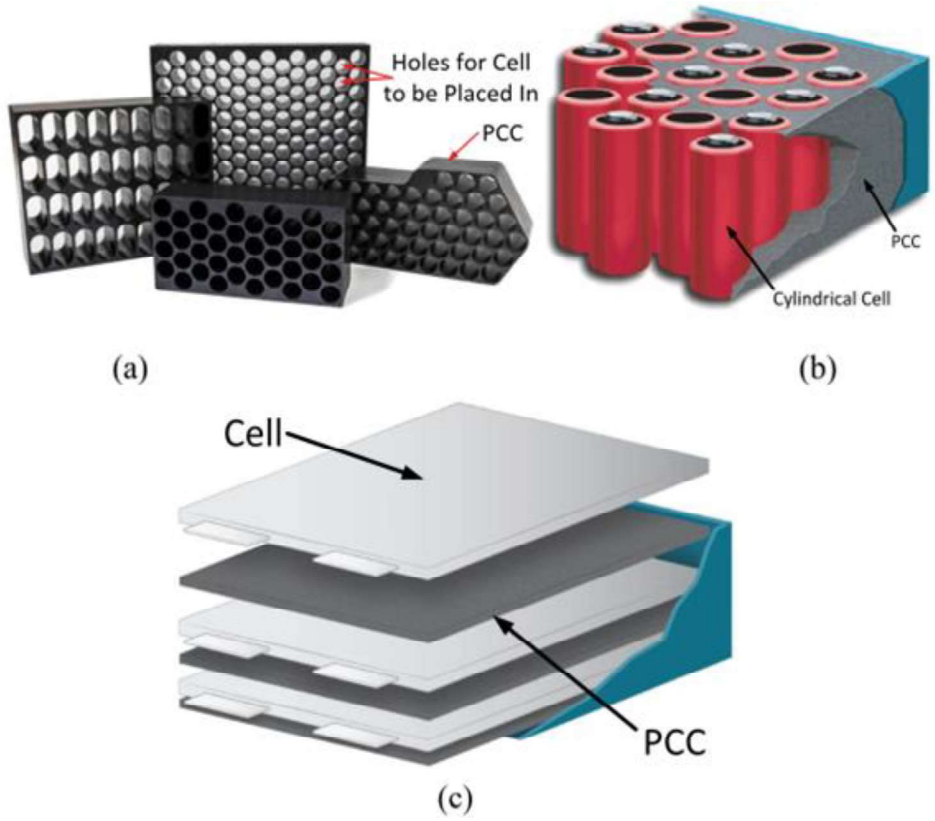


**Fig. 6.** Application forms of the composite PCMs in power systems: (a) fabricated PCM matrix; (b) PCC with cylindrical cells; and (c) PCC plates with prismatic cells [56,57].

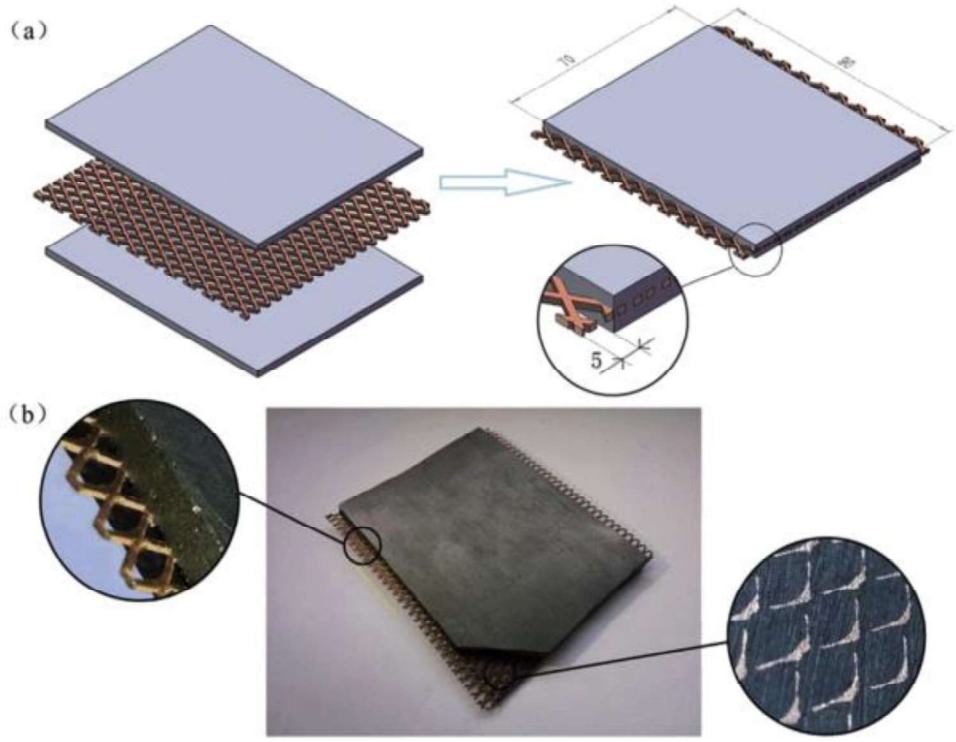


**Fig. 7.** Promoted thermal-conductive PA/EG composite PCMs [88].

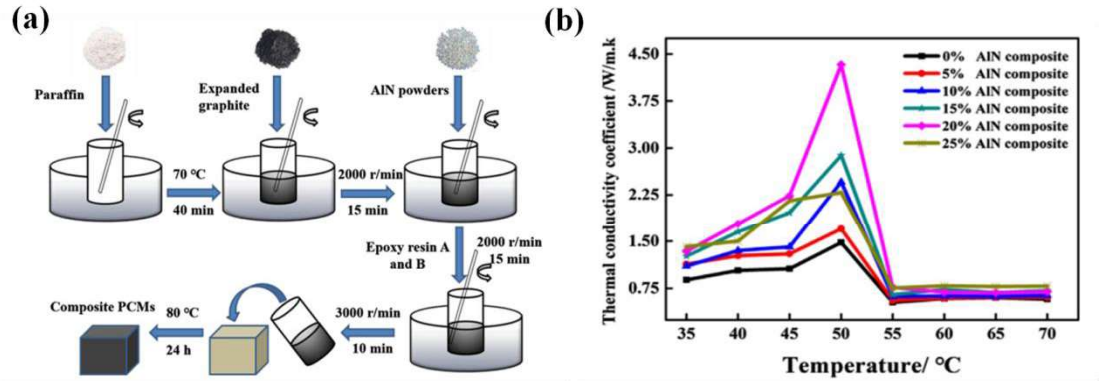


**Fig. 8.** PA/EG/epoxy resin composite PCMs with AlN as additives: (a) specific preparation process and (b) thermal conductivity property changes [89].

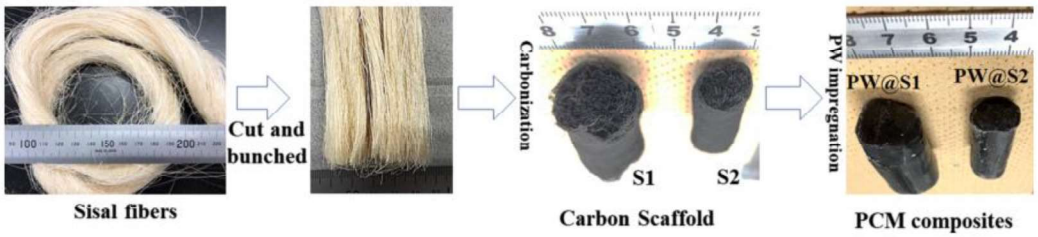


**Fig. 9.** Sisal-derived carbon scaffold and PA-based composite PCMs construction [90].

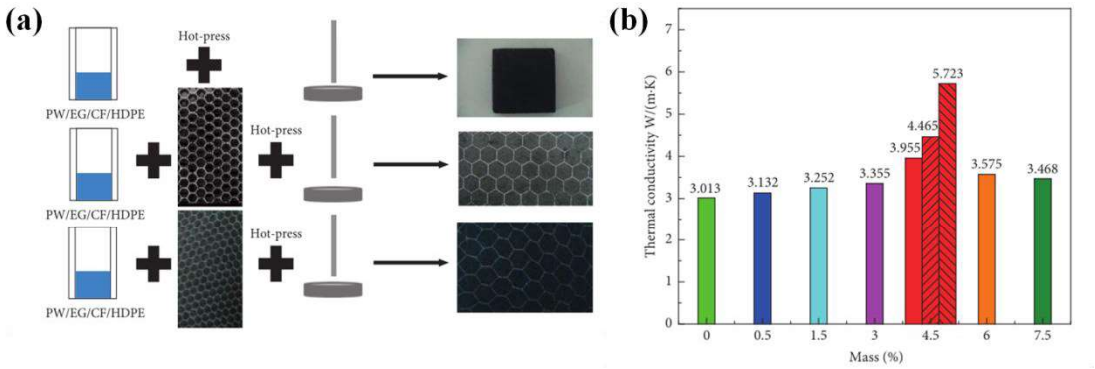


**Fig. 10.** PA/EG/carbon fiber/ HDPE composite PCMs: (a) specific preparation procedures and (b) thermal conductivity coefficient changes with different carbon fiber mass fractions [91].

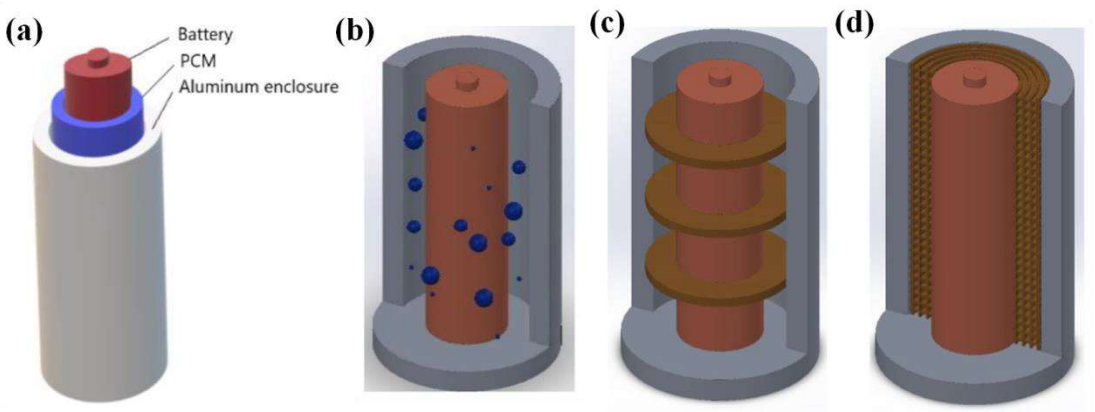

**Fig. 11.** Schematics of BTMS units with (a) pure PCM, (b) PCM/nanoparticles, (c) PCM/fins, and (d) PCM/metal foam [93].

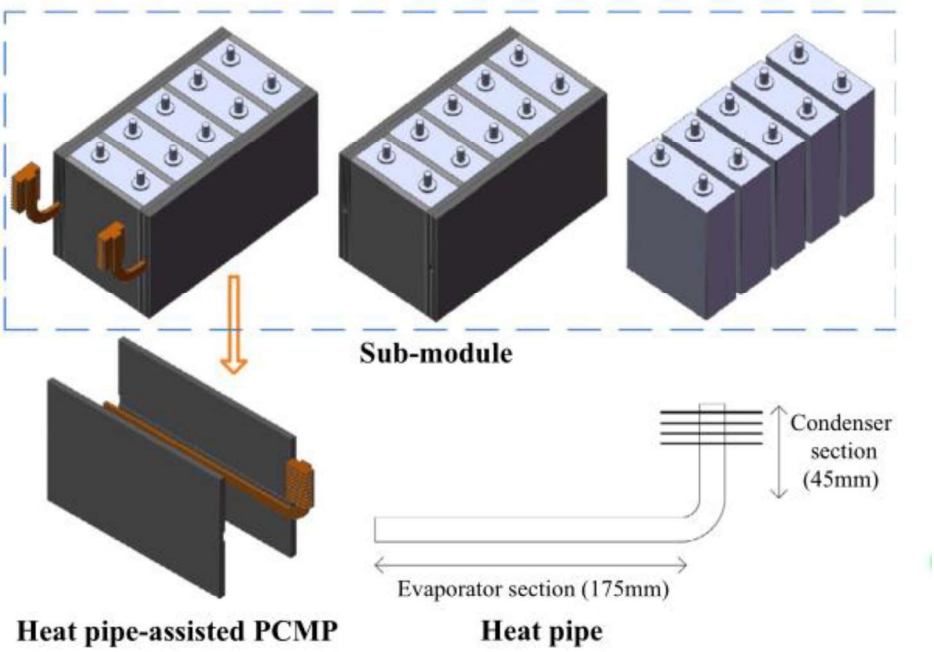


**Fig. 12.** PA/EG BTMS coupling with HP for the square batteries modules [100].


**Fig. 13.** Structural stability problems of PCM matrix during preparation and testing.

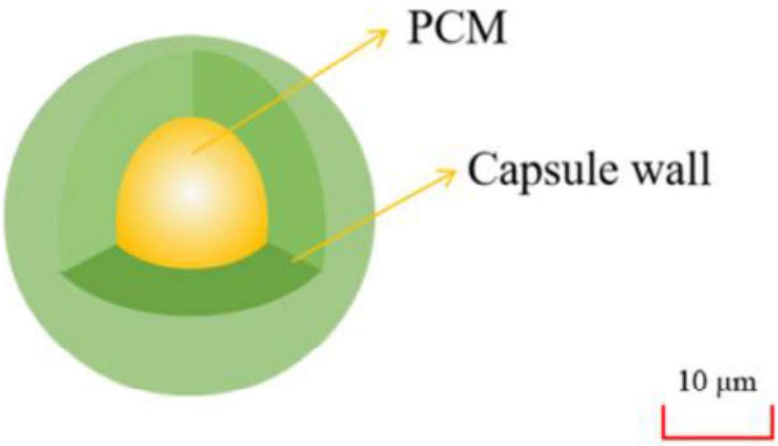


**Fig. 14.** Schematic diagram of MicroPCM.

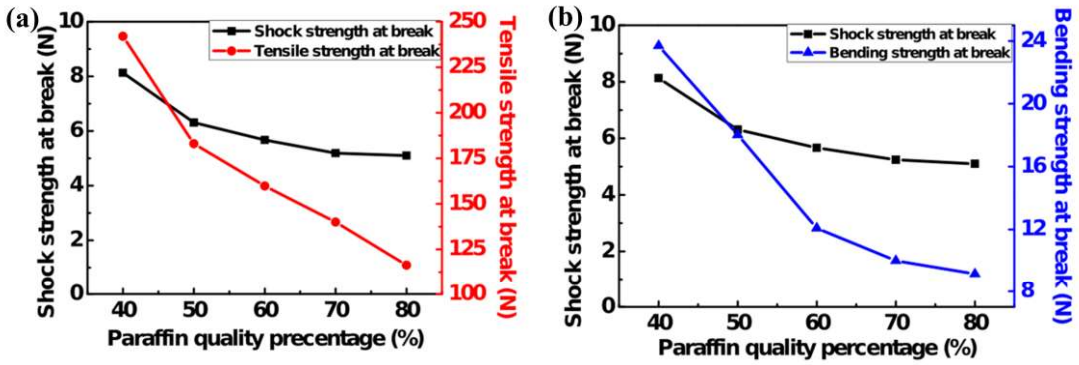


**Fig. 15.** Mechanical strengths variations: (a) shock and tensile strengths at break and (b) shock and bending strengths at break [118].

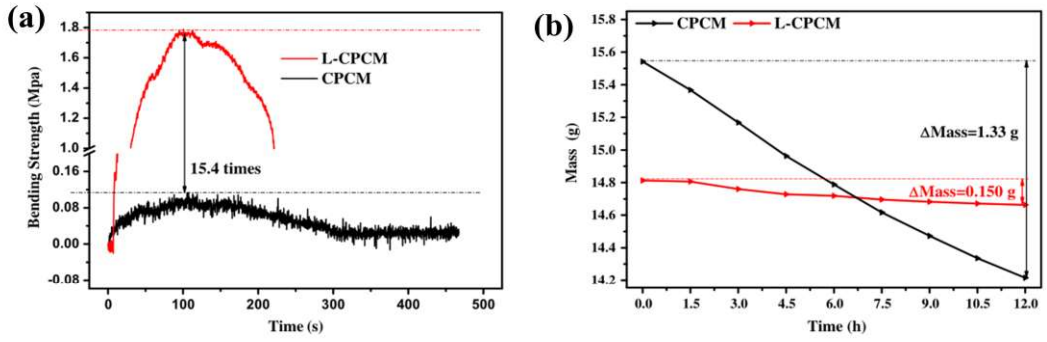


**Fig. 16.** Bending strength and leakage variations: (a) bending strength and (b) mass changes with time [119].

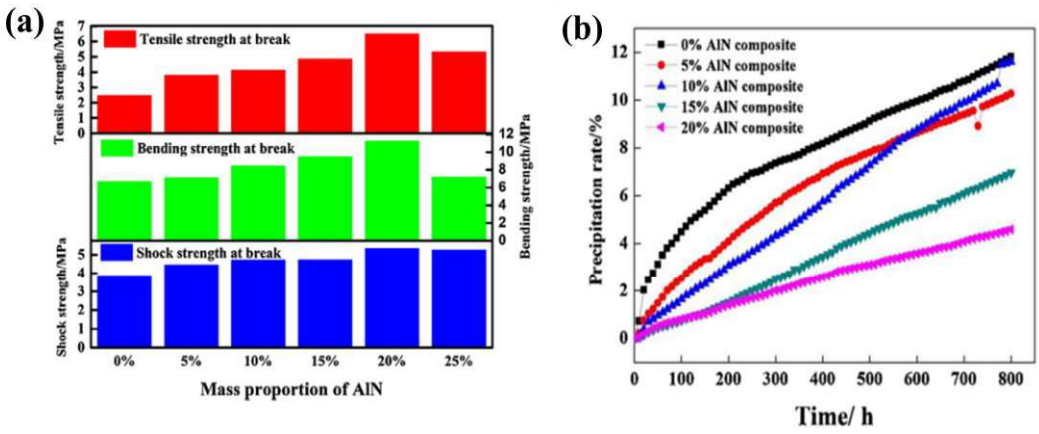


**Fig. 17.** Mechanical strength variations of different proportions of AlN powders in PCC: (a) tensile, bending strength, and shock strength at break and (b) leakage rate changes with testing time [120].

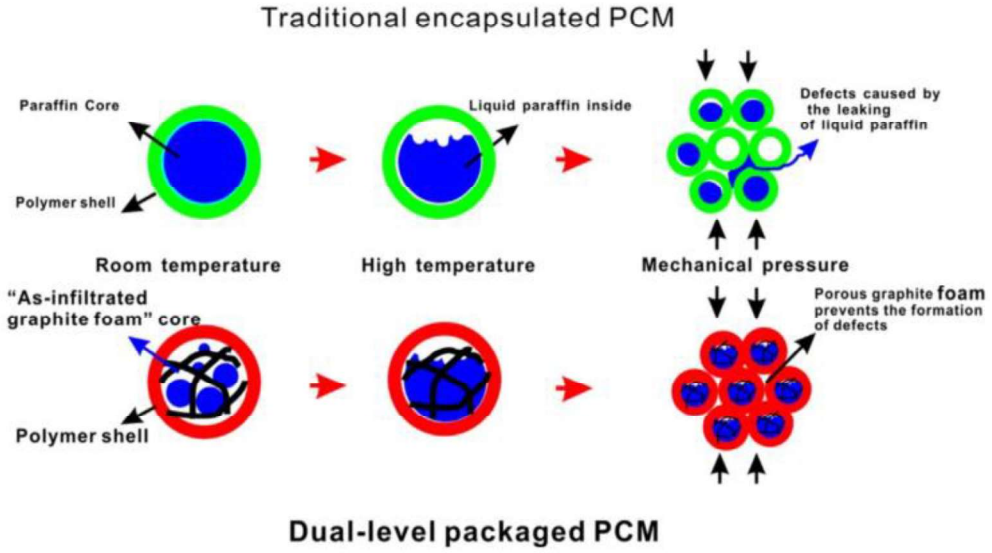


**Fig. 18.** Structure schematic of dual-level packaged PCMs at higher temperatures [123].

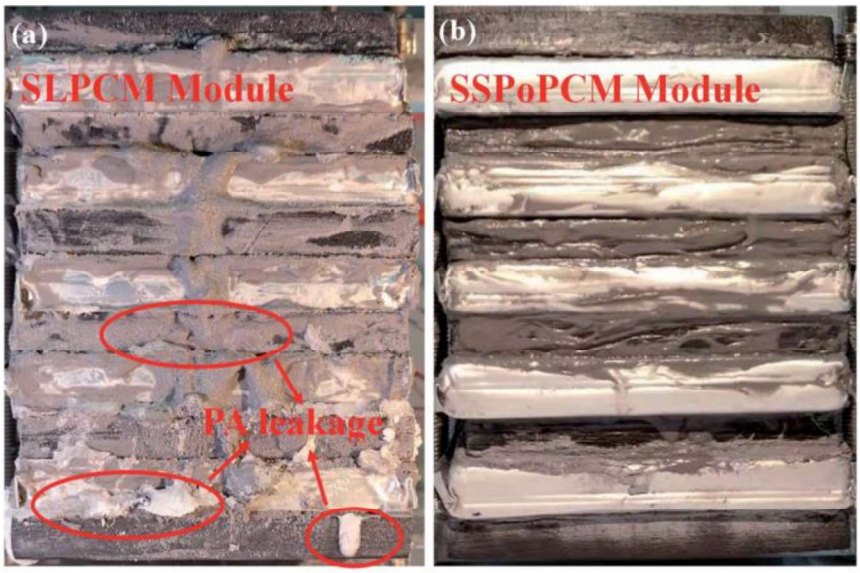


**Fig. 19.** Digital photographs of the PCC: (a) SLPCM and (b) solid-solid polymer PCM (SSPoPCM) modules after cycling [124].

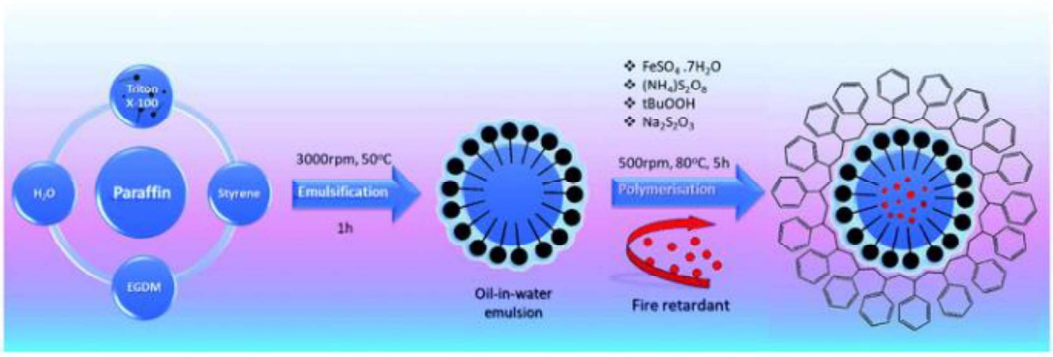


**Fig. 20.** PA-based MicroPCM production using fire-resistant additives [125].

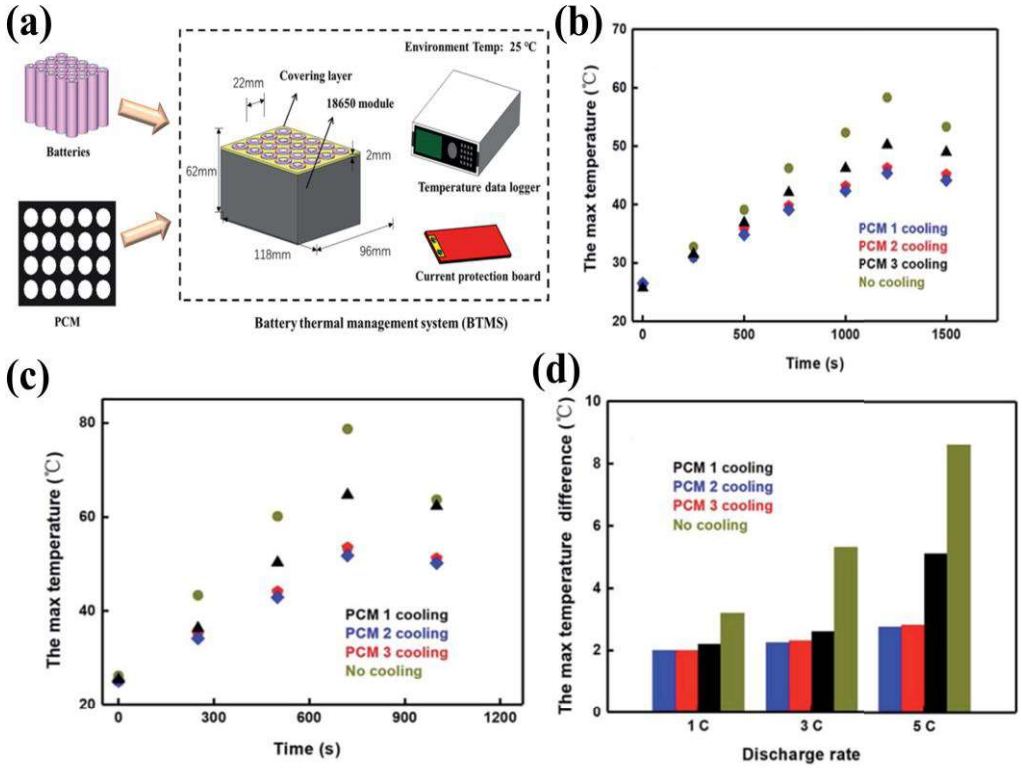


**Fig. 21.** Three kinds of composite PCMs in the 18650 cell: (a) battery module composed of selected cells and PCMs, (b) maximum temperature comparison at a discharge rate of 3.0C, (c) maximum temperature comparison at a discharge rate of 5.0C, and (d) maximum temperature difference comparison [149].

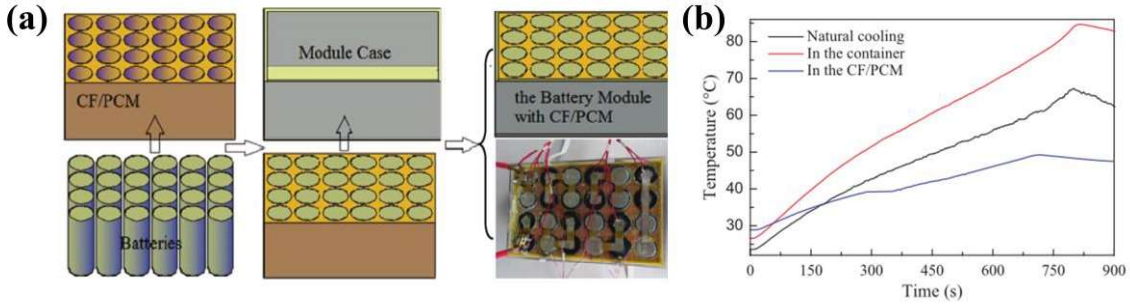


**Fig. 22.** Application of PCM/CF composites in cylindrical 42110-type battery module: (a) PCM/CF battery module and (b) comparison of maximum temperature at a 5C cell discharge with various cooling methods [153].

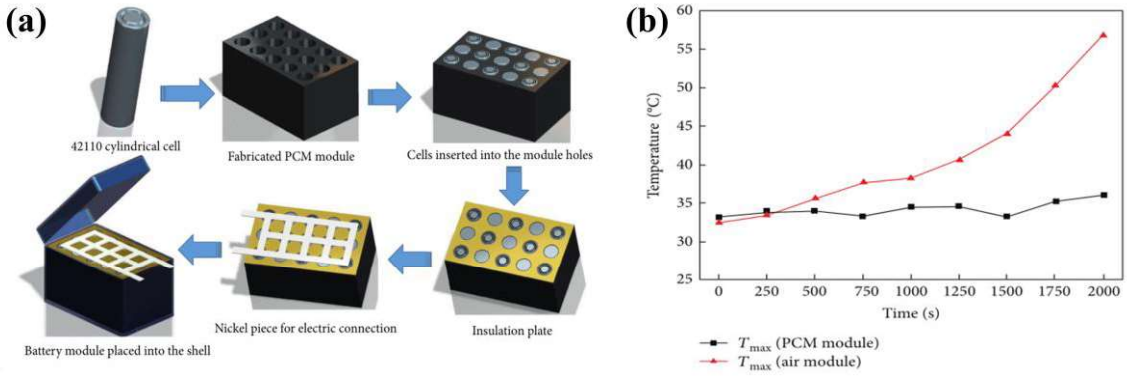


**Fig. 23.** Application of PA/EG composite in cylindrical 18650-type battery module: (a) battery module assembly schematic and (b) comparison of air-cooling module and PCM cooling module maximum temperature test data [160].

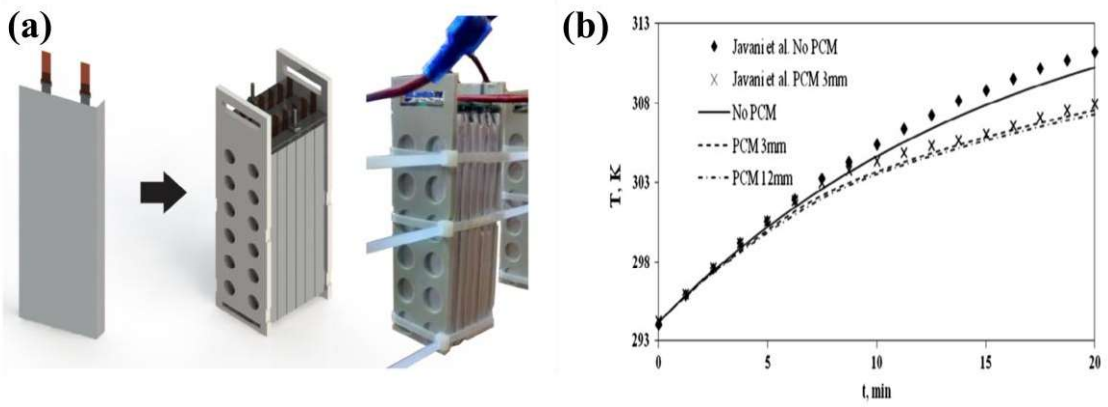


**Fig. 24.** Polymer battery module with PA/EG composite: (a) PCM assembly in battery module, and (b) transient comparison of average battery temperature with and without PCM [163].

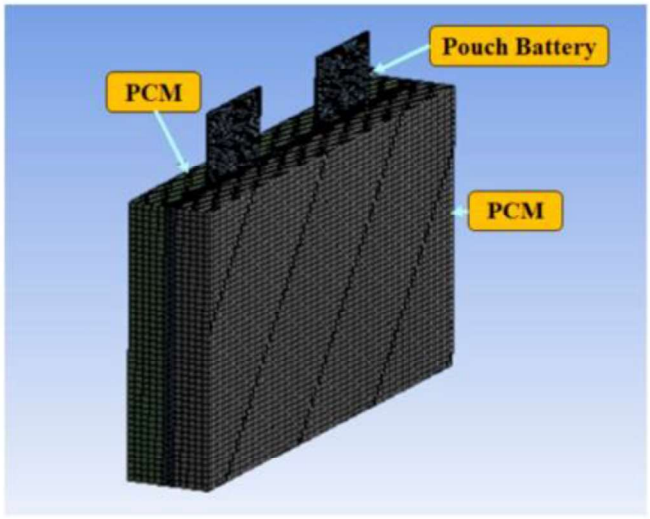


**Fig. 25.** Proposed single lithium-ion polymer pouch BTMS [167].

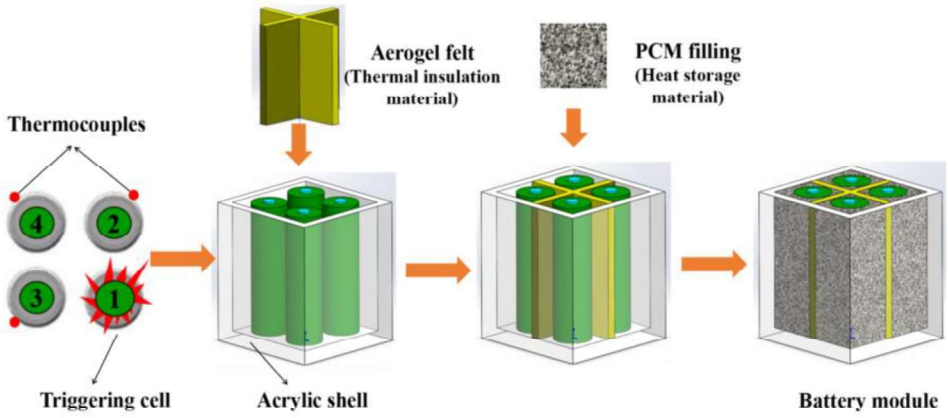


**Fig. 26.** Structure and assembly of designed flame retarded PA/aerogel felt battery module [140].

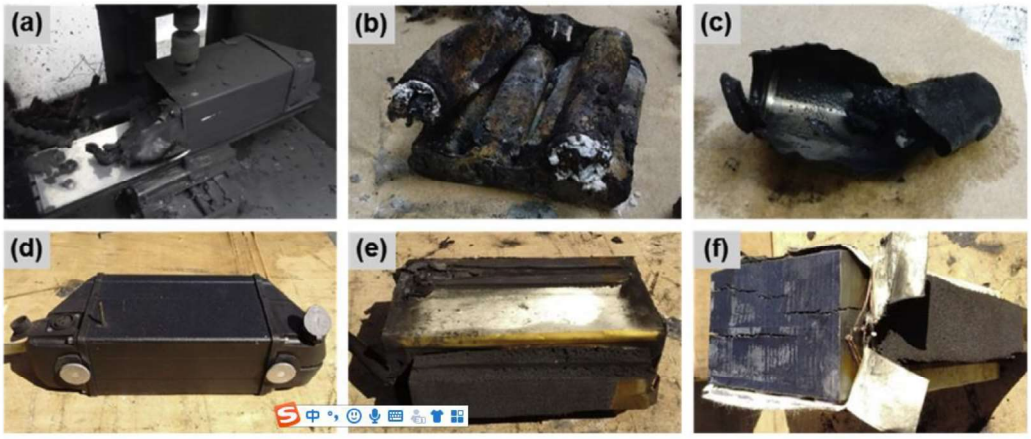


**Fig. 27.** Autopsy images: (a–c) battery pack without PCM and (d–f) battery pack with PCM [161].

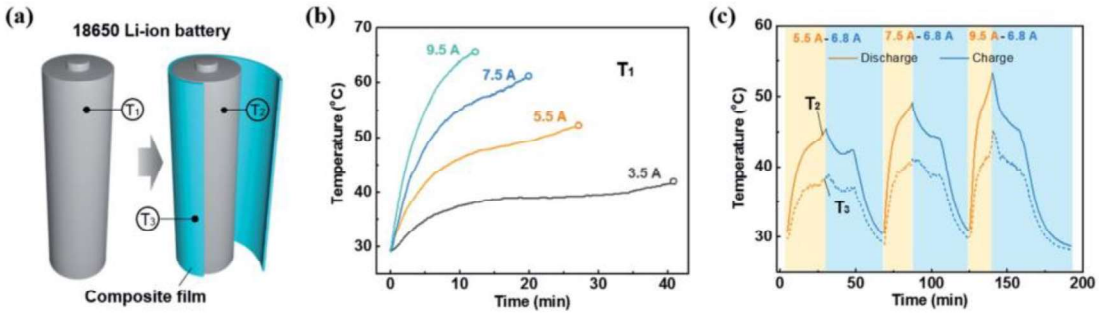


**Fig. 28.** Battery temperature management: (a) commercial 18650 lithium-ion cells with/without composite film wrapped, (b) cell surface temperature evolution at various discharging currents, and (c) temperature evolution of battery monomer wrapped with composite film [175].

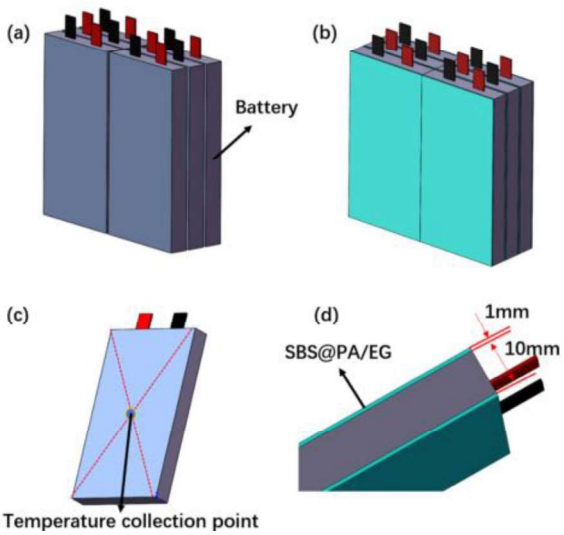


**Fig. 29.** Diagram of battery modules with flexile PCM BTMS: (a) battery module without a BTMS, (b) battery modules with flexible PCM on both sides of each monomer, (c) temperature testing point arrangement, and (d) schematic diagram of the monomer with flexible SBS/PA/EG placed [179].

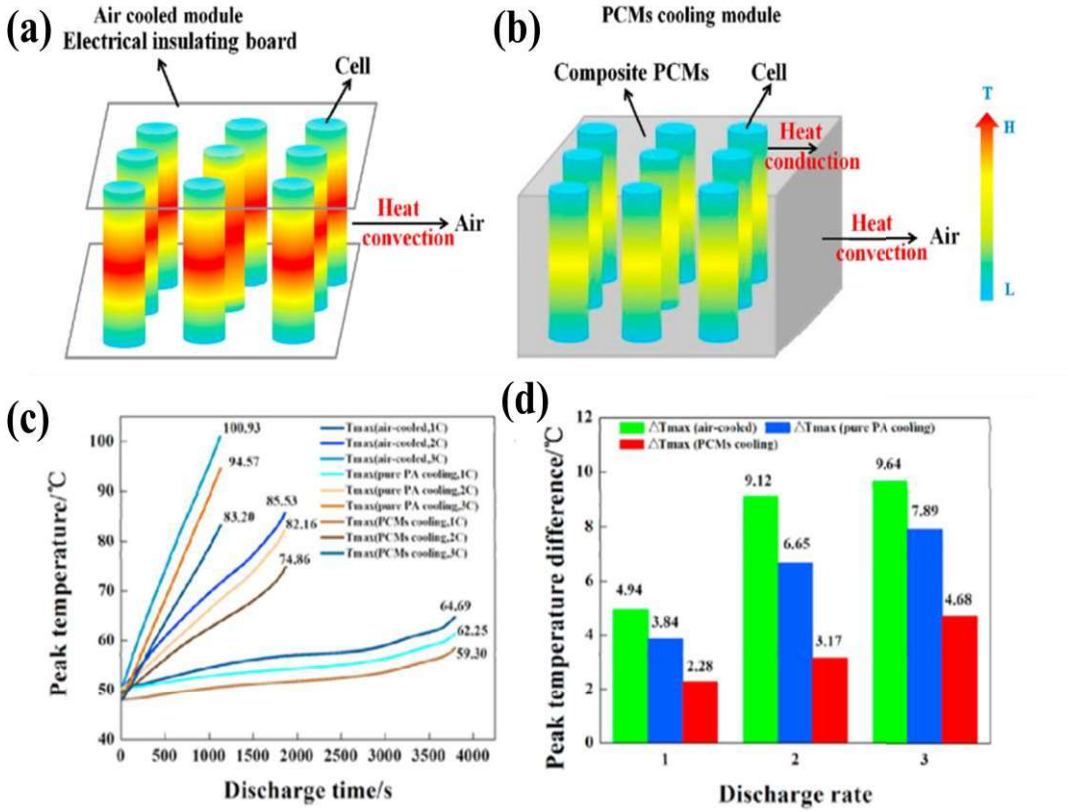


**Fig. 30.** Various BTMS cooling effects: (a) air cooling mode, (b) PCM heat dissipation mode, (c) comparison of peak temperatures (45°C) and (d) maximum temperature difference (45°C) [120].

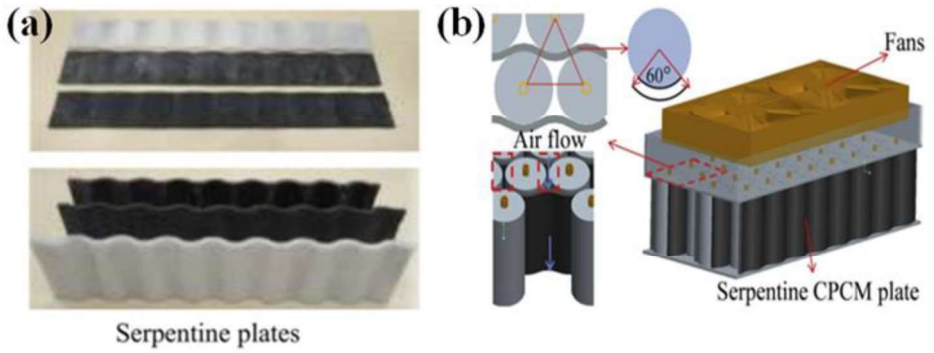


**Fig. 31.** S-CPCM coupled with forced air convection thermal management structure: (a) serpentine plates and (b) S-CPCM plates and air-forced cooling in the battery module [181].

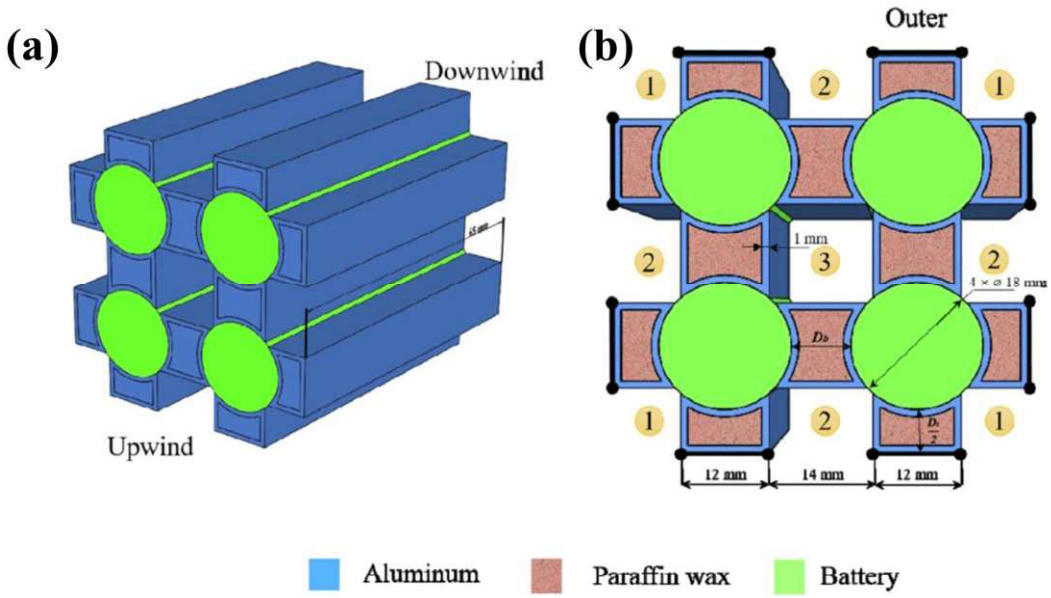


**Fig. 32.** Description of the proposed BTMS: (a) arrangement of air direction and channels and (b) top view of the introduced battery module [184].

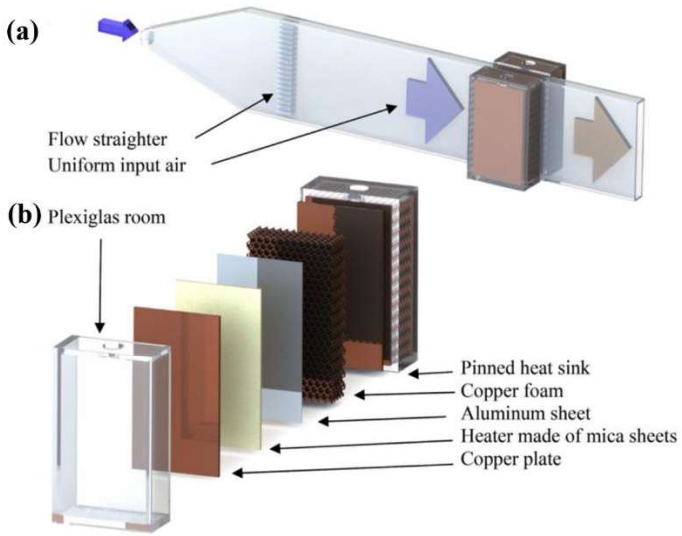

**Fig. 33.** Description of the proposed BTMS: (a) arrangement of air direction and channels and (b) composition of the battery module [187].


**Fig. 34.** Battery pack design with CM-PCM plate [88].

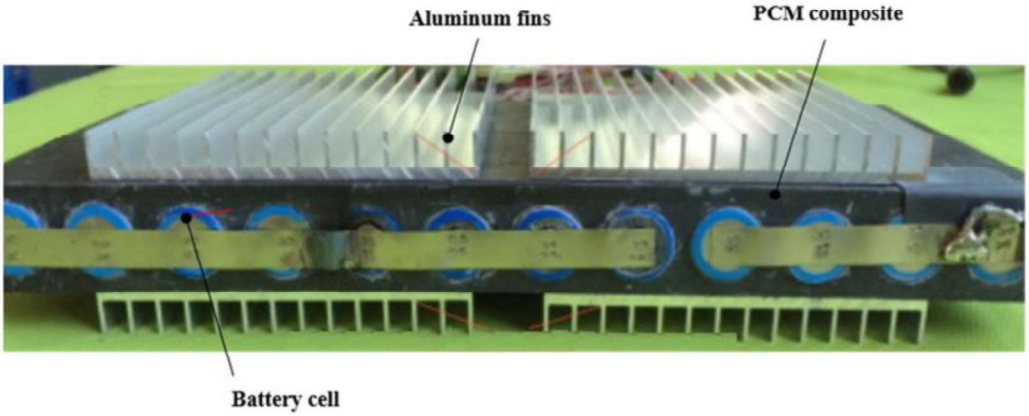


**Fig. 35.** LDPE-CPCM coupled battery pack employing PCM and air-forced cooling [119].

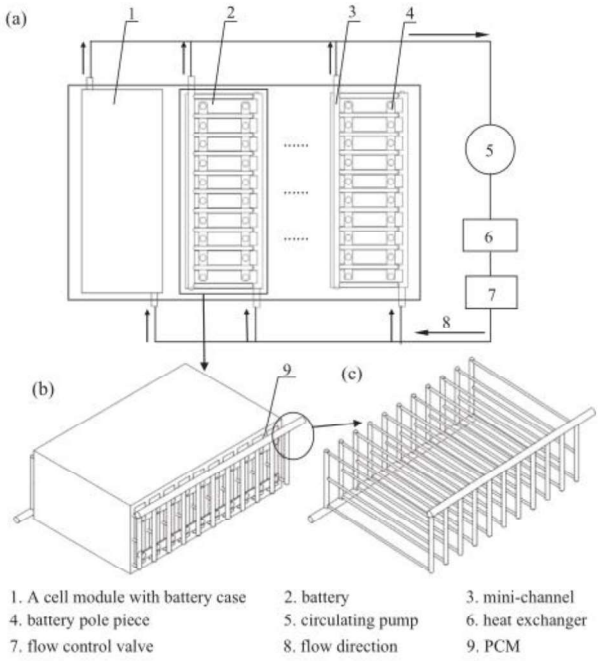

**Fig. 36.** Square lithium-ion battery pack diagram: (a) overall system, (b) a module without battery case, and (c) mini-channel structure [200].

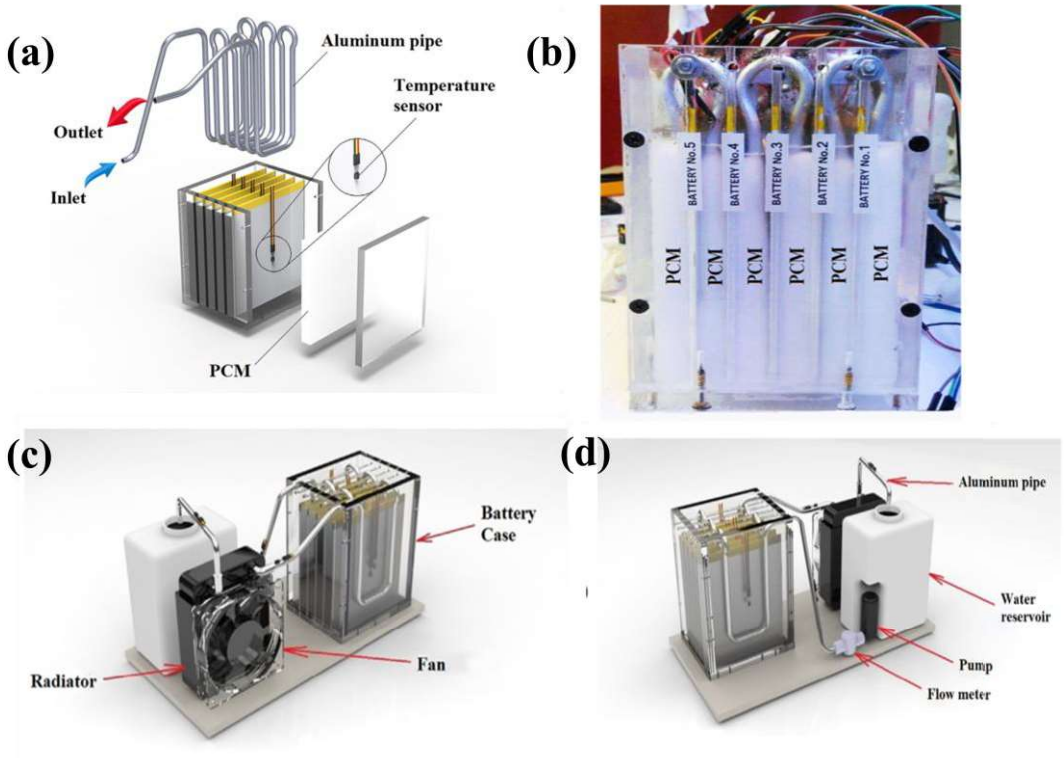


**Fig. 37.** Composite liquid/PCM cooling battery pack: (a) lithium-ion battery module and temperature sensors; (b) prismatic cells, cooling pipes, and PCM; (c) water circulation system and component frontal view; and (d) water circulation system and component back view [202].

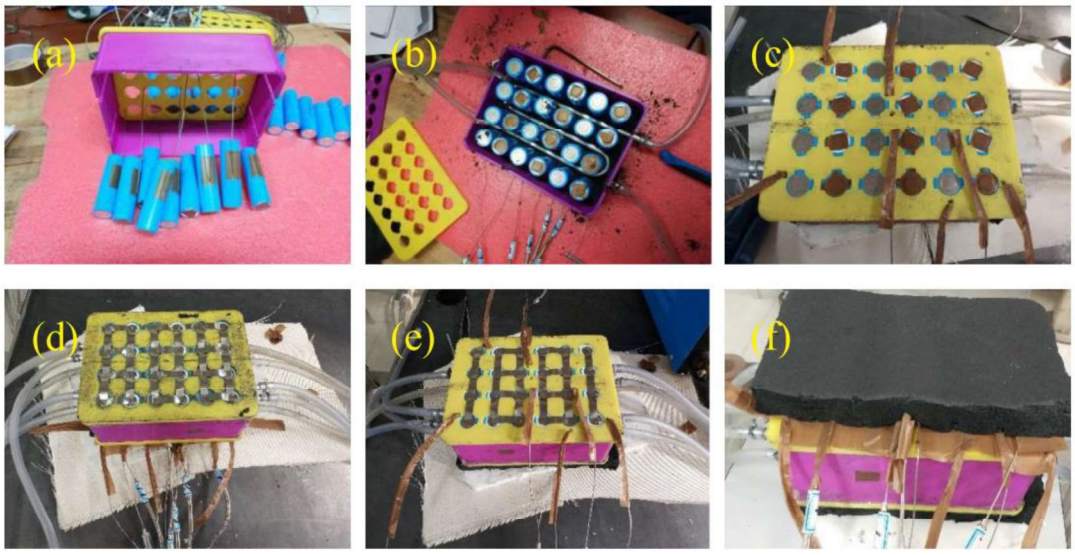


**Fig. 38.** Battery pack and coupled PCM-liquid-cooling system production [205].

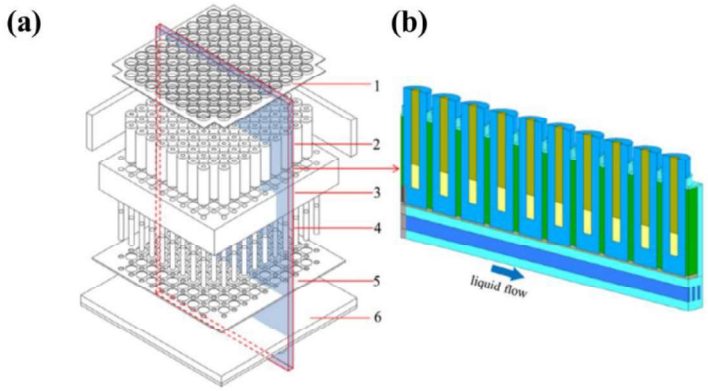


**Fig. 39.** Battery module with conjugated cooling configuration: (a) overall system: (1) heat spreading plate, (2) battery, (3) PCM, (4) thermal column, (5) insulation layer, (6) cold plate assembly, and (b) battery module numerical model [209].

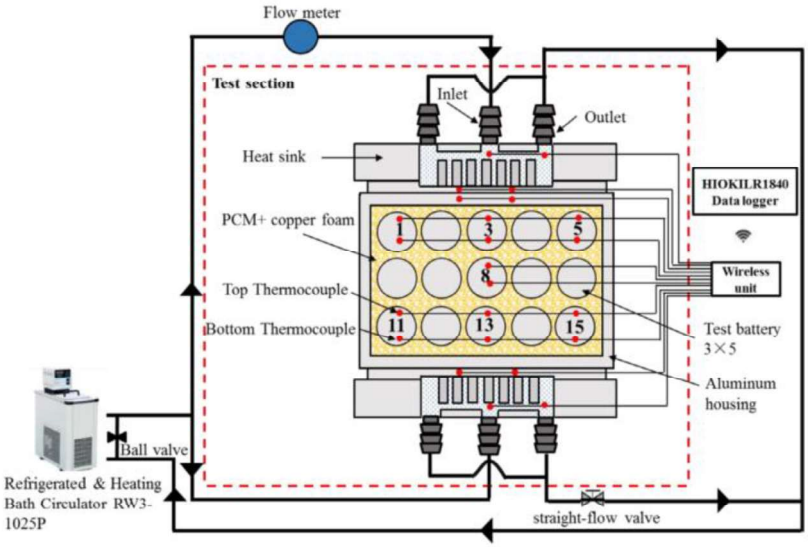


**Fig. 40.** Experimental system and thermocouple locations [212].

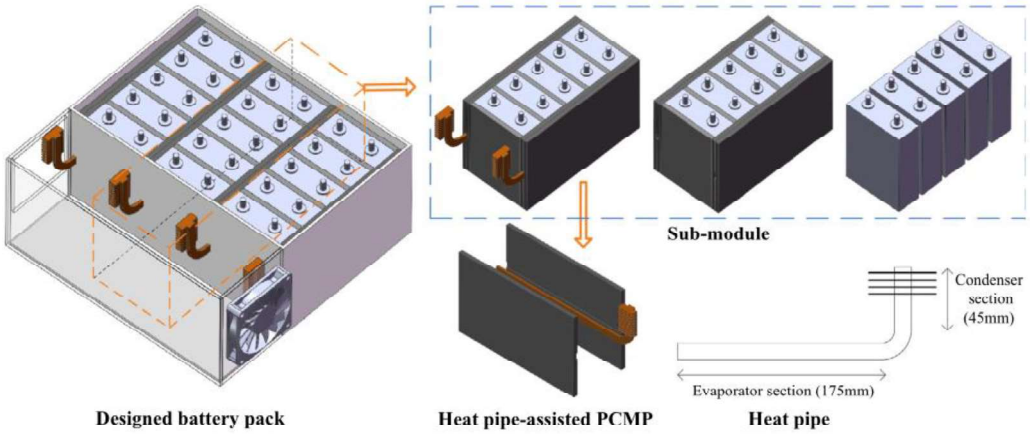


**Fig. 41.** Designed battery pack and sub-modules employing PCM/HP cooling strategies [100].

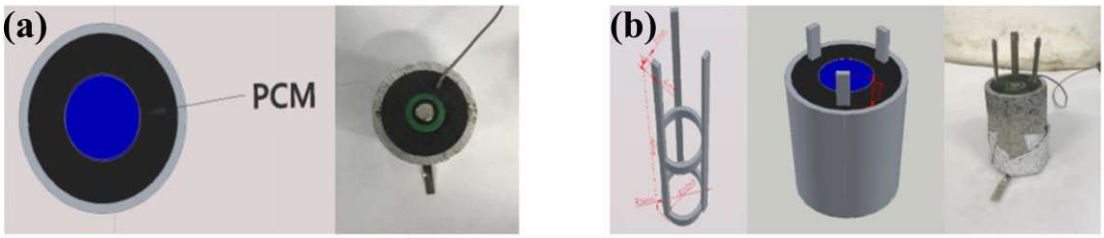


**Fig. 42.** 18650-type cell with PCM/fin structure: (a) PCM cooling and (b) heat dissipation fins and PCM-fin cooling [222].

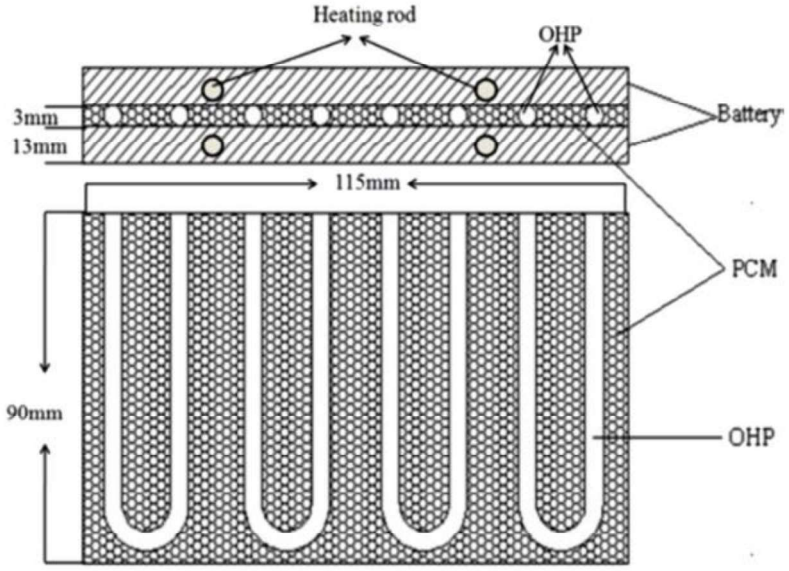


**Fig. 43.** PCM/OHP-based battery cooling system [224].

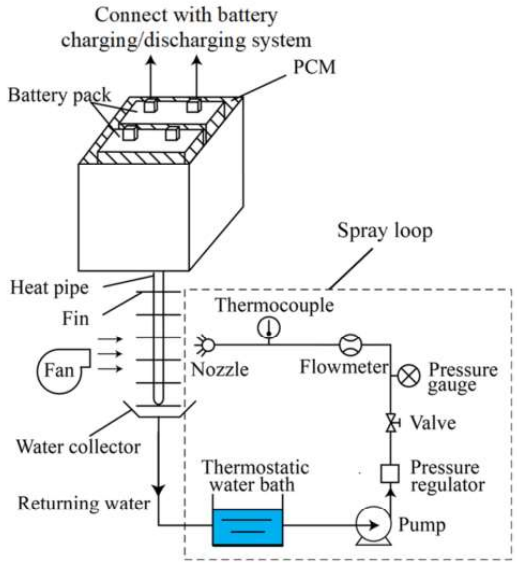


**Fig. 44.** Proposed PCM thermal storage-, HP-, and spray cooling-inspired BTMS design [225].

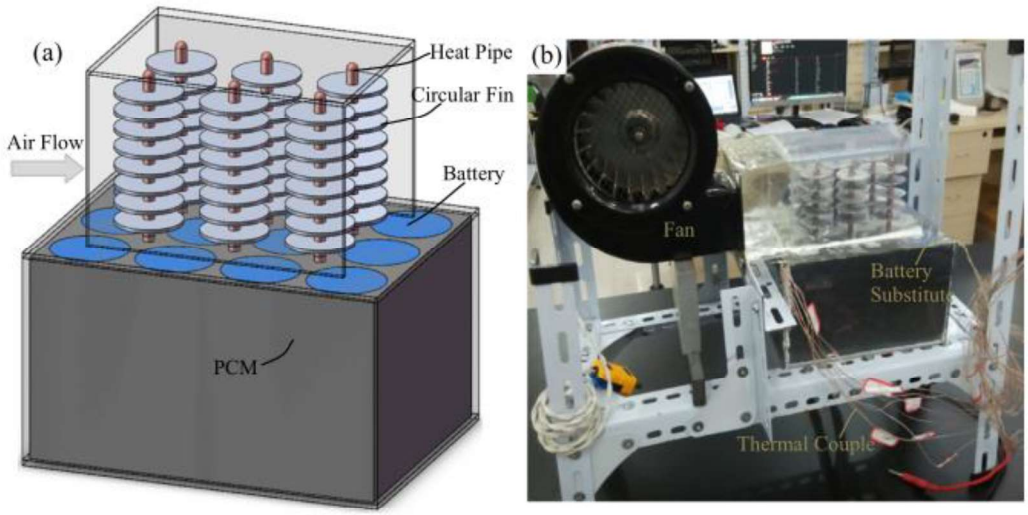


**Fig. 45.** Battery module with PCM/HP composite BTMS: (a) Designed scheme and (b) actual experimental setup [227].

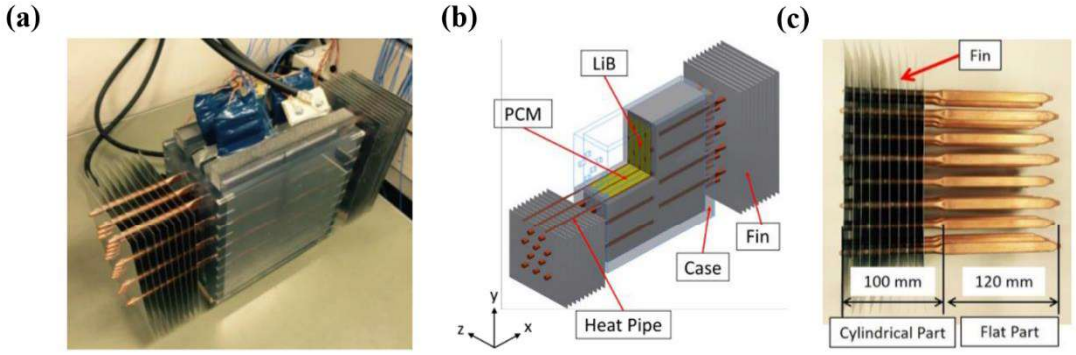


**Fig. 46.** Proposed PCM/HP hybrid cooling system: (a) overview, (b) schematic view, and (c) HPs with fins [228].

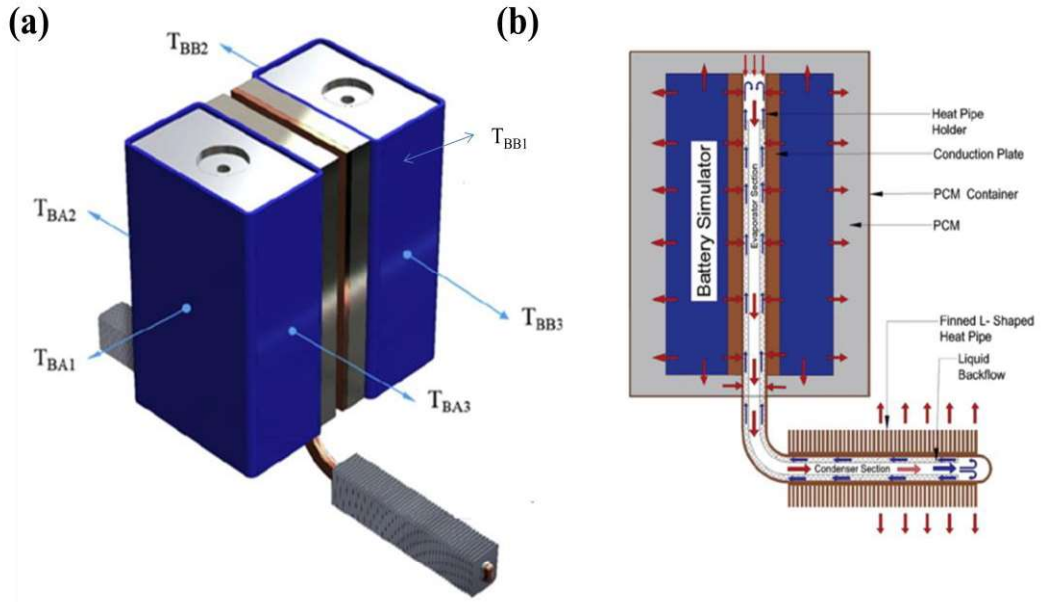

**Fig. 47.** Proposed hybrid PCM/HP cooling system for square batteries: (a) arrangement of power batteries and thermocouples and (b) HP-PCM heat transfer/exchange [230].

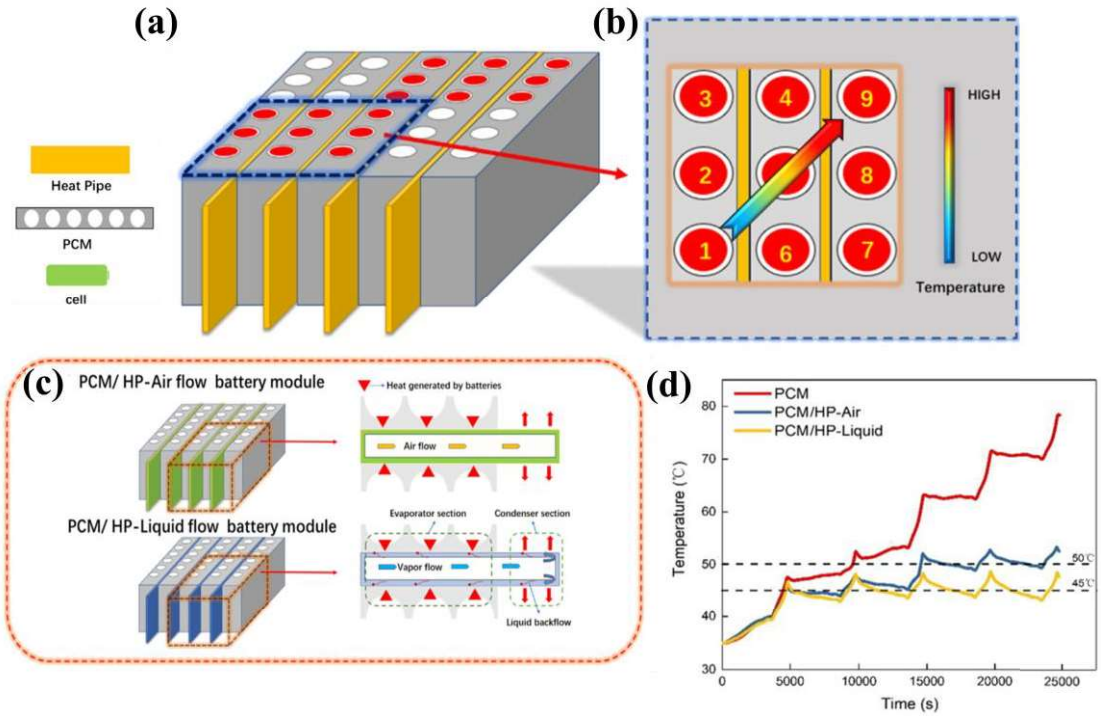


**Fig. 48.** Schematic of proposed hybrid PCM/HP cooling system: (a) designed battery module with integrated BTMS, (b) nine-cell sub-module rectangular region, (c) heat transfer mechanism, and (d) peak temperature variations [233].

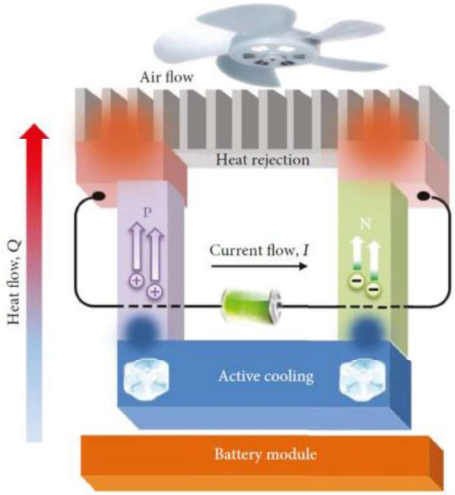


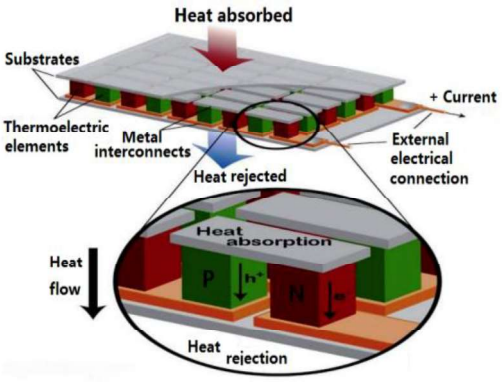


**Fig. 49.** Schematic of a TE module [237-241]. **Fig. 50**. Heat transfer principle of a TE chip [242].

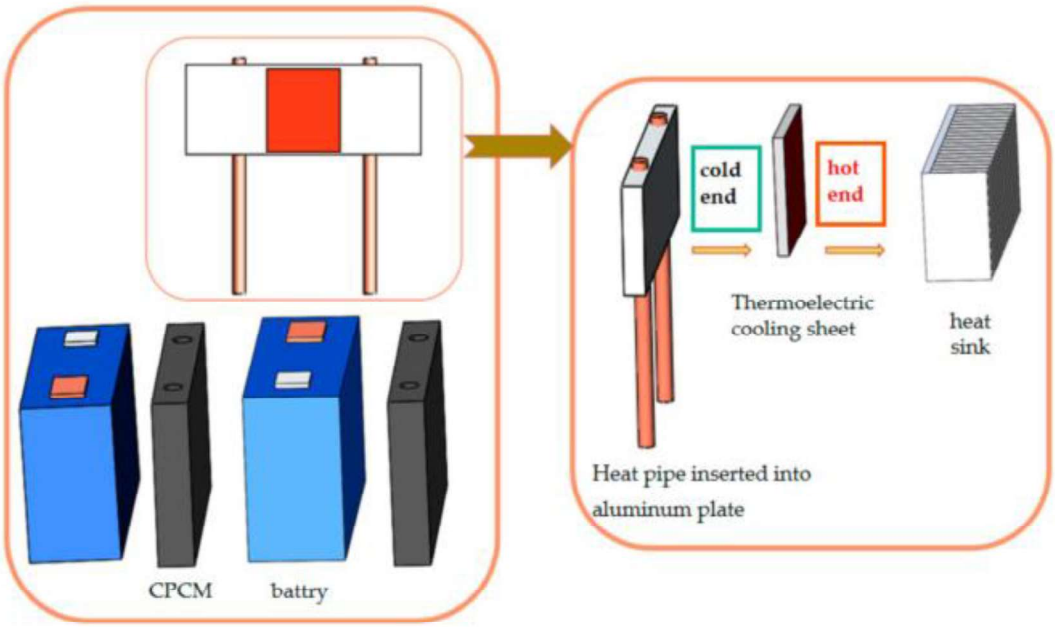


**Fig. 51.** TE sheet-PCM composite thermal management diagram [250].

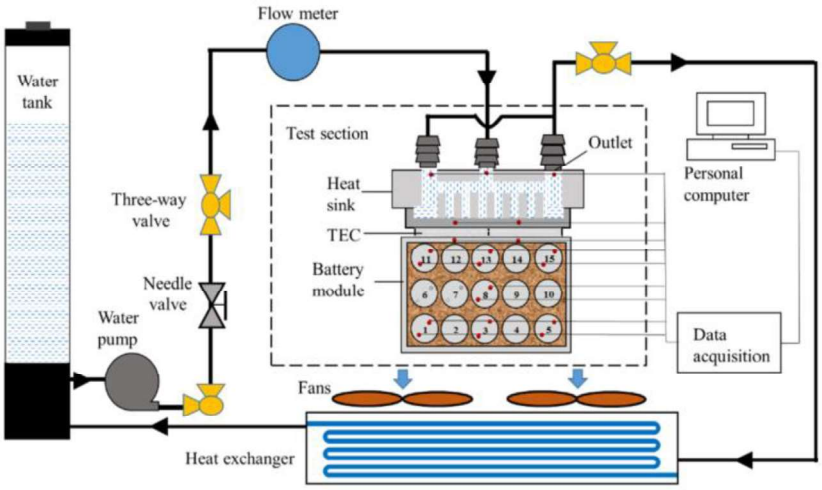


**Fig. 52**. PCM- and TE cooling-based battery module test setup [252].

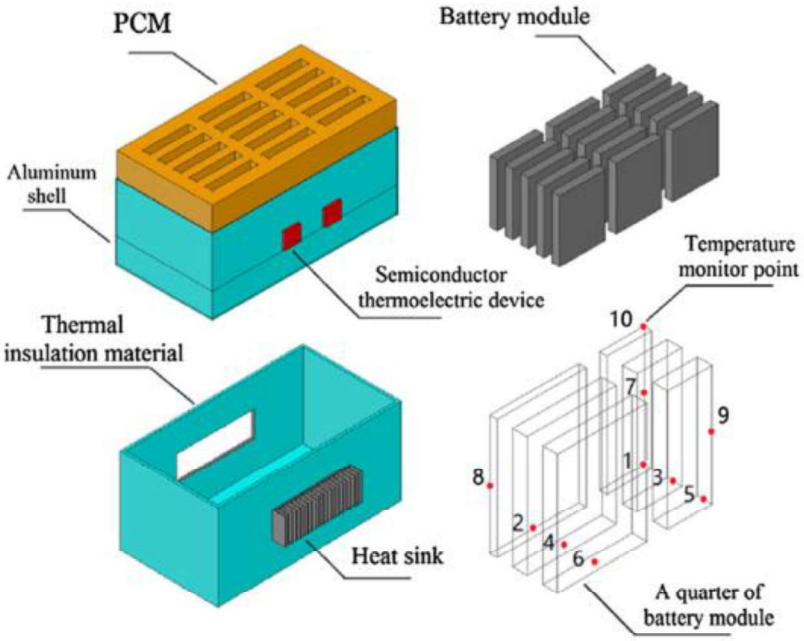


**Fig. 53.** Battery pack with TE semiconductor devices and PCMs [255].

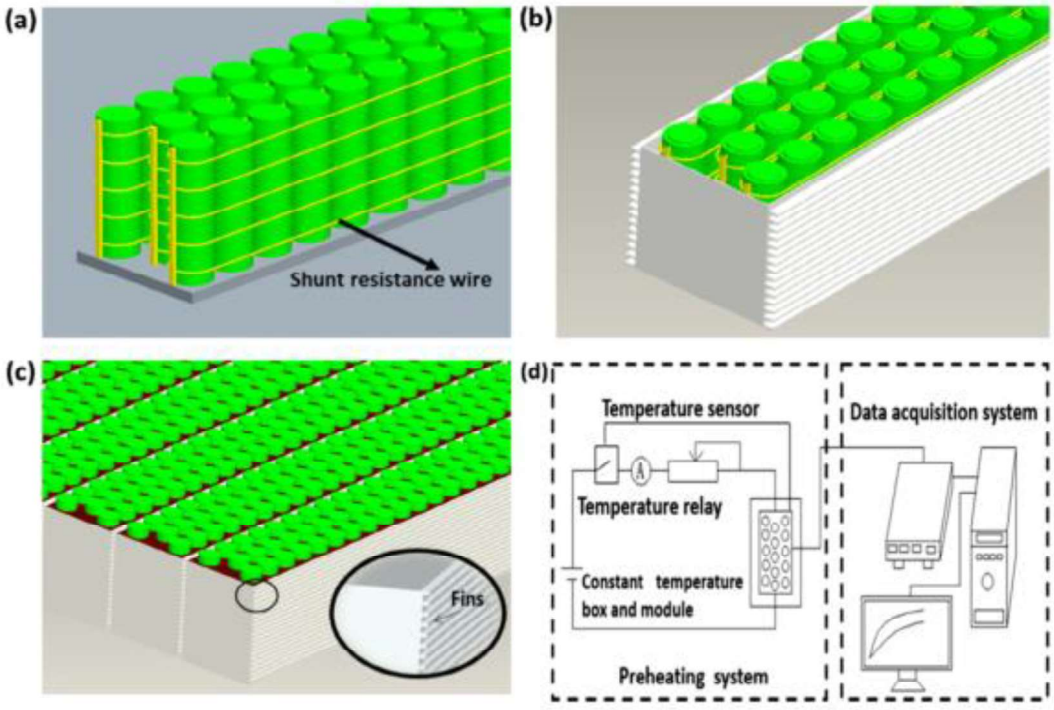


**Fig. 54** Battery module design: (a) resistance wire wrapped around batteries, (b) batteries within the module shell, (c) battery pack composed of battery modules, and (d) preheating experimental setup [270].

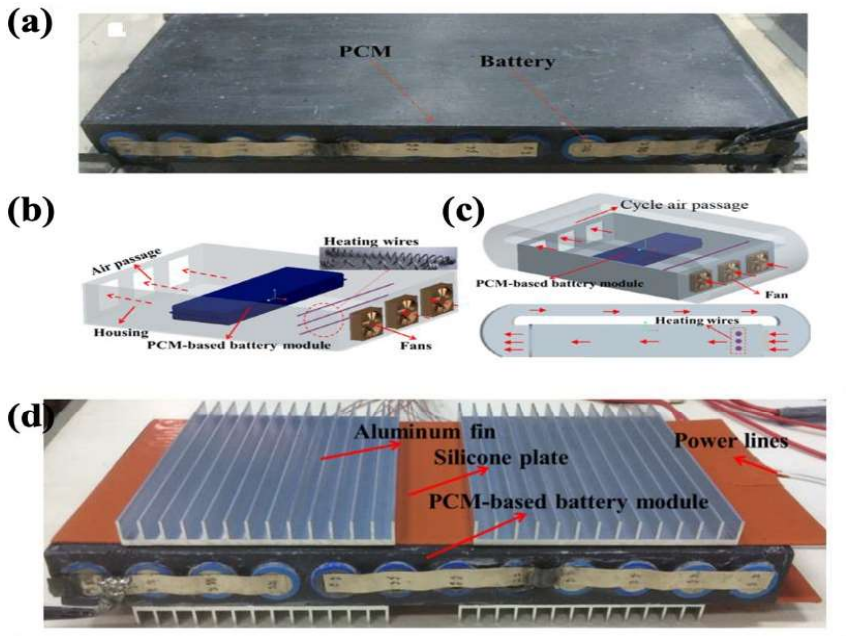


**Fig. 55.** PCM battery module heating strategies: (a) standardized PCM-based battery module, (b) forced air convection heating strategy, (c) optimized forced air convection heating strategy, and (d) silicone plate heating strategy [272].

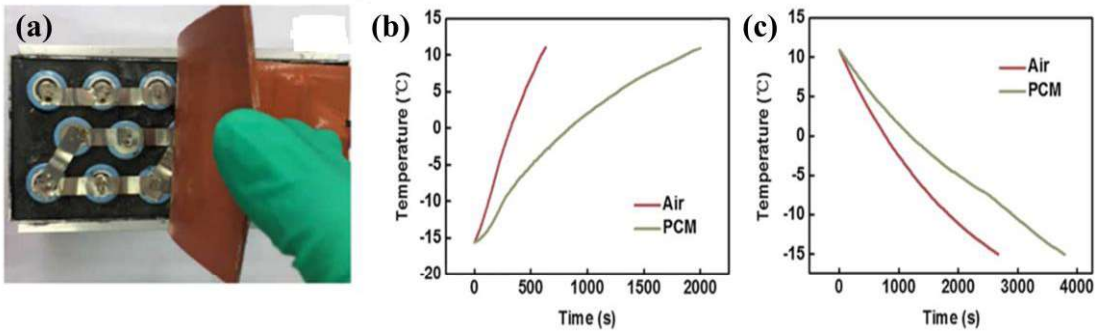


**Fig. 56.** Battery module heating system coupled with PCM and heating sheet: (a) battery module with heat sheet, (b) average air-based battery module surface temperature with two heat sheets at 50°C, and (c) average PCM-based battery module surface temperature with two heat sheets at 50°C [275].

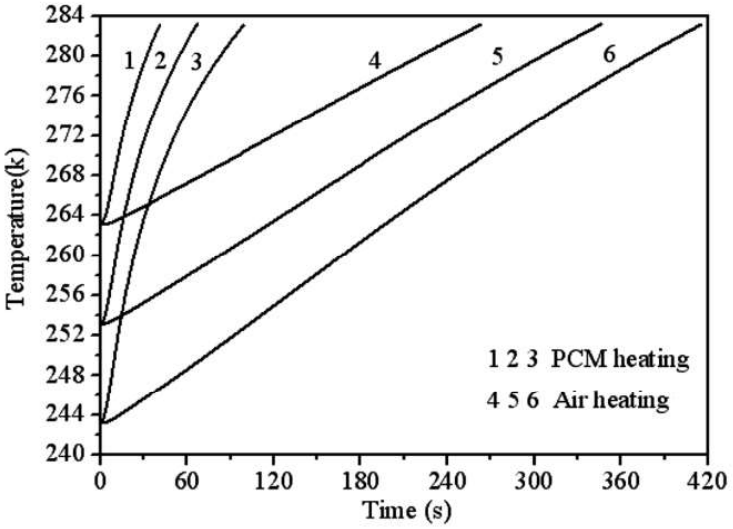


**Fig. 57.** Comparison of temperature responses of PCM and air heating [277].

# Advanced thermal management system driven by phase change materials for power lithium-ion batteries: A review

Jiangyun Zhang[a,*], Dan Shao[d], Liqin Jiang[c], Guoqing Zhang[a], Hongwei Wu[b], Rodney Day[b], Wenzhao Jiang[a]

[a] *School of Materials and Energy, Guangdong University of Technology, Guangzhou, Guangdong 510006, China*

[b] *School of Physics, Engineering and Computer Science, University of Hertfordshire, Hatfield, AL10 9AB, United Kingdom*

[c] *Guangdong Zhuhai Supervision Testing Institute of Quality And Metrology, Zhuhai, 519000, China*

[d] *Guangdong Key Laboratory of Battery Safety, Guangzhou Institute of Energy testing, Guangzhou, Guangdong 511447, China*

The tables in this manuscript are as follows:

**Table 1**

Future plans to ban the sale of traditional fuel vehicles [8-10]

| Countries | Detailed time / year | Specific target |
|---|---|---|
| France | 2040 | A blanket ban on the fuel vehicle sale |
| United Kingdom | 2040 | A complete ban on the sale of traditional diesel-powered cars |
| Germany | After 2030 | Banning the sale of traditional internal combustion engine cars |
| India | 2030 | Banning the sale of conventional fuel cars |
| Holland | 2025 | Banning the sale of conventional fuel cars |
| Norway | 2025 | Banning the sale of conventional fuel cars |
| China | 2040 | Banning the sale of conventional fuel cars |

**Table 2**

Selected lithium-ion battery TR mechanism-induced severe accidents

| Date of accident | Location | Source of accident |
|---|---|---|
| January 6, 2016 | Norway | Tesla Model S suddenly fired when charging in the charge station [11] |
| August 17, 2016 | Biarritz, France | Tesla Model 90D suddenly fired when testing driving [12] |
| September 27, 2017 | Newman Company, Shenzhen City, China | Short circuit-induced spontaneous combustion of stored batteries in a warehouse [13] |
| May 12, 2018 | Florida, USA | Tesla Model S resulted in fire accidents after collisions [14] |
| April 7, 2019 | Hangzhou, China | Battery spontaneously ignited and occurred propagation during the charging process [15] |
| July 18, 2019 | Beijing, China | Batteries suddenly ignited during the rest-time period [16] |
| June 11, 2019 | Daly City, California, USA | Lithium-ion battery-induced fire during charging, which ignited surrounding combustible materials and spread the fire accident [13] |
| May 8, 2020 | Dongguan City, China | Lithium-ion battery-induced spontaneous combustion of car, resulting in a fire [13] |
| August 16, 2020 | Taiyuan City, China | Lithium-ion battery-induced spontaneous combustion of electric car during charging [13] |
| November 6, 2020 | Haikou City, China | EC 30-type electric car suddenly began to smoke and burn [17] |
| November 9, 2020 | Pingxiang City, China | New energy vehicle burst into flames, accompanied by large amount of smoke and explosion [18] |
| November 22, 2020 | Shenzhen City, China | New energy car suddenly sent up smoke, which spread the fire and resulted in an explosion [19] |

**Table 3**

Trade-off analysis of the mainstream lithium-ion power batteries [52,53].

| Cathode chemistry | LCO | LMO | LFP | NCM | NCA |
|---|---|---|---|---|---|
| Voltage (V) | 3.7 | 3.8 | 3.2 | 3.6 | 3.7 |
| Specific energy (mAh/g) | 150 | 120 | 150 | 160 | 170 |

| | | | | | |
|---|---|---|---|---|---|
| Energy density (Wh/kg) | 120-150 | 105-120 | 130 | 160-220 | 220-250 |
| Cycles life | 500 | 300 | 2000 | 1000 | 1000 |
| Thermal Safety | Poor | Excellent | Excellent | Preferable | Poor |
| Operating temperature range/$^{o}$C | -20–60$^{o}$C | -20–60$^{o}$C | -20–60$^{o}$C | -20–55$^{o}$C | -20–60$^{o}$C |
| Cost | Expensive | Cheap | Cheap | More expensive | Low |
| Advantages | Stable charge/discharge properties and simple technology | Low cost and admirable safety | High security, environmentally friendly and longer service life | Good circulation | Eminent low-temperature property and high energy density |
| Disadvantages | Expensive Co and reduced cycle life | Low energy density | Poor low-temperature performance and discharge voltage | High cost of Co | Poor high-temperature property and high technical barrier |

**Table 4**

Lithium-ion power battery heat generation under different temperature ranges.

| Temperature range /$^{o}$C | Chemical reactions | Heat generation/J·g$^{-1}$ | Mechanism analysis |
|---|---|---|---|
| 110–150 | $Li_xC_6$ + | 350 | Rupture of passivation film |
| 130–180 | Melting of PE diaphragm | -190 | Heat absorption |
| 160–190 | Melting of PP diaphragm | -90 | Heat absorption |
| 180–500 | Decomposition of $Li_{0.3}NiO_2$ and electrolyte | 600 | Releasing oxygen temperature 200$^{o}$C |
| 220–500 | Decomposition of $Li_{0.45}CoO_2$ and electrolyte | 450 | Releasing oxygen temperature 230$^{o}$C |
| 150–300 | Decomposition of $Li_{0.1}MnO_4$ and electrolyte | 450 | Releasing oxygen temperature 300$^{o}$C |

| | | | |
|---|---|---|---|
| 130–220 | Solvent and $LiPF_6$ | 250 | Lower energy |
| 240–350 | $Li_xC_6$ and PVDF | 1500 | Violent chain growth |
| 660 | Aluminum melting | -395 | Heat absorption |

**Table 5**

Thermophysical properties of selected straight chain alkanes.

| Molecular formula | Molecular weight | Melting point/$^oC$ | Latent heat/J • $g^{-1}$ |
|---|---|---|---|
| $C_{16}H_{34}$ | 226 | 16.7 | 236.81 |
| $C_{17}H_{36}$ | 240 | 21.4 | 171.54 |
| $C_{18}H_{38}$ | 254 | 28.2 | 242.67 |
| $C_{19}H_{40}$ | 268 | 32.6 | - |
| $C_{20}H_{42}$ | 282 | 36.6 | 246.86 |
| $C_{21}H_{44}$ | 296 | 40.2 | 200.83 |
| $C_{22}H_{46}$ | 310 | 44.0 | 251.04 |
| $C_{23}H_{48}$ | 324 | 47.5 | 234.30 |
| $C_{24}H_{50}$ | 338 | 50.6 | 248.95 |
| $C_{25}H_{52}$ | 352 | 53.5 | - |
| $C_{26}H_{54}$ | 366 | 56.3 | 255.22 |
| $C_{27}H_{56}$ | 380 | 58.8 | 234.72 |

**Table 6**

Literature reviews on fire-retardant PCC applications

| PCM | Type | Form/shell | Fire retardant | Result | Reference |
|---|---|---|---|---|---|
| PA | MicroPCM | Gelatin and Na-alginate | Clay-nano particle shell material, introduced during microencapsulation | Ignition time of treated textile increased by 25%–50 % | [126] |
| PA | MicroPCM | Polymetacrylic acid-*co*-ethyl methacrylate | PCM-diethyl ethylphosphonate (DEEP), introduced during microencapsulation | 6–9% increase in treated foam limiting oxygen index (LOI) | [127] |
| PA or fatty acid | MicroPCM | Melamine-formaldehyde resin, gelatin, | Boric acid, sodium carbonate, and | NA | [128] |

| | | | | | |
|---|---|---|---|---|---|
| | | polyurea, polyurethane, urea-formaldehyde resin, and combinations | sodium silicate applied on the surface of the microcapsule after microencapsulation | | |
| PA | FS | HDPE | Nine $Mg(OH)_2$, $Al(OH)_3$, ammonium polyphosphate (APP), PER, and EG formulations | NA | [129] |
| PA | FS-PCM | HDPE | 15-20-25 APP+PER+melamine (2:1:1) wt%; EG | NA | [130] |
| PA | FS-PCM | HDPE | APP, PER, Fe | 40%–56% lower heat release rate (HRR) | [131] |
| PA | FS-PCM | HDPE | APP, EG, zinc borate | HRR decreased by 60% | [132] |
| PA | FS-PCM | HDPE | APP, EG, zinc borate | HRR decreased by 60%–68% | [133] |
| *n*-Octadecane | Nano encapsulated | Melamine-formaldehyde | Phosphorus–nitrogen containing diamine (PNDA) | Peak heat release rate (PHRR) decreased by 32.8%<br>Total heat release (THR) decreased by 30.3%<br>Total | [134] |

| | | | | | |
|---|---|---|---|---|---|
| | | | | smoke rate (TSR) decreased by 18.6% | |
| *n*-Octadecane | Nano encapsulated | Poly(methylmethacrylate) | Diethyl bis(2-hydroxyethyl acrylate)amino methylphosphonate | pHRR decreased by 39.7%<br>Total heat release (THR) decreased by 18.4%<br>TSR decreased by 12.2%<br>LOI increased from 19.5% to 25.1% | [135] |
| PA | Shape stabilized | - | Acrylic resin/EG; alkyd resin/EG; and epoxy resin/EG | pHRR decreased by 62%–84% | [136] |
| PA | Shape stabilized | HDPE and styrene-butadiene-styrene copolymer | Organomontmorillonite, EG | pHRR decreased by up to 72.7% | [137] |
| Paraffin chlorinated paraffin | FS-PCM | HDPE | EG, antimony trioxide | pHRR decreased up to ~50% | [138] |
| PA (70%) | FS-composite | Olefin block | Acrylic resin/EG, glass fibers | pHRR decreased by 58.8% | [139] |